

## CREEP BEHAVIOR OF SELF-CONSOLIDATING CONCRETE

Except where reference is made to the work of others, the work described in this thesis is my own or was done in collaboration with my advisory committee. This thesis does not include proprietary or classified information.

---

Bryan Palmer Kavanaugh

Certificate of Approval:

---

Robert W. Barnes  
James J. Mallett Associate Professor  
Civil Engineering

---

Anton K. Schindler, Chair  
Gottlieb Associate Professor  
Civil Engineering

---

Mary L. Hughes  
Assistant Professor  
Civil Engineering

---

George T. Flowers  
Interim Dean  
Graduate School

CREEP BEHAVIOR OF SELF-CONSOLIDATING CONCRETE

Bryan Palmer Kavanaugh

A Thesis

Submitted to

the Graduate Faculty of

Auburn University

in Partial Fulfillment of the

Requirements for the

Degree of

Master of Science

Auburn, Alabama  
August 9, 2008

CREEP BEHAVIOR OF SELF-CONSOLIDATING CONCRETE

Bryan Palmer Kavanaugh

Permission is granted to Auburn University to make copies of this thesis at its discretion, upon requests of individuals or institutions and at their expense. The author reserves all publication rights.

---

Signature of Author

---

Date of Graduation

## VITA

Bryan Palmer Kavanaugh, son of Mark Edward and Carole Nichols Kavanaugh, was born May 7, 1980, in Atlanta, Georgia. He is a 1998 graduate of Fayette County High School, located in Fayetteville, Georgia. After graduating from high school, he attended Auburn University, where he earned a Bachelor of Civil Engineering degree in May, 2006. Upon completion of his undergraduate course work, he entered graduate school at Auburn University with the intent of earning the degree of Master of Science in Civil Engineering (Structures). After completing this degree in August, 2008, he was employed as a structural designer with The Preston Partnership, LLC in Atlanta, Georgia.

THESIS ABSTRACT  
CREEP BEHAVIOR OF SELF-CONSOLIDATING CONCRETE

Bryan Palmer Kavanaugh

Master of Science, August 9, 2008  
(B.C.E., Auburn University 2006)

233 Typed Pages

Directed by Anton K. Schindler

Self-consolidating concrete (SCC) is a highly flowable material that has the ability to improve the quality and durability of structures; however, much is still unknown about the hardened properties of this material, including the creep behavior. This thesis presents research aimed at improving knowledge in this area by investigating the creep performance of four SCC mixtures and one conventional-slump mixture. The four SCC mixtures have varying water-to-cementitious materials ratios of 0.28 and 0.32, and use differing powder combinations that include Type III portland cement, Class C fly ash, and Ground Granulated Blast-Furnace (GGBF) slag. All four SCC mixtures' fresh properties were evaluated using the slump flow, T-50, and VSI tests. For each mixture, the following five loading ages were investigated: 18 hours, 2 days, 7 days, 28 days, and 90 days. The 18-hour samples, which had compressive strengths ranging

from 5,800 psi to 8,860 psi, were cured at predetermined elevated temperatures that are typical of those used in the prestressing industry in the Southeastern United States. The samples loaded at 2, 7, 28, and 90 days were moist cured prior to loading. Upon the completion of curing, each sample was loaded to achieve a stress level equal to 40 percent of the concrete compressive strength.

All data collected from the SCC mixtures were compared to the data from the conventional-slump mixture. When curing was accelerated and the load was applied at 18 hours, the creep of all the SCC mixtures was less than the conventional-slump mixture. All SCC mixtures cured under elevated or standard laboratory temperatures exhibited creep values similar to or less than that of the conventional-slump concrete mixture. When curing was not accelerated, the creep behavior of the moderate-strength fly ash SCC and conventional-slump mixtures were similar. The high-strength mixtures had the highest paste content, but exhibited less creep than any of the moderate-strength mixtures. At a fixed water-to-cementitious materials ratio, SCC mixtures made with GGBF slag exhibited less creep than those made with fly ash, regardless of the age at loading.

The accuracy of the following five creep prediction methods was also investigated: ACI 209, AASHTO 2007, CEB 90, GL 2000, and B3. ACI 209 provided the most accurate creep estimations for the accelerated-cured specimens, except for the high-strength concrete mixture. The AASHTO 2007 method underestimated the creep at early concrete ages, but overestimated it for later ages. Overall, the CEB 90 method was the most accurate of the five models investigated in this study. The GL 2000 and B3 methods significantly overestimated the creep for all mixtures.

## ACKNOWLEDGEMENTS

I would like to thank my advisor Dr. Anton K. Schindler for all his help and direction throughout this entire process. His advice and time were of exceptional value to me over the past several years. Additionally, I would like to thank Dr. Robert W. Barnes for his input and guidance throughout the course of this research project.

Furthermore, none of this project would have been possible without the tireless efforts of the many graduate and undergraduate students working in the Structural Research Laboratory at Auburn University. A list of these hard working research assistants includes, but is not limited to: Kurtis Boehm, Darren Dachelet, Dustin Swart, Jason Meadows, Seth Green, Wes Bullock, and Nick Franklin. Special thanks also go to Mr. Billy Wilson, the structural research laboratory technician at Auburn University, for his friendship, guidance, and help throughout the latter course of my time at Auburn University.

The support of my family, namely my mother and father, over the past 28 years has been incredible and is greatly appreciated. I can never repay all they have done for me or express how much it has meant to me, but I thank them for everything and I love them dearly.

Finally, I would like to thank God. All things are truly possible in His name. I thank Him for staying with me throughout all of my pitfalls and for blessing me with such a wonderful life, family, and group of friends.

Style manual or journal used Chicago Manual of Style

---

Computer software used Microsoft® Word, and Microsoft® Excel

---



## TABLE OF CONTENTS

LIST OF TABLES .....	xviii
LIST OF FIGURES .....	xxi
CHAPTER 1: INTRODUCTION .....	1
1.1 BACKGROUND .....	1
1.2 RESEARCH OBJECTIVES .....	3
1.3 RESEARCH SCOPE .....	4
1.4 ORGANIZATION OF THESIS .....	5
CHAPTER 2: LITERATURE REVIEW .....	7
2.1 INTRODUCTION .....	7
2.2 COMPONENTS OF SCC.....	8
2.2.1 SCC CONSTITUENT MATERIALS .....	9
2.2.1.1 Type III Cement.....	10
2.2.1.2 Air-entraining Admixtures.....	10
2.2.1.3 Supplementary Cementing Materials (SCMs) .....	11
2.2.1.4 Viscosity Modifying Admixtures .....	13
2.3 VOLUMETRIC CHANGE.....	13
2.3.1 DRYING SHRINKAGE .....	14

2.3.2	AUTOGENEOUS SHRINKAGE.....	17
2.3.3	CREEP .....	18
2.3.3.1	The Creep Mechanism .....	20
2.3.3.2	Variables Affecting Creep .....	21
2.4	CREEP PREDICTION METHODS .....	24
2.4.1	ACI 209 CREEP PREDICTION METHOD .....	24
2.4.2	AASHTO 2007 CREEP PREDICTION METHOD .....	27
2.4.3	CEB 90 CREEP PREDICTION METHOD.....	28
2.4.4	GL 2000 CREEP PREDICTION METHOD .....	31
2.4.5	B3 CREEP PREDICTION METHOD.....	34
2.5	PREVIOUS FINDINGS RELATED TO CREEP OF SCC.....	38
2.5.1	DESCRIPTION OF PREVIOUS STUDIES .....	38
2.5.1.1	Creep Evaluation by Raghavan et al. (2003) .....	38
2.5.1.2	Study Conducted by Seng and Shima (2005) .....	41
2.5.1.3	Creep Study by Colleparidi et al. (2003) .....	44
2.5.2	CONCLUSIONS FROM PREVIOUS STUDIES .....	46
CHAPTER 3: EXPERIMENTAL PLAN .....		48
3.1	INTRODUCTION .....	48
3.2	EXPERIMENTAL PROGRAM.....	48
3.2.1	REQUIREMENTS FOR SCC MIXTURES.....	49
3.2.1.1	Fresh Properties .....	50
3.2.1.2	Hardened Properties.....	50
3.2.2	SPECIMEN TYPES AND AGES AT LOADING .....	50

3.3 MIXTURE PROPORTIONS .....	53
3.4 TEST SPECIMEN IDENTIFICATION SYSTEM .....	55
3.5 TEST METHODS.....	57
3.5.1 BATCHING.....	57
3.5.1.1 Collection of Materials .....	57
3.5.1.2 Moisture Corrections .....	57
3.5.2 MIXING PROCEDURES .....	58
3.5.2.1 Buttering the Mixer.....	58
3.5.2.2 Mixing Sequence .....	59
3.5.3 METHODS FOR TESTING FRESH CONCRETE.....	61
3.5.3.1 Slump Flow.....	61
3.5.3.2 Visual Stability Index (VSI) .....	63
3.5.3.3 T-50.....	64
3.5.3.4 Air Content and Unit Weight.....	64
3.5.3.5 Fresh Concrete Temperature.....	65
3.5.4 SPECIMEN PREPARATION AND CURING .....	65
3.5.4.1 Specimen Preparation .....	65
3.5.4.2 Curing Regimes .....	68
3.5.5 METHODS FOR TESTING HARDENED CONCRETE .....	70
3.5.5.1 Compressive Strength .....	70
3.5.5.2 Drying Shrinkage .....	71
3.5.6 CREEP TESTING.....	74
3.5.6.1 Creep Frames .....	74

3.5.6.2 The Creep Room .....	80
3.5.6.3 Creep Testing Procedure .....	82
3.6 MATERIALS .....	85
3.6.1 CEMENTITIOUS MATERIALS .....	85
3.6.1.1 Type III Portland Cement .....	85
3.6.1.2 Class C Fly Ash .....	85
3.6.1.3 Ground-Granulated Blast-Furnace (GGBF) Slag .....	86
3.6.2 CHEMICAL ADMIXTURES .....	87
3.6.2.1 High-Range Water-Reducing (HRWR) Admixture.....	87
3.6.2.2 Viscosity Modifying Admixture (VMA).....	87
3.6.3 COARSE AGGREGATE.....	88
3.6.4 FINE AGGREGATE .....	88
CHAPTER 4: PRESENTATION AND ANALYSIS OF RESULTS .....	90
4.1 INTRODUCTION .....	90
4.2 FRESH PROPERTIES .....	90
4.2.1 SLUMP FLOW .....	92
4.2.1.1 Slump Flow Test Results .....	92
4.2.1.2 Discussion of Slump Flow Test Results .....	92
4.2.2 T-50.....	93
4.2.3 VISUAL STABILITY INDEX (VSI).....	94
4.2.4 AIR CONTENT .....	94
4.2.5 UNIT WEIGHT .....	95
4.3 MECHANICAL PROPERTIES .....	95

4.3.1 COMPRESSIVE STRENGTH .....	96
4.3.1.1 Effects of Water-to-Cementitious Materials Ratio .....	96
4.3.1.2 Effects of Cementitious Material System .....	98
4.3.1.3 Behavior of SCC versus Conventional-Slump Concrete .....	98
4.4 RESULTS FROM CREEP TESTING PROCEDURES.....	101
4.4.1 CREEP AND COMPLIANCE RESULTS .....	103
4.4.1.1 Creep Strain Results.....	103
4.4.1.2 Compliance Results .....	106
4.4.1.2.1 Effects of Water-to-Cementitious Materials Ratio .....	107
4.4.1.2.2 Effects of Cementitious Materials System.....	110
4.4.1.2.3 Behavior of SCC versus Conventional-Slump Concrete .....	110
4.4.2 DRYING SHRINKAGE .....	113
4.4.2.1 Effects of Water-to-Cementitious Materials Ratio .....	116
4.4.2.2 Effects of Cementitious Materials System.....	119
4.4.2.3 Behavior of SCC versus Conventional-Slump Concrete .....	119
4.4.3 ENVIRONMENTAL CONDITIONS .....	121
4.4.4 TRACKING AND MAINTAINING THE APPLIED LOAD .....	121
4.5 RAPID CHLORIDE ION PENETRATION TEST .....	124
4.6 LESSONS LEARNED THROUGH TESTING .....	125
4.6.1 DESIGNING AND BUILDING CREEP FRAMES .....	125
4.6.1.1 Creep Frame Design .....	125
4.6.1.2 Creep Frame Construction .....	126
4.6.2 PREPARING SPECIMENS.....	127

4.6.2.1	Mixing and Casting Specimens .....	127
4.6.2.2	Final Specimen Preparation .....	128
4.6.3	CONDUCTING CREEP TESTING .....	128
4.7	SUMMARY OF RESULTS .....	129
4.7.1	FRESH PROPERTIES .....	129
4.7.2	HARDENED PROPERTIES.....	130
CHAPTER 5:	EVALUATION OF CREEP PREDICTION METHODS .....	132
5.1	INTRODUCTION .....	132
5.2	STATISTICAL ANALYSIS OF CREEP PREDICTION METHODS.....	133
5.2.1	COMPARISON STATISTICS .....	133
5.2.2	RESULTS FROM STATISTICAL ANALYSIS .....	135
5.3	ACI 209 CREEP PREDICTION METHOD .....	138
5.4	AASHTO CREEP PREDICTION METHOD.....	143
5.5	CEB 90 CREEP PREDICTION METHOD .....	148
5.6	GL 2000 CREEP PREDICTION METHOD.....	152
5.7	B3 CREEP PREDICTION METHOD .....	156
5.8	CALIBRATION OF THE CEB 90 CREEP PREDICTION METHOD .....	160
5.9	SUMMARY OF CONCLUSIONS.....	167
CHAPTER 6	CONCLUSIONS AND RECOMMENDATIONS.....	170
6.1	SUMMARY OF LABORATORY WORK .....	170
6.2	CONCLUSIONS.....	171
6.2.1	FRESH PROPERTIES .....	171
6.2.2	HARDENED PROPERTIES.....	171

6.2.3 CREEP PREDICTION METHODS .....	172
6.3 RECOMMENDATIONS FOR FUTURE RESEARCH.....	174
APPEDICES .....	183
APPENDIX A: RAW TEST DATA.....	184
A.1 COLLECTED TEST DATA.....	184

## LIST OF TABLES

Table 2-1	Total air content in percent by volume .....	11
Table 2-2	B3 Method Material Parameters .....	34
Table 2-3	Values of $Q(t,t')$ .....	36
Table 2-4	Mixture Proportions from Raghavan et al. (2003).....	39
Table 2-5	Mixture proportions used by Seng and Shima (2005) .....	42
Table 2-6	Mixture proportions used by Collepardi et al. (2005).....	45
Table 2-7	Creep strains published by Collepardi et al. (2005) at 180 days .....	46
Table 3-1	Specimen type and quantity for each mixture.....	52
Table 3-2	Experimental mixing plan.....	53
Table 3-3	Mixture proportions .....	55
Table 3-4	Appropriate VSI values.....	64
Table 3-5	Chemical composition of the powdered materials.....	86
Table 3-6	Gradation for the No. 78 crushed limestone .....	89
Table 3-7	Gradation for the fine aggregate .....	89
Table 4-1	Summary of the fresh properties for all mixtures .....	91
Table 4-2	Compressive strength values for all mixtures and loading ages .....	96



Table 4-3	365-day creep and drying shrinkage strains for all loading ages and mixtures.....	102
Table 4-4	365-day measured compliance values for all loading ages of every mixture .....	106
Table 4-5	Maximum positive and negative percent errors in applied load .....	123
Table 4-6	Chloride ion penetrability based on charge passed.....	124
Table 4-7	Average 91-day total charge measured and resulting penetrability .....	124
Table 5-1	Error calculation results for the non-accelerated-cured specimens for all mixtures.....	136
Table 5-2	Error calculation results for the accelerated-cured specimens for all mixtures.....	137
Table 5-3	Parameters used in the Modified CEB 90 method.....	161
Table 5-4	Error calculations for the non-accelerated-cured specimens .....	163
Table 5-5	Error calculations of the accelerated-cured specimens.....	163
Table A-6-1	Raw collected data for the 18-hour loading age of the control mixture .	185
Table A-6-2	Raw collected data for the 2-day loading age of the control mixture.....	186
Table A-6-3	Raw collected data for the 7-day loading age of the control mixture.....	187
Table A-6-4	Raw collected data for the 28-day loading age of the control mixture...	188
Table A-6-5	Raw collected data for the 90-day loading age of the control mixture...	189
Table A-6-6	Raw collected data for the 18-hour loading age of the MS-FA mixture	190
Table A-6-7	Raw collected data for the 2-day loading age of the MS-FA mixture ....	191
Table A-6-8	Raw collected data for the 7-day loading age of the MS-FA mixture ....	192
Table A-6-9	Raw collected data for the 28-day loading age of the MS-FA mixture ..	193

Table A-6-10	Raw collected data for the 90-day loading age of the MS-FA mixture ..	194
Table A-6-11	Raw collected data for the 18-hour loading age of the HS-FA mixture .	195
Table A-6-12	Raw collected data for the 2-day loading age of the HS-FA mixture.....	196
Table A-6-13	Raw collected data for the 7-day loading age of the HS-FA mixture.....	197
Table A-6-14	Raw collected data for the 28-day loading age of the HS-FA mixture...	198
Table A-6-15	Raw collected data for the 90-day loading age of the HS-FA mixture...	199
Table A-6-16	Raw collected data for the 18-hour loading age of the MS-SL mixture .	200
Table A-6-17	Raw collected data for the 2-day loading age of the MS-SL mixture ....	201
Table A-6-18	Raw collected data for the 7-day loading age of the MS-SL mixture ....	202
Table A-6-19	Raw collected data for the 28-day loading age of the MS-SL mixture ..	203
Table A-6-20	Raw collected data for the 90-day loading age of the MS-SL mixture ..	204
Table A-6-21	Raw collected data for the 18-hour loading age of the HS-SL mixture..	205
Table A-6-22	Raw collected data for the 2-day loading age of the HS-SL mixture .....	206
Table A-6-23	Raw collected data for the 7-day loading age of the HS-SL mixture .....	207
Table A-6-24	Raw collected data for the 28-day loading age of the HS-SL mixture ...	208
Table A-6-25	Raw collected data for the 90-day loading age of the HS-SL mixture ...	209

## LIST OF FIGURES

Figure 2-1	Influence of w/c ratio and aggregate content on shrinkage .....	16
Figure 2-2	Creep of concrete under simultaneous loading and drying.....	20
Figure 2-3	Effect of aggregate type on creep .....	22
Figure 2-4	Creep strain measured by Raghavan et al. (2003) .....	40
Figure 2-5	Testing apparatus used by Seng and Shima (2005) .....	43
Figure 2-6	Creep results found in Seng and Shima (2005) study compared with predicted strains .....	44
Figure 3-1	Outline of experimental work .....	49
Figure 3-2	Specimen identification system .....	56
Figure 3-3	The 12-ft <sup>3</sup> mixer used for mixing operations .....	59
Figure 3-4	Equipment used to conduct the slump flow test .....	62
Figure 3-5	Schematic of slump flow apparatus .....	63
Figure 3-6	Match-curing mold used in this study.....	66
Figure 3-7	Schematic of match-curing system .....	67
Figure 3-8	A 6 in. x 12 in. concrete cylinder inside a match-curing sleeve .....	69

Figure 3-9	Temperature profile used by the match-curing system with typical measured temperatures.....	70
Figure 3-10	The Forney compression testing machine used for this study .....	71
Figure 3-11	Concrete cylinder fitted with DEMEC points.....	73
Figure 3-12	DEMEC gauge used for all strain measurements .....	73
Figure 3-13	Elevation views of creep frame.....	75
Figure 3-14	Plan views of reaction plates used in creep frame .....	76
Figure 3-15	Example of creep frame used during this research project .....	77
Figure 3-16	The layout of the environmentally-controlled creep testing room.....	81
Figure 4-1	Slump flow values for each batch of every SCC mixture.....	93
Figure 4-2	T-50 values for each batch of all SCC mixtures .....	94
Figure 4-3	Air content of every batch for all SCC mixtures .....	95
Figure 4-4	18-hr compressive strengths for all SCC mixtures .....	97
Figure 4-5	Change in compressive strength of each mixture with time .....	97
Figure 4-6	Compressive strength of all SCC mixtures compared to the conventional-slump mixture at all ages .....	100
Figure 4-7	Creep strain development for the conventional-slump mixture.....	103
Figure 4-8	Creep strain development for SCC-MS-FA.....	104
Figure 4-9	Creep strain development for SCC-HS-FA .....	104
Figure 4-10	Creep strain development for SCC-MS-SL .....	105
Figure 4-11	Creep strain development for SCC-HS-SL.....	105
Figure 4-12	18-hr compliance for all mixtures.....	107
Figure 4-13	2-day compliance for all mixtures .....	108

Figure 4-14	7-day compliance for all mixtures .....	108
Figure 4-15	28-day compliance for all mixtures .....	109
Figure 4-16	90-day compliance for all mixtures .....	109
Figure 4-17	365-day compliance values for all SCC mixtures and the conventional- slump mixture .....	112
Figure 4-18	Drying shrinkage strain development for the conventional-slump mixture .....	113
Figure 4-19	Drying shrinkage strain development for the SCC-MS-FA mixture .....	114
Figure 4-20	Drying shrinkage strain development for the SCC-HS-FA mixture.....	114
Figure 4-21	Drying shrinkage strain curve for the SCC-MS-SL mixture .....	115
Figure 4-22	Drying shrinkage strain curve for the SCC-HS-SL mixture.....	115
Figure 4-23	18-hr drying shrinkage strains for all SCC mixtures .....	116
Figure 4-24	2-day drying shrinkage strains for all SCC mixtures.....	117
Figure 4-25	7-day drying shrinkage strains for all SCC mixtures.....	117
Figure 4-26	28-day drying shrinkage strains for all SCC mixtures.....	118
Figure 4-27	90-day drying shrinkage strains for all SCC mixtures.....	118
Figure 4-28	365-day drying shrinkage strains for all SCC mixtures and the conventional-slump mixture .....	120
Figure 4-29	The applied load on the 18-hour specimen of the control mixture .....	122
Figure 5-1	Measured versus estimated creep strain for the conventional-slump mixture using the ACI 209 procedure.....	140
Figure 5-2	Measured versus estimated creep strain for the MS-FA mixture using the ACI 209 procedure.....	141

Figure 5-3	Measured versus estimated creep strain for the HS-FA mixture using the ACI 209 procedure.....	141
Figure 5-4	Measured versus estimated creep strain for the MS-SL mixture using the ACI 209 procedure.....	142
Figure 5-5	Measured versus estimated creep strain for the HS-SL mixture using the ACI 209 procedure.....	142
Figure 5-6	Measured versus estimated creep strain for the conventional-slump mixture using the AASHTO 2007 procedure .....	145
Figure 5-7	Measured versus estimated creep strain for the MS-FA mixture using the AASHTO 2007 procedure .....	146
Figure 5-8	Measured versus estimated creep strain for the HS-FA mixture using the AASHTO 2007 procedure .....	146
Figure 5-9	Measured versus estimated creep strain for the MS-SL mixture using the AASHTO 2007 procedure .....	147
Figure 5-10	Measured versus estimated creep strain for the HS-SL mixture using the AASHTO 2007 procedure .....	147
Figure 5-11	Measured versus estimated creep strain for the conventional-slump mixture using the CEB 90 procedure.....	150
Figure 5-12	Measured versus estimated creep strain for the MS-FA mixture using the CEB 90 procedure.....	150
Figure 5-13	Measured versus estimated creep strain for the HS-FA mixture using the CEB 90 procedure.....	151

Figure 5-14	Measured versus estimated creep strain for the MS-SL mixture using the CEB 90 procedure.....	151
Figure 5-15	Measured versus estimated creep strain for the HS-SL mixture using the CEB 90 procedure.....	152
Figure 5-16	Measured versus estimated creep strain for the conventional-slump mixture using the GL 2000 procedure .....	154
Figure 5-17	Measured versus estimated creep strain for the MS-FA mixture using the GL 2000 procedure .....	154
Figure 5-18	Measured versus estimated creep strain for the HS-FA mixture using the GL 2000 procedure .....	155
Figure 5-19	Measured versus estimated creep strain for the MS-SL mixture using the GL 2000 procedure .....	155
Figure 5-20	Measured versus estimated creep strain for the HS-SL mixture using the GL 2000 procedure .....	156
Figure 5-21	Measured versus estimated creep strain for the conventional-slump mixture using the B3 procedure.....	158
Figure 5-22	Measured versus estimated creep strain for the MS-FA mixture using the B3 procedure.....	158
Figure 5-23	Measured versus estimated creep strain for the HS-FA mixture using the B3 procedure.....	159
Figure 5-24	Measured versus estimated creep strain for the MS-SL mixture using the B3 procedure.....	159

Figure 5-25	Measured versus estimated creep strain for the HS-SL mixture using the B3 procedure.....	160
Figure 5-26	Measured versus estimated creep strain for the conventional-slump mixture using the Modified CEB 90 method.....	165
Figure 5-27	Measured versus estimated creep strain for the MS-FA mixture using the Modified CEB 90 method.....	165
Figure 5-28	Measured versus estimated creep strain for the HS-FA mixture using the Modified CEB 90 method.....	166
Figure 5-29	Measured versus estimated creep strain for the MS-SL mixture using the Modified CEB 90 method.....	166
Figure 5-30	Measured versus estimated creep strain for the HS-SL mixture using the Modified CEB 90 method.....	167



# **CHAPTER 1**

## **INTRODUCTION**

### **1.1 BACKGROUND**

Concrete is a material used in construction applications throughout the world. When properly placed and cured, it exhibits excellent compressive-force-resisting characteristics and engineers rely on it to perform in a myriad of situations; however, if proper consolidation is not provided, its strength and durability could be questionable. To help alleviate these concerns and provide a more uniform, well consolidated end product on a consistent basis, Japanese researchers in the early 1980's created a concrete mixture that deformed under its own weight, thus filling around and encapsulating reinforcing steel (Okamura and Ouchi 1999).

The Japanese researchers at Kochi University were led by Hajime Okamura and acted to lessen the strain in Japan brought on by the shortage of skilled labor (Okamura and Ouchi 1999). Okamura's creation was termed self-consolidating concrete (SCC) and exhibited high flowability without experiencing the segregation issues found in conventional-slump concrete mixtures (Khayat 1999). To achieve these properties, SCC relies on a higher fine aggregate content than conventional-slump concrete, along with a smaller-sized coarse aggregate. Additionally, large doses of high-range water-reducing (HRWR) admixtures must be employed in conjunction with increased volumes of

powdered materials. The inclusion of the proper quantities of these materials allows SCC to achieve high flowability while maintaining cohesiveness (Khayat, Hu, and Monty 1999).

The ability of SCC to act in the manner described above makes the material especially attractive to the precast, prestressed concrete industry, which traditionally constructs narrow members that are highly congested. However, the industry has been slow to adopt this high-performance concrete because many governing agencies and specification-writing bodies have been slow to provide guidelines for its use. Additionally, because of the limited use of SCC in this application, there is a lack of long-term performance data available for evaluation. Groups like the Precast/Prestressed Concrete Institute (PCI) and the National Cooperative Highway Research Program (NCHRP) have, or are currently working to provide, such guidelines in an effort to make SCC more accessible. Additionally, many state departments of transportation are interested in implementing SCC for the construction of prestressed concrete girders.

This fact is true in the state of Alabama, where the Alabama Department of Transportation (ALDOT) is actively researching the implementation of SCC for use in prestressed bridge girder applications. Prior use has been restricted due to a lack of standardization of testing and placement techniques; however, recent American Society for Testing and Materials (ASTM) guidelines have been created to address these issues, and similar specifications are being produced to further fulfill these needs. This fact, coupled with the data produced through additional research efforts, is helping to increase the acceptance and routine use of SCC.

## 1.2 RESEARCH OBJECTIVES

This research effort is part of a larger research project sponsored by the Alabama Department of Transportation (ALDOT) and is aimed at furthering the knowledge of the behavior of SCC designed for use in prestressed bridge girder applications. Previous phases of this effort have covered the development and testing of 21 SCC mixtures and two conventional-slump mixtures with varying water-to-cementitious materials ratios ( $w/cm$ ) and sand-aggregate ( $s/agg$ ) ratios. Thorough testing and evaluation has reduced the number of suitable concrete mixtures down to four SCC mixtures and one conventional-slump mixture.

This thesis outlines the testing and analysis of the creep behavior of these final five mixtures to provide better understanding of the creep response of SCC. In order to accomplish this objective, five levels of concrete maturity, or loading ages, were chosen to provide a full picture of the behavior of each mixture. The primary objectives associated with this study include

- Compare the creep exhibited by SCC to that of conventional-slump concrete typically used in prestressed applications,
- Compare the creep exhibited by SCC mixtures consisting of a cement replacement of Class C Fly Ash with that of SCC mixtures having a cement replacement of Ground-Granulated Blast-Furnace (GGBF) Slag,
- Evaluate the effect of the water-to-cementitious materials ratio ( $w/cm$ ), and thus concrete strength, on the amount of creep experienced, and

- Compare the creep of the SCC mixtures to the estimated values produced by the following creep prediction methods:
  - ACI 209 (ACI Committee 209 1997)
  - AASHTO (2007)
  - CEB 90 (CEB 1990)
  - GL 2000 (Gardner and Lockman 2001), and
  - B3 (Bazant and Baweja 2000).

### **1.3 RESEARCH SCOPE**

As stated in Section 1.2, this study was conducted to determine the creep performance of four SCC mixtures and one conventional-slump mixture. Each of the four SCC mixtures utilized supplementary cementing materials (SCMs) and can be grouped into two categories. The first category is comprised of two SCC mixtures (one moderate-strength and one high-strength) which utilized a cement replacement of Class C Fly Ash. The second is also comprised of a moderate- and high-strength mixture; however, this category used a cement replacement of Ground Granulated Blast-Furnace (GGBF) Slag. The cementitious material portion of the conventional-slump mixture was comprised entirely of Type III portland cement, which was the cement type used in all five mixtures.

It was determined that the researchers conducting investigation needed to address the manner in which each of the SCC mixtures behaved relative to the conventional-slump mixture and the manner in which SCC mixtures of various strength levels creep. To accommodate these objectives, researchers involved in the study looked at each mixture at five loading ages, which included: 18 hours, 2 days, 7 days, 28 days, and 90 days. All

specimens were non-accelerated-cured for 7 days, or until it was time for the application of load, whichever came first. The only exception to this was made with regard to the 18-hour specimens. They were match-cured at controlled, elevated temperatures in a similar fashion to the method used by the prestressing industry in the Southeastern United States.

Once the appropriate curing regime had completed, the specimens were loaded to 40 percent of the ultimate strength that was determined immediately prior to load application. Strain readings were then taken at specific intervals for a duration of 365 days, and the data were analyzed to determine the creep behavior for each loading age of each mixture. Once these data were available, a comparison was made to compare the creep behavior of each SCC mixture relative to the conventional-slump mixture and to the other SCC mixtures of similar strengths. Additionally, the data gathered were compared to the estimated values produced using the following five creep prediction methods: ACI 209, AASHTO 2007, CEB 90, GL 2000, and B3.

#### **1.4 ORGANIZATION OF THESIS**

A critical review of relevant literature is presented in Chapter 2 of this report. This chapter includes sections on: an introduction to SCC along with a discussion of components of SCC, volumetric changes in concrete, creep prediction methods, and previous studies of creep associated with SCC.

The experimental plan utilized during the course of the research effort is outlined in Chapter 3, which includes information regarding the preparation and curing of specimens, along with a description of the type and quantities of materials used. Additionally, the test setup used for this study is presented in this chapter. This

description includes detailed information on the dimensions and materials used to construct the creep frames, and also includes a description of the climate-controlled room constructed to contain them.

The data that were gathered over the course of this project and the subsequent analysis of the data is provided in Chapter 4. Here the creep response generated from the gathered data is presented, along with the conclusions that were formed from the data.

A description of the data with regards to the five creep prediction methods that were chosen for evaluation is given in Chapter 5. In addition, the accuracy of each method is reported with regards to estimating the creep values of SCC. Further conclusions are also presented here on the performance of each method.

General conclusions and recommendations are provided in Chapter 6, along with a summary of the laboratory work performed during this study.

## **CHAPTER 2**

### **LITERATURE REVIEW**

#### **2.1 INTRODUCTION**

Self-Consolidating Concrete (SCC) owes its origins to a skilled labor shortage in early 1980's Japan. This deficiency led to a decrease in the durability of the structures being built throughout the country and was the subject of much concern (Okamura and Ouchi 1999). In 1988, a professor at the University of Tokyo, Dr. Hajime Okamura, developed a solution for this problem by creating a type of concrete that would deform under its own weight, eliminating the need for the application of external vibration to insure a durable and aesthetically pleasing concrete structure (Okamura and Ouchi 1999). SCC's deformability brought with it additional benefits that greatly improved all construction processes involving its use. Most notable are reductions in both the overall construction time and in the noise commonly associated with the vibratory consolidation of reinforced concrete (Khayat and Daczko 2003).

While deformability is the most prominent difference between SCC and conventional concrete, several other requirements must be met to truly classify the material as self-consolidating. In fact, a report co-authored by Khayat and Daczko (2003) states that four such requirements must be met:

- 1) High deformability or ability to flow around reinforcement and into crevices without the use of external vibration.
- 2) The deformability must be retainable throughout the duration of transport and placement.
- 3) The mixture must be highly stable and resistant to segregation throughout its entire fresh life cycle.
- 4) The bleeding of free water should be minimized.

Meeting these goals often proves difficult, and compromises must be made during the design of each mixture to ensure the proper fresh and hardened properties for each job are obtained (Khayat and Daczko 2003). In fact, the concessions made during this process illustrate yet another facet of the difference between a conventional and self-consolidating mixture.

## **2.2 COMPONENTS OF SCC**

In order to meet the requirements listed above, the designer of an SCC mixture needs to decide on a strategy to properly proportion the constituents. Domone (2000) says these mixture attributes may be attained by: limiting coarse aggregate volumes, lowering water-powder ratios, and using a superplasticizer.

Limiting the coarse aggregate content helps to reduce the internal particle friction within a mixture. Thus, the mixture is able to flow around obstacles and through reinforcing steel (Domone 2000; Khayat et al. 1999). Additionally, when the coarse aggregate content is limited, a subsequent increase in paste volume results. This increase magnifies the mixture's flowing ability and allows it to flow around reinforcing steel and



into crevices without producing blockages (Domone 2000). As a result, a more durable end product is produced, which is one of the main reasons for choosing to use SCC.

While fluidity and filling ability are integral to the success of any SCC mixture, these two characteristics can be detrimental if not handled correctly. Providing fluidity through an increase in water content can lead to segregation issues and a reduction in desirable hardened properties (Tangtermsirikul and Khayat 2000). To prevent this from happening, it is important to use a low water-powder ratio, which translates into less free water and a consequent reduction of bleeding. These characteristics in turn, will lead to higher static and dynamic stability of the mixture, allowing it to be transported and placed without concern (Assaad et al. 2004).

While a reduction in the water-powder ratio is good for mixture stability, it also leads to a reduction in workability, and precautions must be taken to provide a good finished product. The use of a superplasticizer, also known as high-range water reducer (HRWR), a chemical admixture aimed at increasing flowability without reducing stability, helps to alleviate this concern. HRWRs work to disperse the fine particles in a mixture, providing fluidity without the use of additional water (Tangtermsirikul and Khayat 2000). This dispersion proves to be especially advantageous because water alone will not provide the particle distance needed for proper friction reduction, and as previously stated, excess water can lead to segregation and bleeding issues (Tangtermsirikul and Khayat 2000).

### **2.2.1 SCC CONSTITUENT MATERIALS**

While the basic structure of an SCC mixture is discussed above, it should be noted that each mixture can be tailored to fit the needs of most any job. This means that various

additional materials may be added to the design to fulfill job-specific requirements such as: environmental concerns, availability of supplementary cementing materials (SCMs), use of local materials, and increased viscosity requirements. The following sections outline the constituent materials used for this research project in order to achieve the desired fresh and hardened properties.

#### **2.2.1.1 Type III Cement**

The five types of portland cement ASTM C 150 (2006) recognizes are designated Type I through Type V, each varying in fineness and composition. Type III cement has high early-strength characteristics and is thus conducive for use in the precast, prestressed concrete industry. These high early-strengths are primarily due to the high fineness of the material. This means a large amount of surface area comes into contact with water, producing rapid hydration (Mindess et al. 2003).

#### **2.2.1.2 Air-entraining Admixtures**

Like conventional concrete mixtures, SCC is susceptible to frost-and-deicing salt-related failure issues and requires an elevated air content for prolonged life spans in ice-prone environments. To ensure proper air content, an air-entraining admixture is often proportioned into the mix design. However, this addition can lead to a reduction in strength and must be accounted for during the mixture design process. Table 2-1, which was taken from the PCI Design Handbook (2004), details the proper air content needed for particular aggregate sizes and environmental conditions. It should be noted that all values in Table 2-1 are permitted to be reduced by 1% for all mixtures having a compressive strength in excess of 5,000 psi (PCI 2004).

**Table 2-1:** Total air content in percent by volume (PCI 2004)

Nominal maximum aggregate size, in.	Total air content, %	
	Severe Exposure	Moderate Exposure
Less than 3/8	9.0%	7.0%
3/8	7.5%	6.9%
1/2	7.0%	5.5%
3/4	6.0%	5.0%
1	6.0%	5.0%
1-1/2	5.5%	4.5%

### 2.2.1.3 Supplementary Cementing Materials (SCMs)

Type III portland cement is among the most expensive cementitious materials currently used in concrete production, requiring large amounts of energy and raw materials to produce. When one considers that an increased volume of cementitious materials is required as the mixture's aggregate content decreases, it becomes clear that a cheaper cementitious material would greatly reduce the cost associated with SCC production (Khayat 1999). Moreover, as the cement level rises, an increase in mixture temperature follows, leading to undesirable effects.

To combat these factors and still raise the level of cementitious materials, SCMs are used, most commonly: fly ash, ground-granulated blast-furnace (GGBF) slag, and limestone filler. Each helps to enhance flowability while providing cohesiveness to the mixture (Khayat 1999). Two of the more commonly used SCMs are fly ash and GGBF slag. These two materials bring additional benefits because they are waste materials from other industrial processes. They allow the SCC designer to lower production costs while reducing SCC's impact on the environment.

Fly ash is “the inorganic, noncombustible residue of powdered coal after burning in power plants” and is the most widely used SCM (Mindess et al. 2003). It can be classified into two classes: Class C and Class F, the latter of which is mainly considered to be a pozzolanic material.

Concrete made with class C fly ash exhibits more rapid strength-gaining characteristics than that made with Class F fly ash and is better suited for applications associated with precast, prestressed concrete construction. It is produced during the combustion of lignitic coals, which are predominately found in the western portions of the U.S., while Class F fly ash is found in the eastern portion of the U.S. and is formed when bituminous and sub-bituminous coals are burnt (Mindess et al. 2003).

GGBF slag is defined as “the nonmetallic product, consisting essentially of silicates and aluminosilicates of calcium and of other bases that is developed in a molten condition simultaneously with iron in a blast furnace” (ACI Committee 116 2000). It is not considered a pozzolanic material. Rather, it is a cementitious material comprised of the same oxides that make up portland cement, e.g. lime, silica, and alumina, with the difference being exhibited in the proportions of the constituents (Neville 1996). The inclusion of GGBF slag into a mixture will provide greater workability and improved durability over a mixture without GGBF slag, while reducing dependence on costly portland cement (ACI Committee 233 2000; Neville 1996).

While limestone filler was not used during the course of this research project, it should be noted that it is a popular mineral additive throughout the world. Limestone is a hydraulic material that reacts well with portland cement. For this reason, ENV 197-1:1992 permits it for use in concentrations of up to 35 percent, where other fillers are

only allowed in concentrations of 5 percent (Neville 1996). Using this material helps to increase workability while providing cohesiveness and preventing bleeding (Khayat 1999).

#### **2.2.1.4 Viscosity Modifying Admixtures**

Viscosity modifying admixtures (VMA) work to improve static and dynamic stability within a SCC mixture. Static stability is the resistance of a mixture to bleeding and segregating once cast into place, while dynamic stability is the mixture's resistance to segregation and blocking while being transported and placed (Assaad et al. 2004). It should also be noted that VMA in small dosages works to improve robustness in SCC mixtures thus decreasing sensitivity to changes in material properties and environmental conditions (Khayat 1999).

Khayat (1999) states that “mixtures containing VMA exhibit shear-thinning, a behavior whereby the apparent viscosity decreases with the increase in shear rate.” This decrease allows the mixture to deform during placement and then to regain viscosity after placement, when the shear rate diminishes. Having these attributes allows a mixture greater workability while reducing segregation, bleeding, and surface settlement after being cast (Khayat 1999).

### **2.3 VOLUMETRIC CHANGE**

Volume changes in concrete specimens are an intrinsic characteristic of the material itself and can be attributed to several different mechanisms occurring simultaneously within the specimen of interest. While the processes ultimately leading to volumetric change are complex, it is widely accepted that three main components comprise the vast majority of

volumetric change: drying shrinkage, autogeneous shrinkage, and basic creep (Bazant 2001).

It is easy to imagine that each of the mechanisms listed above occurs for different reasons. In fact, they each owe their existence to various combinations of mixture proportions, environmental conditions, geometric properties, and stress conditions. This section, which is organized according to the three volumetric change components, details these factors.

### **2.3.1 DRYING SHRINKAGE**

Neville (1996) defines drying shrinkage as a decrease in specimen volume due to the “withdrawal of water from concrete.” It is important to take this into account when designing a mixture because it can lead to “cracking or warping of elements of the structure due to restraints present during shrinkage” (Mindess et al. 2003).

According to Bazant (2001), drying shrinkage occurs due to three mechanisms acting simultaneously within the hardened specimen: capillary tension, solid surface tension, and a withdrawal of absorbed water. From a design standpoint these three mechanisms can be minimized through limiting the total water content and paste volume, where paste volume is the “binder (cement and fillers), the water, the air, and the fine particles of sand” (Chopin et al. 2003).

An increase in total water content results in a higher water-cement ratio ( $w/c$ ) and greater workability of a mixture. However, this will lead to more evaporable water in a mixture and thus lead to higher shrinkage strains (Neville 1996). In fact, research has shown shrinkage to be directly proportional to the  $w/c$  when it falls between 0.2 and 0.6,

while higher  $w/c$  show no appreciable shrinkage as the additional water is removed (Neville 1996).

To further clarify the importance paste volume plays in drying shrinkage, additional explanation is required. To this end, consider the following: as the cement content of a mixture is increased while holding the  $w/c$  constant, a subsequent increase in shrinkage occurs (Neville 1996). This can be attributed to the increased volume of hydrated cement paste, which can be as much as ten times more deformable than the aggregate constituent of a mixture (Chopin et al. 2003). Conversely, if the cement content were increased while holding the water content steady, shrinkage would show no increase because the higher cement content would allow for a stronger paste (Neville 1996). Thus the paste would have a greater ability to resist the forces caused by shrinkage.

As mentioned above, aggregate is stiffer than hydrated cement paste and thus plays a role in the resistance of shrinkage. In fact, Neville (1996) states that aggregate type and stiffness are “the most important influence” with regards to shrinkage resistance. Figure 2-1 illustrates how an increase in total aggregate content works to reduce shrinkage.

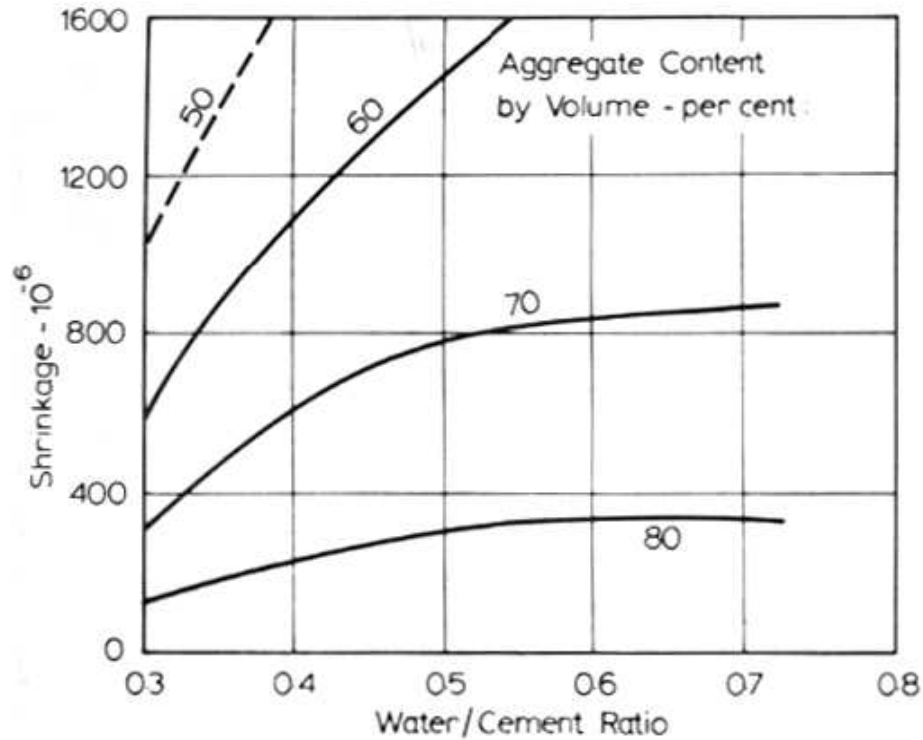


**Figure 2-1:** Influence of w/c ratio and aggregate content on shrinkage (Neville 1996)

It should also be noted that the curing regime used to mature a concrete specimen affects the amount of shrinkage that occurs (Neville 1996). Prolonging moist curing allows a greater amount of cement paste to hydrate prior to drying, thus reducing the concrete specimen's susceptibility to shrinkage (Neville 1996).

When the drying shrinkage of SCC is compared to that of conventional concrete, intuition would suggest that SCC will exhibit higher shrinkage values. This reasoning can be attributed to the higher paste content required by SCC to attain the fluidity necessary to be classified as self-consolidating. Chopin et al. (2003) found shrinkage in SCC to be upwards of 20 percent higher than the shrinkage found in their conventional mixture. It



should also be noted that the conventional concrete mixture used in that research had a high gravel/sand ratio, which will also lead to a large amount of shrinkage.

In contrast to the findings in Chopin et al. (2003), Schindler et al. (2006) found that SCC mixtures exhibited drying shrinkage values on the same order of magnitude as conventional-slump concrete. This held true for all mixtures investigated, even as the sand-aggregate (S/Agg) ratio changed from 0.38 to 0.46. These findings led the researchers in that study to conclude that SCC performs in a manner similar to conventional-slump concrete with regards to drying shrinkage.

### **2.3.2 AUTOGENEOUS SHRINKAGE**

Autogeneous shrinkage is a phenomenon that occurs in concrete in which a decrease in volume takes place without a change in mass or temperature (Lee et al. 2006). It differs from drying shrinkage in that it occurs due to water consumption brought on by the hydration process. As the hydration process continues in a hardened concrete specimen, self-desiccation occurs, consuming available water and causing a subsequent decrease in volume (Pierard et al. 2005).

Autogeneous shrinkage increases as the  $w/c$  decreases, but can vary according to the type of cementitious material present (Pierard et al. 2005). Portland cement gains strength rapidly as compared to other cementitious materials, due in part to its high speed of hydration, which is a function of the material's fineness. Consequently, the majority of autogeneous shrinkage associated with portland cement is complete within the first three days (Pierard et al. 2005). Ground granulated blast-furnace (GGBF) slag exhibits a much more retarded development of autogeneous shrinkage. In fact, it is not uncommon to see

swelling of a specimen over the first few days, followed by a decrease in volume as the specimen continues to age (Pierard et al. 2005). Mixtures utilizing this cementitious material tend to undergo the majority of their shrinkage at later ages.

Knowing that autogenous shrinkage is directly related to cement content and thus paste content, it can be easily seen that an increase in paste volume may result in an increase in this type of shrinkage. That being said, it should also be easy to see that SCC mixtures are especially susceptible to autogenous shrinkage due to their dependence on high paste content for fluidity.

### **2.3.3 CREEP**

D'Ambrosia et al. (2005) define creep as “the time-dependent viscoelastic response to stress generated from externally applied loads”. Its importance in the design of precast, prestressed concrete structures is paramount, as creep results in partial loss of prestress force, which can be detrimental to a structure’s functionality if the loss is underestimated. It is a complex phenomenon dependent on many of the factors that influence shrinkage and some additional parameters.

Creep and shrinkage act together to account for the total time-dependent increase in strain occurring in loaded concrete specimens (Neville 1996; Mindess et al. 2003). This is evident considering most concrete is drying under load and increases in creep strain have been measured under such conditions (Mindess et al. 2003). To this end, terminology has been developed to take this into account. For instance, total time-dependent volumetric change can be broken down into three categories: free shrinkage, basic creep, and drying creep (Neville 1996; Mindess et al. 2003).

Free shrinkage, also known as drying shrinkage, was discussed in detail in Section 2.3.1. Basic creep is the time-dependent increase in strain due to the applied load without drying. However, the sum of these two fails to account for the total time-dependent deformation a loaded concrete specimen undergoes. To account for this, a drying creep term is introduced (Mindess et al. 2003). Figure 2-2 clearly illustrates how the sum of the three components combines to account for the total deformation. In this figure, the following notation is used:  $\epsilon_{sh}$  = drying shrinkage strain,  $\epsilon_{bc}$  = basic creep strain,  $\epsilon_{dc}$  = drying creep strain,  $\epsilon_{CT}$  = total creep strain,  $\epsilon_{tot}$  = total strain.

It should also be noted that in spite of the validity of the mechanisms discussed above, common practice does not account for the individual effects (Mindess et al. 2003). The reasoning behind this spawns from a proliferation of available data which considers creep and shrinkage additive (Neville 1996).

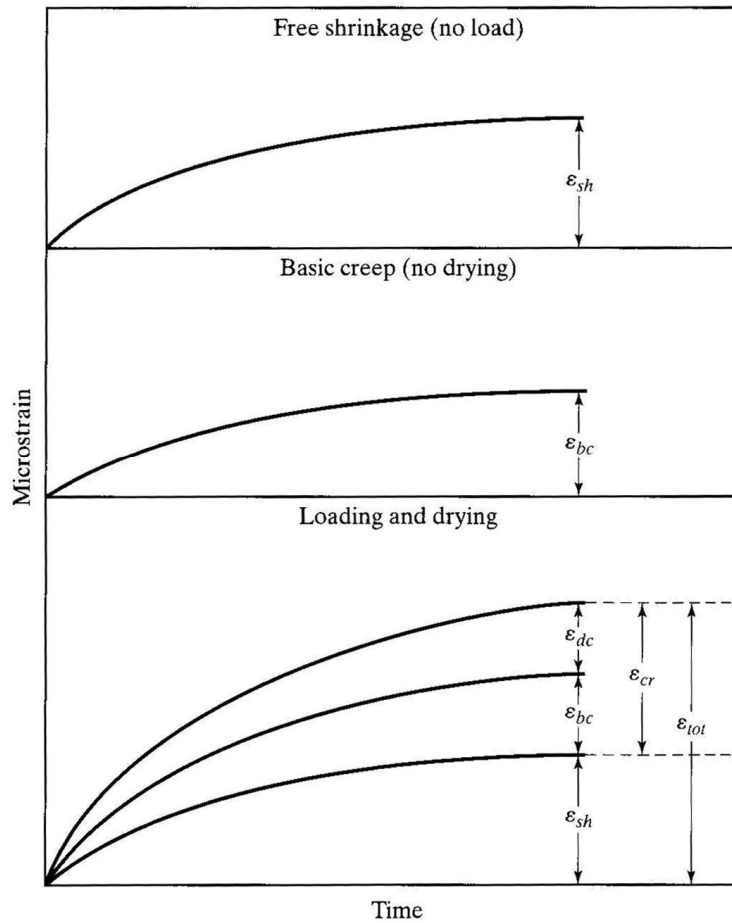


**Figure 2-2:** Creep of concrete under simultaneous loading and drying

(Mindess et al. 2003)

### 2.3.3.1 The Creep Mechanism

As mention in Section 2.3.3, creep is a complex phenomenon, which is likely not fully understood. However, the most widely accepted view involves shearing forces acting on individual particles causing them to slip past each other (Mindess et al. 2003). The amount of slip is highly dependent on the attractive forces binding the particles together. For instance, if the particles are chemically bonded, no slip will be able to occur. However, if the particles are held together by van der Waals' forces, slip is possible.

Bound water within the concrete works to weaken the bond between particles, allowing slip to occur (Mindess et al. 2003).

While particle slip is a widely accepted mechanism of creep, it is not the only way creep can occur. According to Mindess et al. (2003) the application of external force works to push bound water out of micropores within the hardened paste structure. The water is moved from micropores to capillary pores where the stress levels are much lower. As this occurs, the concrete specimen undergoes a noticeable change in volume (Mindess et al. 2003).

Some of the water being moved is able to work its way to the surface and evaporate, which is a form of drying creep. However, since the total amount of water being redistributed is a small portion of the total bound water, this movement can occur with no external loss of water. Therefore, creep can occur in fully saturated specimens, which is referred to as basic creep (Mindess et al. 2003).

### **2.3.3.2 Variables Affecting Creep**

Due to the overwhelmingly complex nature of creep itself, many factors influence the total amount of creep a specimen experiences. According to Neville (1996) it is the hydrated cement paste which actually experiences creep, while the aggregate structure serves to restrain or prevent creep from happening. Therefore, the most important factors affecting the amount of creep are the stiffness of the chosen aggregate and its content within the mixture (Neville 1996 Mindess et al. 2003). Figure 2-3 illustrates how different aggregate types affect total creep. In this figure, it can be seen that sandstone

allows the most creep of the four aggregate types. Then, moving down the right vertical axis, gravel, granite, and limestone each exhibit decreasing amounts of creep.

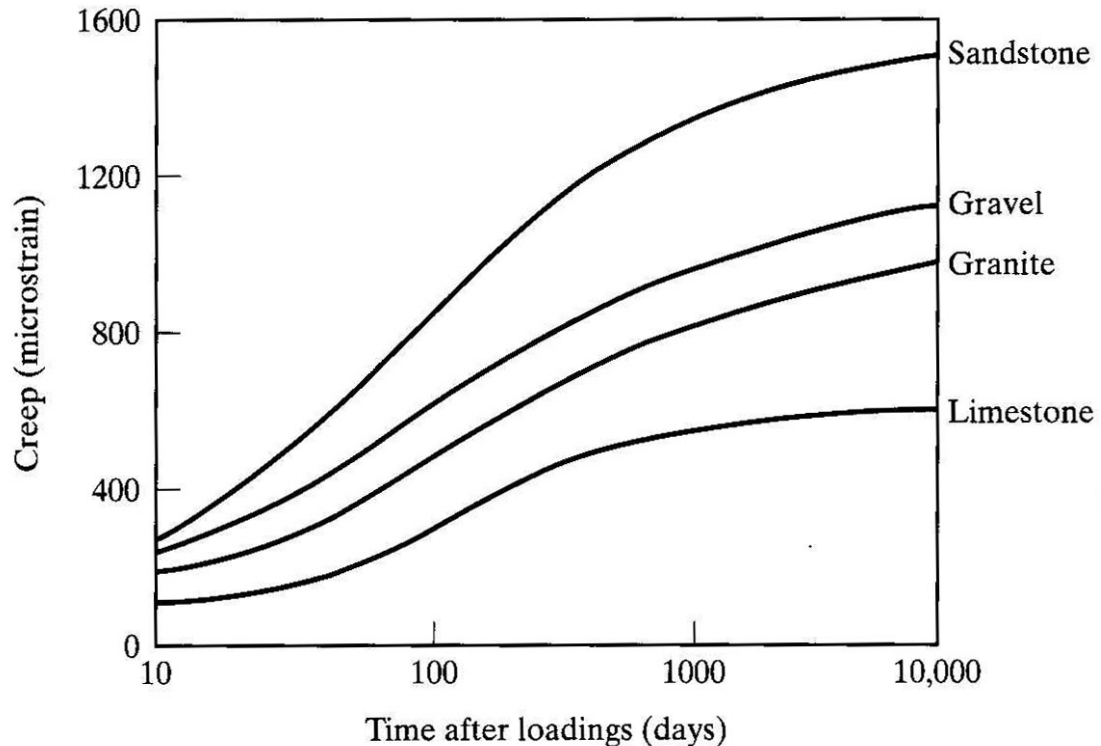


**Figure 2-3:** Effect of aggregate type on creep (Mindess et al. 2003)

While aggregate is the most important factor affecting creep, total paste content is also of large concern. As previously stated, the paste portion of the mixture is what actually experiences creep. Therefore, the higher the paste content, the higher the creep; however, this is by no means a linear relationship (Neville 1996).

In a similar fashion, creep is dependent on the  $w/c$  of a concrete mixture. As the  $w/c$  increases, an associated increase in creep will occur. This is due in part to an increase in bound water, which can be displaced as described in Section 2.3.3.1, causing a volumetric change in the concrete specimen. A change in  $w/c$  could also signify a change

in cement content, which will affect strength and thus the amount of creep (Mindess et al. 2003). If the cement content were to increase, then the strength would increase. This would lead to less creep because the higher strength concrete would be better able to resist the creep forces (Mindess et al. 2003).

Concrete strength is directly related to total creep in that the higher the compressive strength of a mixture, the lower the measured deformation. Curing conditions play a large role in maturing concrete, and proper curing increases the compressive strength to levels better suited for resisting creep. The longer a specimen is allowed to cure, the more hydrated cement exists, and the higher the compressive strength (Mindess et al. 2003). This makes it extremely important to properly cure specimens in order to reduce creep.

Other factors that influence concrete strength consequently play a role in the amount of creep observed. For instance, the composition of the chosen cement can play a large role. Type I cement gains strength slower than Type III cement and consequently experiences more creep at early ages (Mindess et al. 2003). Likewise, the use of chemical admixtures such as superplasticizers can increase creep. However, it should be noted that strength gains achieved by the low  $w/c$  ratios resulting from superplasticizers can offset the undesirable effects of increased creep (Neville 1996; Mindess et al. 2003).

Ambient conditions such as elevated temperature and low relative humidity will also increase creep. While experiencing elevated temperature, a specimen will undergo an increased rate of creep; however, the net result should be less overall creep due to the increased concrete maturity brought on by the elevated temperatures (Mindess et al. 2003). A reduction in relative humidity works to increase drying creep as more internal moisture is pulled away from the specimen (Neville 1996; Mindess et al. 2003).

Another large contributing influence on creep is the applied stress level within the specimen of interest. It is widely accepted that the amount of creep witnessed is approximately proportional to the applied stress (Neville 1996; Mindess et al. 2003). However, this is only true for stress levels below 40% to 60% of the strength at loading (Neville 1996). Above these stress levels, microcracking begins to occur and the stress-strain relationship becomes increasingly nonlinear.

## **2.4 CREEP PREDICTION METHODS**

The following sections outline the procedures for five commonly used creep prediction methods and provide the reader with a terse explanation of how each works.

### **2.4.1 ACI 209 CREEP PREDICTION METHOD**

The creep prediction method set forth by ACI Committee 209 (1997) uses an ultimate creep coefficient that may be adjusted to account for various environmental conditions and mixture-specific properties. In addition to the ultimate creep coefficient, this method uses a time-rate function to account for the growth in creep over time (ACI Committee 209 1997).

The ultimate creep coefficient, which is defined as the ratio of creep strain to initial strain resulting from the application of load, is determined using the following equation:

$$v_u = 2.35(\gamma_{la} \times \gamma_{\lambda} \times \gamma_{vs} \times \gamma_{\psi} \times \gamma_s \times \gamma_a)$$

where,

$v_u$  = ultimate creep coefficient



with,

$\gamma_{la}$  being the loading age correction factor:

$$\gamma_{la} = 1.25(t_{la})^{-0.118} \text{ (for non-accelerated-cured concrete)}$$

$$\gamma_{la} = 1.13(t_{la})^{-0.094} \text{ (for steam-cured concrete)}$$

where,

$t_{la}$  = loading age (days), only to be used for ages later than  
7 days for non-accelerated-cured concrete and later than  
1-3 days for steam-cured concrete.

$\gamma_{\lambda}$  being the relative humidity correction factor:

$$\gamma_{\lambda} = 1.27 - 0.0067 \times RH \text{ (for } RH > 40\%)$$

where,

$RH$  = relative humidity (%)

$\gamma_{vs}$  being the volume-to-surface area ratio correction factor:

$$\gamma_{vs} = (2/3) \times [1 + 1.13 \times \exp(-0.54(v/s))]$$

where,

$v/s$  = volume-to-surface area ratio (in.)

$\gamma_{\psi}$  being the fine aggregate percentage correction factor:

$$\gamma_{\psi} = 0.88 + 0.0024\Psi$$

where,

$\Psi$  = ratio of fine to total aggregate by weight (%)

$\gamma_s$  being the slump correction factor:

$$\gamma_s = 0.82 + 0.067s$$

where,

$s$  = observed slump (in.)

$\gamma_a$  being the air content correction factor:

$$\gamma_a = 0.46 + 0.09a \geq 1.0$$

where,

$a$  = air content (%)

To determine the predicted creep coefficient for each time step of interest, the ultimate creep coefficient,  $v_u$ , must be multiplied by  $v_t$ , which is the parameter that accounts for the concrete age:

$$v_u(t) = v_u \times v_t$$

with,

$$v_t = \frac{t^{0.6}}{10 + t^{0.6}}$$

where,

$t$  = length of time after loading (days)

It is important to note that the above equation is applicable to loading ages later than 7 days and 1-3 days for non-accelerated-cured and steam-cured samples, respectively.

With  $v_u(t)$  determined, the estimated creep can be calculated by multiplying  $v_u(t)$  by the elastic strain resulting from loading as follows:

$$\text{predicted creep}(t) = v_u(t) \times (\text{elastic strain resulting from loading}).$$

#### 2.4.2 AASHTO 2007 CREEP PREDICTION METHOD

The AASHTO 2007 method is much like the ACI 209 method previously discussed, in that it too uses an ultimate creep coefficient. It is based on the results of the research described in NCHRP Report 496 (2003), which was sponsored by the National Cooperative Highway Research Program (NCHRP). This report was created in an effort to develop guidelines for predicting prestress loss in high-strength concrete girders. AASHTO 2007 allows the user to take into account factors such as the relative humidity surrounding the specimen of interest, the volume-to-surface area ratio, concrete strength, and the development of strength with time (AASHTO 2007).

To determine the creep coefficient the following equation is given, along with several modifiers to account for various environmental and mixture specific factors:

$$\psi(t, t_i) = 1.9 \times k_s \times k_{hc} \times k_f \times k_{td} \times t_i^{-0.118}$$

where,

$k_s$  being the factor accounting for the effect of the volume-to-surface area ratio component:

$$k_s = 1.45 - 0.13(v/s) \geq 1.0$$

$k_{hc}$  being the humidity factor for creep:

$$k_{hc} = 1.56 - 0.008H$$

where,

$$H = \text{relative humidity (\%)}$$

$k_f$  being the factor for the effect of concrete strength:

$$k_f = \frac{5}{1 + f'_{ci}}$$

where,

$f'_{ci}$  = compressive strength of concrete at 28 days (ksi)

$k_{td}$  being the time development factor:

$$k_{td} = \frac{t}{61 - 4f'_{ci} + t}$$

where,

$t$  = age of concrete (days), defined as age of concrete between time of loading for creep calculations and time being considered for analysis of creep effects

$t_i$  = age of concrete when load is initially applied for accelerated curing (days), minus 6 days for moist-curing. For moist-curing, when age of concrete is less than 7 days,  $t_i$  = age of concrete (days) divided by 7.

Once the creep coefficient is calculated for each time step of interest, it is multiplied by the elastic strain resulting from loading to determine the predicted creep, as follows:

$$\text{predicted creep}(t, t_i) = \psi(t, t_i) \times (\text{elastic strain resulting from loading}).$$

#### **2.4.3 CEB 90 CREEP PREDICTION METHOD**

The CEB 90 method is the current creep model endorsed by the European design code, CEB-FIP Model Code 1990, and is applicable for use with concrete mixtures subjected to normal conditions (Al-Manaseer and Lam 2005). That is to say, it is applicable to concrete mixtures not subjected to extremely high temperatures or low relative humidities, and normal weight mixtures. Moreover, this method contains provisions allowing for the cement type, curing temperature, and high stress levels to be taken into account (CEB 1990; Muller and Hillsdorf 1990).

The procedure for obtaining the estimated creep from this model is similar in nature to that used in the ACI 209 method. A creep coefficient is determined based on each mixture's fresh and hardened properties and the environmental conditions to which the concrete is exposed.

$$\Phi(t, t_0) = \Phi_0 \times \beta_c(t - t_0)$$

where,

$\Phi(t, t_0)$  = creep coefficient

$\Phi_0$  = notational creep coefficient

$\beta_c(t - t_0)$  = coefficient describing the development of creep with time after loading

$t$  = age of concrete at the moment considered (days)

$t_0$  = age of concrete at time of loading (days)

The notational creep coefficient,  $\Phi_0$ , is dependent on the compressive strength of the concrete and the relative humidity of its surroundings.

$$\Phi_0 = \Phi_{RH} \times \beta(f_{cm}) \times \beta(t_0)$$

where,

$$\Phi_{RH} = 1 + \frac{1 - RH / RH_0}{0.46(h / h_0)^{1/3}}$$

$$\beta(f_{cm}) = \frac{5.3}{(f_{cm} / f_{cm0})^{0.5}}$$

$$\beta(t_0) = \frac{1}{0.1 + (t_0 / t_1)^{0.2}}$$

where,

$$h = 2A_c/u \text{ (mm)}$$

$$f_{cm} = \text{mean compressive strength of concrete at 28 days (MPa)}$$

$$f_{cmo} = 10 \text{ MPa}$$

$$RH = \text{relative humidity of the ambient environment (\%)}$$

$$RH_0 = 100\%$$

$$A_c = \text{cross-sectional area (mm}^2\text{)}$$

$$u = \text{perimeter of the member in contact with the atmosphere (mm)}$$

$$h_0 = 100 \text{ mm}$$

$$t_1 = 1 \text{ day}$$

The manner in which the creep develops with time is accounted for in the following equation:

$$\beta_c(t-t_0) = \left[ \frac{(t-t_0)/t_1}{\beta_H + (t-t_0)/t_1} \right]^{0.3}$$

where,

$$\beta_H = 150 \left\{ 1 + \left( 1.2 \frac{RH}{RH_0} \right)^{18} \right\} \frac{h}{h_0} + 250 \leq 1500$$

After the creep coefficient has been calculated, it can be multiplied by the elastic strain resulting from the applied load to determine the estimated creep at each time step, as follows:

$$\text{predicted creep}(t, t_0) = \Phi(t, t_0) \times (\text{elastic strain resulting from loading}).$$

For the purposes of this research, an elevated-temperature curing cycle was used. The CEB 90 method allows for this to be taken into account by using a maturity approach. The age of the concrete in days was adjusted to account for the elevated temperatures which each sample experienced during curing. The following equation allowed for the adjusted time to be determined:

$$t_T = \sum_{i=1}^n \Delta t_i \exp \left[ 13.65 - \frac{4000}{273 + \{T(\Delta t_i)/T_o\}} \right]$$

where,

$t_T$  = temperature-adjusted concrete age, which replaces  $t$  in the corresponding equations (days)

$\Delta t_i$  = increment of days where  $T$  prevails

$T(\Delta t_i)$  = the temperature (°C) during the time period  $\Delta t_i$

$T_o$  = 1° C

#### **2.4.4 GL 2000 CREEP PREDICTION METHOD**

The GL 2000 method, published by Gardner and Lockman in 2001, is a modified version of the GZ model proposed by Gardner and Zhao in 1993, and again in 1997 (Al-Manaseer and Lam 2005). It allows for the prediction of creep associated with all types of concrete mixtures, regardless of the inclusion of chemical admixtures or SCMs, and is non-dependent on casting temperature and method of curing. Furthermore, this method takes into account several important factors related to concrete quality and performance, including 28-day specified concrete strength, strength at loading, element size, and relative humidity. This method is based on strength development with time, and the

relationship between modulus of elasticity and strength, and includes equations to predict creep and shrinkage (Gardner and Lockman 2001).

To calculate the predicted creep, termed here “specific creep”, this method uses the following relationship between the creep coefficient and the modulus of elasticity at 28 days. Since  $\Phi_{28}$  varies with time, the far right side of the equation was included to more accurately describe what is meant by the creep coefficient and the modulus of elasticity at 28 days.

$$\text{specific creep } (t, t_0) = \frac{\Phi_{28}}{E_{cm28}} = \frac{\Phi(t, t_0)}{E_{cm}(28 \text{ days})} \quad (1/\text{ksi})$$

where,

$E_{cm28}$  = modulus of elasticity at 28 days (ksi)

$\Phi_{28}$  = creep coefficient

$\Phi(t, t_0)$  = creep coefficient at any time  $t$  (days) and for any loading age  $t_0$  (days)

$E_{cm}(28 \text{ days})$  = modulus of elasticity at 28 days (ksi)

Using the specific creep coefficient calculated for each time step of interest, the compliance for the same time step can be calculated with the following equation:

$$\text{compliance } J(t, t_0) = \frac{1}{E_{cm}(t_0)} + \text{specific creep } (t, t_0) \quad (1/\text{ksi})$$

where,

$E_{cm}(t_0)$  = modulus of elasticity at time of loading (ksi)



The equation for the creep coefficient,  $\Phi(t, t_0)$ , is shown below. It is followed by the same equation, but in expanded form, which shows all the variables on which  $\Phi_{28}$  is dependent. The reader should note one correction in the expanded equation. The coefficient, 77, on the far right side has been changed from its original value of 97, based upon correspondence with Dr. John Gardner. This coefficient was found by Dr. Gardner to be in error in the original publication.

$$\Phi(t, t_0) = \Phi(t_c) \left[ 2 \left( \frac{(t-t_0)^{0.3}}{(t-t_0)^{0.3} + 14} \right) + \left( \frac{7}{t_0} \right)^{0.5} \left( \frac{t-t_0}{t-t_0+7} \right)^{0.5} + 2.5(1-1.086h^2) \left( \frac{t-t_0}{t-t_0+77 \cdot (v/s)^2} \right)^{0.5} \right]$$

where,

$h$  = relative humidity expressed as a decimal

$t$  = age of concrete (days)

$t_0$  = age at loading (days)

If  $t_0 = t_c$ , then  $\Phi(t_c) = 1$ ,

When  $t_0 > t_c$

$$\Phi(t_c) = \left[ 1 - \left( \frac{t_0 - t_c}{t_0 - t_c + 77 \cdot (v/s)^2} \right)^{0.5} \right]^{0.5}$$

where,

$t_c$  = age drying commenced (days)

The previously mentioned  $\Phi(t_c)$  is used in this method to take drying before loading into account, and it serves to reduce both the basic creep and drying creep values (Gardner and Lockman 2001). Again, the reader should note one correction. Like the  $\Phi(t, t_0)$

equation above, the coefficient, 77, has been changed from the original value of 97, based upon correspondence with Dr. John Gardner. It too was found in error by Dr. Gardner and was thus changed.

#### 2.4.5 B3 CREEP PREDICTION METHOD

The B3 creep prediction method, the latest version in a series of creep prediction models, was developed by Dr. Bazant in 2000. It is a mathematically complex model aimed at providing the most accurate creep estimations for use in the design structures sensitive to creep strains. Intended to be an improvement on the ACI 209 model, it was designed for use with portland cement concrete mixtures with parameters that range within the boundaries listed in Table 2-2 (Bazant and Baweja 2000).

**Table 2-2: B3 Method Material Parameters (Bazant and Baweja 2000)**

<b>Parameter</b>	<b>Range</b>
Water-to-Cement Ratio	$0.35 \leq w/c \leq 0.85$
Aggregate-to-Cement Ratio	$2.5 \leq a/c \leq 13.5$
Compressive Strength	$2500 \text{ psi} \leq f'_c \leq 10,000 \text{ psi}$
Cement Content	$270 \text{ pcy} \leq c \leq 1215 \text{ pcy}$
Service Stress	up to $0.45f'_c$

In addition, the method is applicable for mixtures cured for at least one day and can be applied to any portland cement mixture provided calibration tests are conducted (Bazant and Baweja 2000).

This method is based on complex mathematical equations intended to accurately predict the intricate nature of creep behavior. A creep compliance function is employed that takes into account instantaneous strain due to a unit stress, creep at constant moisture

content with no moisture migration throughout the specimen, and creep due to drying (Bazant and Baweja 2000). The following equation shows the compliance function which brings the various components together to describe creep behavior:

$$J(t, t') = q_1 + C_0(t, t') + C_d(t, t', t_0) \quad (1 \times 10^{-6} \text{ psi})$$

where,

$$q_1 = \text{instantaneous strain due to unit stress } (1 \times 10^{-6} / \text{psi})$$

$$C_0(t, t') = \text{compliance function describing basic creep } (1 \times 10^{-6} / \text{psi})$$

$$C_d(t, t', t_0) = \text{compliance function describing simultaneous drying} \\ (1 \times 10^{-6} / \text{psi})$$

$$t = \text{time step of interest (days)}$$

$$t' = \text{loading age (days)}$$

$$t_0 = \text{age when drying commenced (days)}$$

The basic creep component of the creep compliance equation is a time-rate function that can be tailored according to mixture-specific properties. The equation below details this computation:

$$C_0(t, t') = q_2 Q(t, t') + q_3 \ln[1 + (t - t')^n] + q_4 \ln\left(\frac{t}{t'}\right) \quad (1 \times 10^{-6} / \text{psi})$$

where,

$$q_2 = 451.1 \sqrt{c} f'_c{}^{-0.9} \quad (1 \times 10^{-6} / \text{psi})$$

$$Q(t, t') = \text{coefficient given in Table 2-3 (unitless)}$$

$$q_3 = 0.29(w/c)^4 q_2 \quad (1 \times 10^{-6} / \text{psi})$$

$$q_4 = 0.14(a/c)^{-0.7} \text{ (1x10}^{-6}\text{/psi)}$$

$$n = 0.1 \text{ (unitless)}$$

$$a = \text{aggregate content (lb/ft}^3\text{)}$$

$$c = \text{cement content (lb/ft}^3\text{)}$$

$$w = \text{water content (lb/ft}^3\text{)}$$

**Table 2-3: Values of  $Q(t,t')$  (Bazant and Baweja 2000)**

log(t-t')	log t'								
	0.0	0.5	1.0	1.5	2.0	2.5	3.0	3.5	4.0
-2.0	0.4890	0.2750	0.1547	0.08677	0.04892	0.02751	0.01547	0.008699	0.004892
-1.5	0.5347	0.3009	0.1693	0.09519	0.05353	0.03010	0.01693	0.009519	0.005353
-1.0	0.5586	0.3284	0.1848	0.10400	0.05846	0.03288	0.01849	0.01040	0.005846
-0.5	0.6309	0.3571	0.2013	0.11330	0.06372	0.03583	0.02015	0.01133	0.006372
0.0	0.6754	0.3860	0.2185	0.21310	0.06929	0.03897	0.02192	0.01233	0.006931
0.5	0.7108	0.4125	0.2357	0.13340	0.07516	0.04229	0.02379	0.01338	0.007524
1.0	0.7352	0.4335	0.5140	0.14360	0.08123	0.04578	0.02576	0.01449	0.008149
1.5	0.7505	0.4480	0.2638	0.15290	0.08727	0.04397	0.02782	0.01566	0.008806
2.0	0.7597	0.4570	0.2724	0.16020	0.09276	0.05239	0.02994	0.01687	0.009494
2.5	0.7652	0.4624	0.2777	0.16520	0.09708	0.05616	0.03284	0.01812	0.01021
3.0	0.7684	0.4656	0.2808	0.16830	0.10000	0.05869	0.03393	0.01935	0.01094
3.5	0.7703	0.4675	0.2827	0.17020	0.10180	0.06041	0.03541	0.02045	0.01166
4.0	0.7714	0.4686	0.2838	0.17130	0.10290	0.06147	0.03641	0.02131	0.01230
4.5	0.7720	0.4692	0.2844	0.17190	0.10360	0.06210	0.03702	0.02190	0.01280
5.0	0.7724	0.4696	0.2848	0.17230	0.10380	0.06247	0.03739	0.02225	0.01314

The creep associated with shrinkage and drying is described with the following function, which takes into account the environmental conditions surrounding the specimen:

$$C_d(t, t', t_0) = q_5 [\exp\{-8H(t)\} - \exp\{-8H(t'_0)\}]^{(1/2)} \text{ (1x10}^{-6}\text{/psi)}$$

with,

$$q_5 = 7.57 \times 10^5 f'_c{}^{-1} |\epsilon_{ss}|^{-0.6} \text{ (1x10}^{-6}\text{/psi)}$$

$$H(t) = 1 - (1 - h)S(t) \text{ (unitless)}$$

$t'_0 = \max(t', t_0)$  if  $t \geq t'_0$ , otherwise  $C_d(t, t', t'_0) = 0$ ;  $t'_0$  is the time at

which drying and loading first act simultaneously (days)

where,

$$\varepsilon_{\infty} = -\alpha_1 \alpha_2 \left[ 26\omega^{2.1} f'_c{}^{-0.28} + 270 \right] \quad (1 \times 10^{-6} \text{ in./in.})$$

$h$  = relative humidity (unitless)

$$S(t) = \tanh \sqrt{\frac{t - t_0}{\tau_{sh}}} \quad (\text{unitless})$$

$$\tau_{sh} = k_t (k_s D)^2 \quad (\text{days})$$

$$\alpha_1 \begin{cases} 1.0 & \text{for Type I cement} \\ 0.85 & \text{for Type II cement} \\ 1.1 & \text{for Type III cement} \end{cases} \quad (\text{unitless})$$

$$\alpha_2 \begin{cases} 0.75 & \text{for steam - cured} \\ 1.2 & \text{for sealed or normal curing in air} \\ 1.0 & \text{for curing in water or at 100\% humidity} \end{cases} \quad (\text{unitless})$$

$\omega$  = water content (lb/ft<sup>3</sup>)

$$k_t = 190.8 t_0^{-0.08} f'_c{}^{-1/4} \quad (\text{days / in}^2)$$

$$k_s \begin{cases} 1.00 & \text{for an infinite slab} \\ 1.15 & \text{for an infinite cylinder} \\ 1.25 & \text{for an infinite square prism} \\ 1.30 & \text{for a sphere} \\ 1.55 & \text{for a cube} \end{cases} \quad (\text{unitless})$$

$D$  =  $2V/S$  (in)

$V$  = specimen volume (in<sup>3</sup>)

$S$  = specimen surface area (in<sup>2</sup>)

Once the compliance is calculated, it is possible to determine the associated creep strain by multiplying the compliance value by the stress resulting from loading and subtracting out the initial elastic strain.

$$\text{predicted creep}(t,t') = [J(t,t') \times \sigma(t')] - \varepsilon(t') \text{ (in./in.)}$$

where,

$\sigma(t')$  = stress resulting from loading (psi)

$\varepsilon(t')$  = initial elastic strain (in./in.)

## **2.5 PREVIOUS FINDINGS RELATED TO CREEP OF SCC**

Limited studies have been conducted in recent years to investigate the behavior creep of SCC compared to that of conventional-slump concrete. This section is dedicated to outlining three of these studies, including their experimental procedures and results. A summary is located at the end of this section to serve as an overview of these results.

### **2.5.1 DESCRIPTION OF PREVIOUS STUDIES**

Recent studies in which creep of SCC has been investigated include those conducted by Raghavan et al. (2003) in India, Seng and Shima (2005) at Kochi University of Technology in Japan, and Collepari et al. (2005) at Enco in Ponzano Veneto, Italy. The details of each study will be described in this section, along with the results and conclusions presented by each.

#### **2.5.1.1 Creep Evaluation by Raghavan et al. (2003)**

The study conducted by Raghavan et al. (2003) in India involved a comparison of the mechanical properties of an SCC mixture with those of a conventional concrete mixture.

The mixture proportions chosen for the research project were similar for both mixtures employed. Both contained similar quantities of ordinary portland cement; however, the SCC mixture incorporated the addition of fly ash as a supplementary cementing material. To obtain SCC characteristics, a high-range water reducer (HRWR) was used, along with a viscosity modifying admixture (VMA) for stability. A sulfonated naphthalene formaldehyde (SNF) based admixture was used in the control mixture to achieve the required consistency. The specific mixture proportions can be seen in Table 2-4 below.

**Table 2-4: Mixture Proportions from Raghavan et al. (2003)**

Mixture Constituents	Mixtures	
	SCC	Control
Cement, kg/m <sup>3</sup>	400	450
Fly ash, kg/m <sup>3</sup>	175	----
Sand, kg/m <sup>3</sup>	830	714
Coarse aggregate, k/m <sup>3</sup>	735	1072
Water, kg/m <sup>3</sup>	173	173
HRWR, L/m <sup>3</sup>	2.20	----
SNF, L/m <sup>3</sup>	----	2.50
VMA, L/m <sup>3</sup>	3.00	----

The test specimens used in this project were 150mm x 300mm in size and were cast and stored at 23°C for a period of 24 hours. At the end of the 24-hour period, the specimens were removed from their molds and non-accelerated-cured at 23°C for 7 and 28 days. When the curing period was over, the compressive strength of each mixture was determined and 30% of that load was applied to a representative specimen for testing purposes. Creep strain was then measured using a fender gauge for a period of 90 days

for the 7 day specimens and 70 days for the 28 day specimens. Figure 2-4, which was taken directly from the research report, shows the creep strain measured over the entire testing period. The reader should note that the left vertical axis is creep strain in the units of  $1 \times 10^{-3}$  mm/mm.

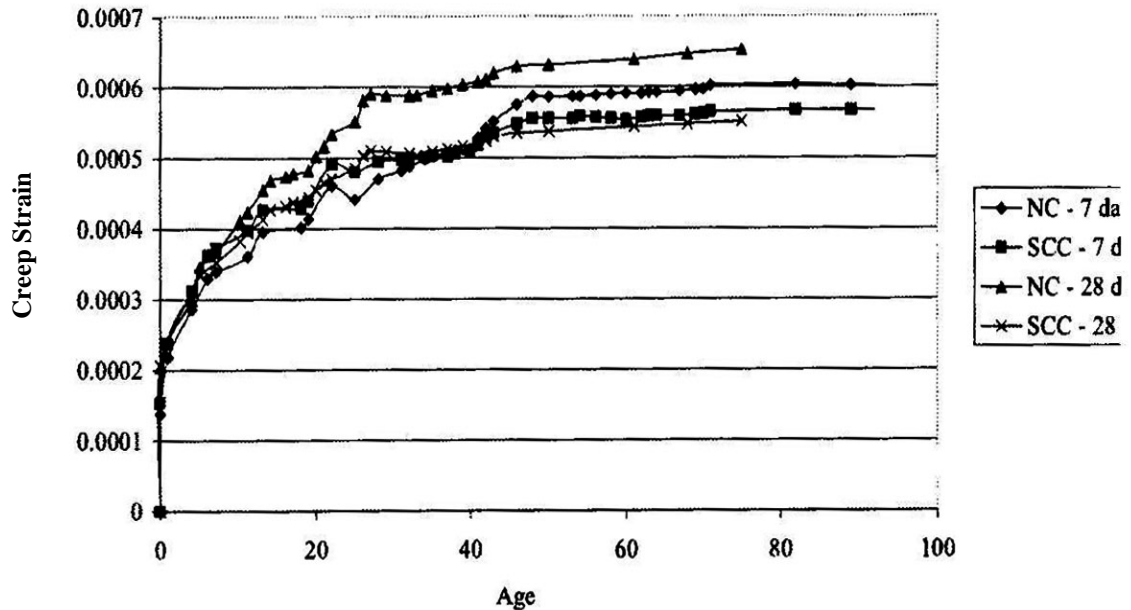


**Figure 2-4:** Creep strain measured by Raghavan et al. (2003)

The results found during this study indicate that the SCC mixture experienced a higher initial elastic deformation than the control mixture; however, the total creep strain measured over the entire testing period was less in the SCC mixture than it was in the control mixture. Additionally, it was concluded in the study that the rate of creep was reduced by 33% for the control mixture and by 50% for the SCC mixture between non-accelerated-cured times of 7 and 28 days.



### **2.5.1.2 Study Conducted by Seng and Shima (2005)**

Seng and Shima (2005) at Kochi University in Japan investigated the creep behavior of SCC compared to that of conventional concrete. To do this, three SCC mixtures were evaluated against a control mixture, which was designed to perform in a conventional manner. Each SCC mixture had varying amounts of constituent materials including ordinary portland cement, crushed stone, sand, and limestone filler. The mixture design process began by creating a conventional mixture having a compressive strength of 55 MPa. The three SCC mixtures were designed by increasing the powder content while using different limestone filler contents, which was done to reduce the coarse aggregate content. SCC characteristics were achieved in the SCC mixtures by using a superplasticizer. The mixture proportions for each of the four mixtures are listed in Table 2-5.

**Table 2-5:** Mixture proportions used by Seng and Shima (2005)

Descriptions		CC		SCC1		SCC2		SCC3	
		Mass	Volume	Mass	Volume	Mass	Volume	Mass	Volume
W/C ratio		0.4	1.27	0.4	1.27	0.35	1.10	0.31	0.97
S/(S+G) ratio (%)		44.05	44.98	49.05	50.00	49.05	50.00	49.05	50.00
LF/(C+LF) ratio (%)		0	0	20.58	23.33	10.29	11.56	0	0
Unit mass (kg/m <sup>3</sup> ) Unit volume (m <sup>3</sup> /m <sup>3</sup> )	W	175	0.175	175	0.175	175	0.175	175	0.175
	C	437.5	0.138	437.5	0.138	500.85	0.159	567	0.180
	LF	0	0	113.4	0.042	56.7	0.021	0	0
	S	777	0.300	777	0.300	777	0.300	777	0.300
	G	987	0.367	807	0.300	807	0.300	807	0.300
	SP	2.174	-	6.303	-	6.969	-	7.645	-
	A	-	0.02	-	0.045	-	0.045	-	0.045
Fresh properties	flow(mm)	Slump = 10.5 cm		675		625		605	
	V-funnel(s)			10.15		11.45		12.48	
	Box(mm)			325		315		305	
Strength	4days(MPa)	38.19		42.75		52.58		61.70	
	28days(MPa)	56.34		65.36		72.55		80.67	

Square specimens 100 x 100 and 600 mm long were cast with a 25 mm hole in the center running the entire length. After 24 hours each specimen was removed from its mold and air-cured at a constant temperature of  $20 \pm 2^\circ\text{C}$  and relative humidity of  $60 \pm 5\%$ . Creep testing began after four days of curing under the conditions specified above by tensioning a 21 mm prestressing bar, which was placed through the center hole of each specimen. The test apparatus can be seen below in Figure 2-5. A load equaling 40% of the compressive strength was applied and maintained within 2% over the duration of the test, which ran for just over 30 days.

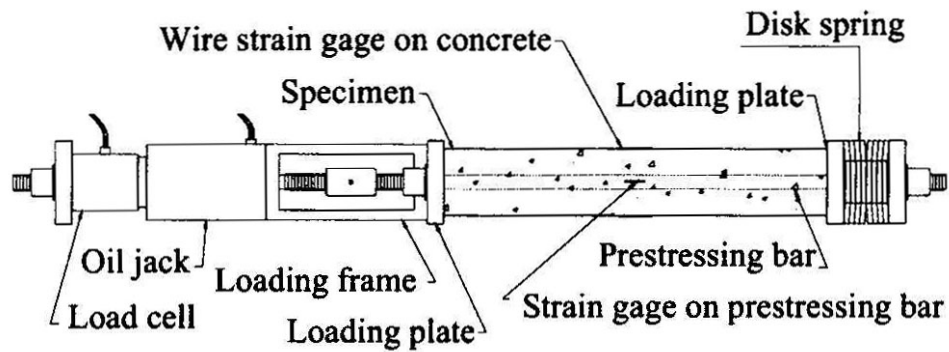


**Figure 2-5:** Testing apparatus used by Seng and Shima (2005)

The researchers concluded that SCC has comparable creep properties to those of conventional concrete. It was determined that the limestone content was directly related to the amount of creep measured; the higher the limestone content, the higher the creep. Additionally, the researchers compared creep coefficients calculated from ACI 209, CEB 90, and JSCE (Japan Society of Civil Engineers) 2002 and found results that varied considerably. They concluded that none of these models work well for predicting creep of SCC mixtures containing high limestone filler contents (Seng and Shima 2005). The graphs depicted in Figure 2-6 illustrate the large disparity between the experimentally-determined values and those found using each model.

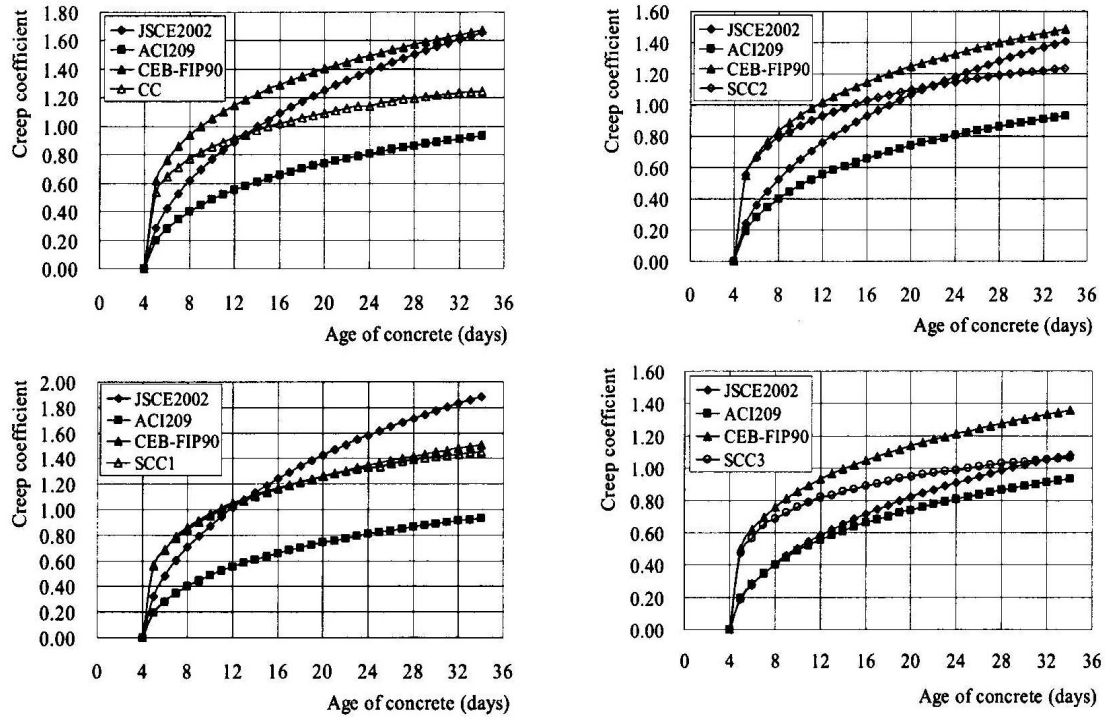


**Figure 2-6:** Creep results found in Seng and Shima (2005) study compared with predicted strains

### 2.5.1.3 Creep Study by Colleparidi et al. (2005)

Colleparidi et al. (2005) used three mixtures (two SCC mixtures and one conventional-slump mixture) to evaluate the creep performance of SCC versus conventional concrete. A similar amount of cement was used for each mixture; however, additional mineral additives were used in the SCC mixtures. Limestone filler was used in one SCC mixtures, and fly ash was used as the supplementary cementing material (SCM) in the other SCC mixture. Superplasticizers were used in the SCC mixtures along with viscosity modifying admixtures to achieve SCC characteristics. All the constituent materials and their proportions are given in Table 2-6, which was taken directly from the research report.

**Table 2-6:** Mixture proportions used by Collepari et al. (2005)

Ingredients/Properties		MIX		
		OFC	L/SCC	F/SCC
CEM I 52.5R (kg/m <sup>3</sup> )		400	400	400
Filler (kg/m <sup>3</sup> )		----	Limestone 160	Fly Ash 135
Aggregate	Sand (0-4 mm) kg/m <sup>3</sup>	760	785	785
	Gravel (4-20 mm) kg/m <sup>3</sup>	1040	845	845
Water (kg/m <sup>3</sup> )		180	180	180
Superplasticizer* (kg/m <sup>3</sup> )		2,4	4,5	5,2
VMA** (% cem)		----	0,25	0,20
water/cement ratio		0,45	0,45	0,45 (0,34)****
aggregate/cement ratio		4,5	4,1 (4,5)***	4,1 (3,1)****
Slump (mm)		180	----	----
Slump flow (mm)		----	750	740

\* Polycarboxylate-based superplasticizer

\*\* VMA = Viscosity Modifying Agent

\*\*\* Within brackets the values with limestone as aggregate

\*\*\*\*Within brackets the values with fly ash as cementitious material

Cubic specimens were cast and then cured at 20°C for 7 days, at which time they were tested in air having a relative humidity of 65%. For testing purposes, the specimens were loaded to 25% of their respective compressive strengths and creep strains were measured from 7 to 180 days. Table 2-7 shows the creep strains measured for each mixture at 180 days. In this table the variables are defined as follows:  $\epsilon_E$  = elastic strain,  $\epsilon_S$  = drying shrinkage strain,  $\epsilon_C$  = creep strain, and  $\epsilon_T$  = total measured strain.

**Table 2-7:** Creep strains published by Collepardi et al. (2005) at 180 days

Strain Type	Measured Strain ( $1 \times 10^{-6}$ in./in.)		
	Control	Limestone SCC	Fly Ash SCC
$\epsilon_E$	265	260	270
$\epsilon_S$	470	470	470
$\epsilon_C$	275	270	430
$\epsilon_T$	1010	1000	1170

It was concluded that the SCC mixtures containing limestone filler experienced approximately the same creep that the conventional mixture exhibited; however, the fly ash mixture exhibited more creep than the control mixture. Collepardi et al. (2005) attributes the higher creep of the fly ash mixture to the presence of cenospheres within the fly ash, which were believed to have been deformed when the specimens were loaded.

### **2.5.2 CONCLUSIONS FROM PREVIOUS STUDIES**

The results in Section 2.5.1 clearly show the variability of data resulting from different creep studies. From these results no clear consensus can be reached as to how arbitrary SCC mixtures perform relative to conventional mixtures, except to say they are similar in magnitude. Too many variables are present to draw specific conclusions that can relate to the behavior of all SCC mixtures.

These variables include differences in constituent materials, specimen sizes, loading apparatus, and testing duration. Each of the research projects detailed in the preceding sections consisted of different combinations of the variables listed. It can be assumed that these factors contributed to the difference in results. That being said, some general conclusions may be drawn.

For instance, each group of researchers reported similarities in magnitude with respect to creep in conventional concrete and that found in SCC. It can therefore be concluded that SCC performs similarly to conventional concrete while providing improvements in labor costs and durability. Only further testing under uniform conditions will yield data that can be compared to form universal conclusions.

## **CHAPTER 3**

### **EXPERIMENTAL PLAN**

#### **3.1 INTRODUCTION**

One of the primary objectives of this study was to gain increased knowledge of SCC by studying its creep characteristics in comparison to that of conventional-slump concrete. As stated in Section 1.2, this was accomplished by selecting five concrete mixtures from a list of 21, which were created in an earlier phase of this research effort. This chapter details the procedures used to achieve all of the objectives of this study, including the one listed above. Here the reader will find information regarding the experimental program, mixture proportions, test setup, and raw materials.

#### **3.2 EXPERIMENTAL PROGRAM**

The experimental program used during this study was comprised of two main phases. The first was the specimen preparation phase, which involved all mixing, casting, and curing procedures. The second was the creep testing phase, during which all creep data were collected. As the first phase was completed for a mixture, phase two began. These phases are illustrated in Figure 3-1.



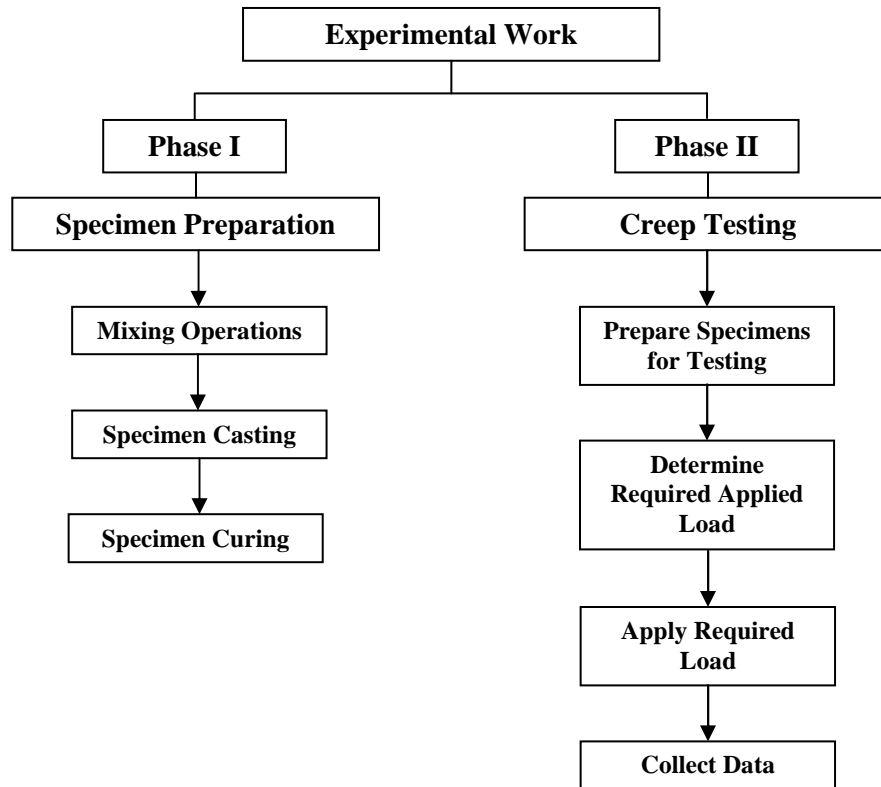


**Figure 3-1:** Outline of experimental work

The slump flow, T-50, visual stability index (VSI), unit weight, temperature, and air content quantities were measured for all SCC mixtures to ensure uniform, high-quality concrete. This was done in conjunction with inspecting the concrete in the mixer during the mixing process to further determine if the concrete would meet all the requirements of SCC.

### **3.2.1 REQUIREMENTS FOR SCC MIXTURES**

The following sections outline the requirements for the fresh and hardened properties for all SCC mixtures. These requirements were chosen in the early stages of the parent project and were agreed upon by all vested parties.

### **3.2.1.1 Fresh Properties**

The slump flow range for this study was specified to be 27 in.  $\pm$  3 in. to allow good filling ability and to take into account variations in materials and weather conditions. The VSI value exhibited by each mixture was required to be below 2.0. At this VSI rating, concrete begins to show signs of segregation as a noticeable layer of mortar is present on the surface of the concrete while in the mixer, and a mortar halo is present around the patty. Additionally, the air content range was chosen to be below 6%. If a mixture did not meet all the specified requirements, it was discarded and remixed. The T-50, temperature, and unit weight measurements were recorded but had no bearing on the approval of each mix.

### **3.2.1.2 Hardened Properties**

The compressive strength at release ( $f'_{ci}$ ) for all SCC mixtures was specified to be between 5,000 and 9,000 psi (34 to 62 MPa) because the average  $f'_{ci}$  value used by the prestressing industry in Alabama is 6,500 psi (45 MPa). A strength in this range was required of all specimens that were cured using elevated temperatures over a duration of 18 hours.

## **3.2.2 SPECIMEN TYPES AND AGES AT LOADING**

In order to gain a more thorough understanding of the nature of the creep behavior exhibited by each mixture, five different levels of maturity, termed “loading ages”, were investigated. These loading ages included: 18 hours, 2 days, 7 days, 28 days, and 90 days. While more information about these loading ages and the characteristics that differentiate them is provided in Section 3.4.4, it should be noted that the 18-hour specimens were put

through an accelerated curing process. The specimens for the other loading ages were simply non-accelerated-cured.

As explained in Section 2.3, multiple mechanisms are responsible for volumetric changes in concrete specimens. However, for the purposes of this research effort, three main components were considered to be the key factors: drying shrinkage, autogenous shrinkage, and creep.

Accurately measuring the creep exhibited by each mixture required that all of these mechanisms be tracked and recorded. To do this, both a creep and a shrinkage specimen were utilized for each mixture at each loading age, and both were cast in the form of 6 in. x 12 in. cylinders. The creep specimens were placed in the creep frame and loaded at a constant stress. They deformed due to elastic response, creep, drying shrinkage, and the effects of autogenous shrinkage. In contrast, the shrinkage specimen had no externally applied load and deformed only due to drying and autogenous shrinkage. Table 3-1 illustrates the number and type of specimens that were mixed for every loading age of every mixture. Two additional things should be noted about this table. The first pertains to the organization of the table, in which the appropriate curing method is noted for each loading age. Secondly, a Strength specimen was a specimen used to determine the ultimate strength of the test specimens immediately prior to load application.

**Table 3-1:** Specimen type and quantity for each mixture

Curing Method	Loading Age	Specimen Type		
		Creep Specimen	Shrinkage Specimen	Strength Specimen
Accelerated	18-hr	2	3	2
Non-accelerated	2-day	2	3	2
	7-day	2	3	2
	28-day	2	*	2
	90-day	2	*	2
<b>Column Totals</b>		10	9	10
<b>Specimen Total</b>		<b>29</b>		

Note: \* Indicates that shrinkage specimens are shared with the 7-day shrinkage specimens

In addition to test specimens, ASTM C 512 requires plugs to be used above and below the creep testing specimens while they are in the creep frames. This helps to ensure an even stress distribution across the actual creep testing specimen. For this study, 25 - 6 in. x 12 in. concrete cylinders (one cylinder for each frame) were cut in half and capped similarly to the test specimens. They were cast using the high-strength slag mixture which was tested during this study and allowed to cure for at least 28 days before being put into service. The choice of the high-strength slag mixture was made because when properly cured, the plugs would have an ultimate strength that exceeded any test specimen.

### 3.3 MIXTURE PROPORTIONS

As mentioned earlier, this study is only a sub-phase of a larger study conducted at Auburn University (Roberts 2005). The project began by designing and studying 21 SCC mixtures in an effort to determine the fresh and hardened properties for each. As the research progressed to later phases, the number of mixtures being studied was reduced as researchers came closer to finding the most suitable mixtures for use by ALDOT. By the time this portion of the study began, only four SCC mixtures remained. Table 3-2, taken from Schindler et al. (2006), illustrates the water-to-cementitious materials ( $w/cm$ ) ratios, sand-to-aggregate ratios, and cementitious material types used in each of the 21 SCC mixes. It should be noted that the mixture identification tags used in Table 3-2 remain in the form used during that research phase.

**Table 3-2:** Experimental mixing plan (Schindler et al. 2006)

Cementitious Material Types	Sand/Aggregate (by volume)	Water-to-Cementitious Materials Ratio			
		0.28	0.32	0.36	0.40
Type III Cement + 30% Class C Fly Ash	0.38	SCC-1	SCC-2	SCC-3	
	0.42	SCC-4	SCC-5	SCC-6	
	0.46	SCC-7	SCC-8	SCC-9	
Type III Cement + x% Grade 120 GGBF Slag	0.42	(30% Slag) SCC-10	(40% Slag) SCC-11	(50% Slag) SCC-12	
	0.46	SCC-13	SCC-14	SCC-15	
Type III Cement + 22% Class C Ash + 8% Silica Fume	0.42		SCC-16	SCC-17	SCC-18
	0.46		SCC-19	SCC-20	SCC-21

Table 3-2 clearly depicts the ratios of each of the constituent materials and shows the various cementitious material combinations used during the early phases of research. For

the current phase of the study, mixtures SCC-7, SCC-9, SCC-13, and SCC-15 were used. SCC-7 and SCC-9, which correspond to SCC-HS-FA and SCC-MS-FA respectively in this thesis, consist of a 30% cement replacement of Class C fly ash and have a sand-to-aggregate ratio of 0.46. However, both mixtures have differing  $w/cm$  of 0.28 and 0.36, respectively. SCC-13 and SCC-15, corresponding to SCC-HS-SL and SCC-MS-SL respectively, consist of differing percentages of a Grade 120 GGBF Slag cement replacement. SCC-13 has a 30% cement replacement, while SCC-15 has a 50% replacement. Both share the same sand-to-aggregate ratio of 0.46; however, like their fly ash counterparts, each has its own  $w/cm$ , which are 0.28 and 0.36, respectively. In addition to the four SCC mixtures, a conventional-slump mixture similar to one found in use by the prestressing industry in the state of Alabama was used as the control for the study.

It should be noted that the  $w/cm$  of the conventional-slump mixture is higher than the  $w/cm$  for both the SCC-MS-SL and SCC-MS-FA mixtures. This was done to provide 18 hour release strengths for the SCC-MS-SL and SCC-MS-FA mixtures that were equivalent in magnitude to that of the conventional-slump mixture.

The proportions for each mixture are listed in Table 3-3. The table includes the proportioning of the water, cementitious materials, aggregates, and chemical admixtures. A full description of each of the raw materials used is given in Section 3.5. One additional note should be made about the mixture constituent materials and proportions. Due to knowledge gained during preliminary mixing, the air-entraining admixture was withheld from the constituent list for the final mixtures, in an effort to provide uniformity, with regard to air content, across all batches of the same mixture.

**Table 3-3: Mixture proportions**

Constituent Materials	Mixtures				
	CTRL	SCC-MS-FA	SCC-HS-FA	SCC-MS-SL	SCC-HS-SL
Water (pcy)	270	270	260	270	260
Cement (pcy)	640	525	650	375	650
Fly Ash (pcy)	----	225	279	----	----
GGBF Slag (pcy)	----	----	----	375	279
Coarse Agg. (pcy)	1,964	1,607	1,529	1,613	1,544
Fine Agg. (pcy)	1,114	1,316	1,252	1,321	1,265
AEA (oz/cwt)	0.33	0.40	0.80	1.50	3.75
Mid-Range WRA (oz/cwt)	4.0	4.0	4.0	6.0	6.0
HRWR Admixture (oz/cwt)	5.0	6.0	6.0	7.0	5.5
VMA (oz/cwt)	0.0	2.0	2.0	2.0	2.0

Note: AEA = Air-Entraining Admixture, WRA = Water-Reducing Admixture, VMA = Viscosity-Modifying Admixture

### 3.4 TEST SPECIMEN IDENTIFICATION SYSTEM

To keep track of each of five mixes, a labeling system had to be developed which would limit data collection errors. Figure 3-2 clearly illustrates this system, which allows the mixture type, strength level, supplemental cementing material (SCM), and loading age all

to be denoted. When this classification system is used for labeling the control mixture (CTRL), the Concrete Strength and SCM portion of the labeling system are not used.

In addition to the labeling system used to identify each mixture and loading age, a system had to be developed to track the data collected for each set of cylinders. As stated earlier, each loading age had three shrinkage cylinders and two creep cylinders, with the exception of the 28- and 90-day loading ages which shared shrinkage cylinders with the 7-day loading age. To track all of these cylinders, they were labeled. The shrinkage cylinders were labeled X, Y, and Z, while the creep cylinders were identified as TOP and BOTTOM based on their alignment in the creep frames. For all of these cylinders, strain readings were taken at three locations around the cylinder perimeter. To limit errors, these three locations were labeled A, B, and C.

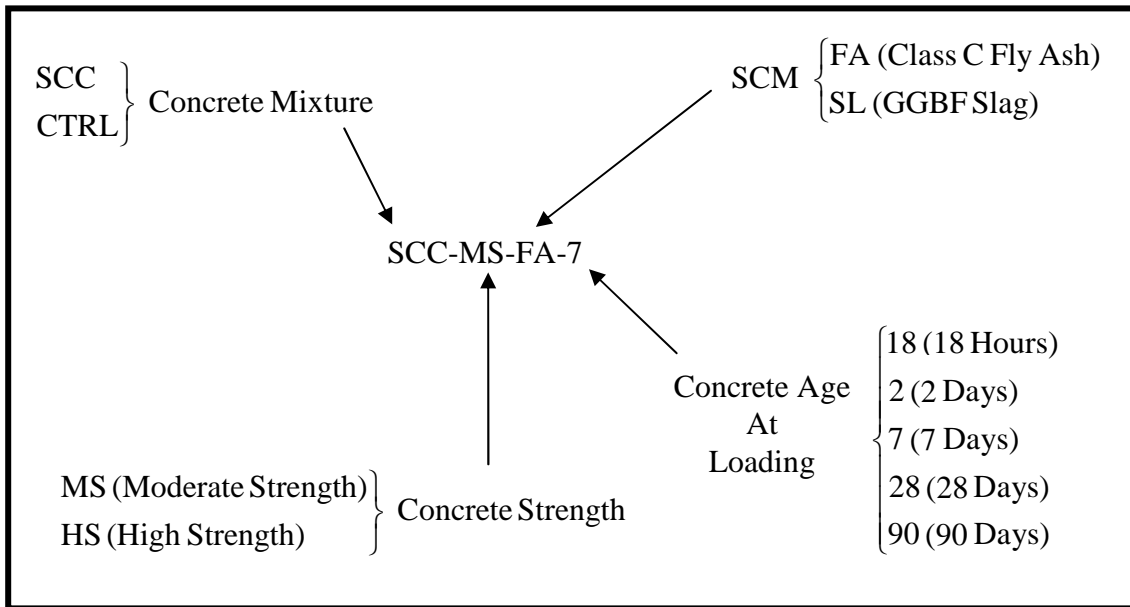


**Figure 3-2:** Specimen identification system



## **3.5 TEST METHODS**

This section outlines the test procedures used to conduct this research project. The information found here includes a description of the batching, mixing, curing, and testing procedures.

### **3.5.1 BATCHING**

In preparation for mixing, all the necessary raw materials for each mixture were gathered in the proper quantities. This section details those actions.

#### **3.5.1.1 Collection of Materials**

Both the fine and coarse aggregates used in each mixture were stockpiled at Twin City Concrete, a ready-mix plant located in Auburn, AL. As these materials were needed, they were gathered in manageable quantities and brought to Auburn University's Structural Research Laboratory and stored in 55-gallon drums, where they remained sealed until needed.

Prior to final batching, all materials were initially batched into five-gallon buckets and were sealed to prevent moisture loss. They remained there until moisture corrections were performed and the correct batch weights were finalized.

#### **3.5.1.2 Moisture Corrections**

Immediately prior to mixing, moisture corrections were performed on the coarse and fine aggregates for each mixture. To do this, all of the five-gallon buckets containing coarse aggregate were mixed together to aid in achieving a more homogeneous moisture distribution. This process was repeated with the fine aggregate. After homogenizing each

aggregate, pans were weighed to determine the mass of each pan. This value was subtracted out later to accurately determine the mass of the moisture each constituent lost.

With the aggregates homogenized and the pan masses determined, samples were taken from each material and weighed to determine the initial mass of each. Having recorded each mass, the pans containing each sample were placed on a hot plate and dried. As the drying progressed, masses were periodically checked until no appreciable decrease was noticed; the mass at this time was then taken to be the dry mass of each aggregate. These values were used to determine the final batch weights of the water, as well as of the fine and coarse aggregate.

### **3.5.2 MIXING PROCEDURES**

After batching the required raw materials, mixing was begun. Several procedures were followed to accomplish the task and to ensure a consistent end product.

#### **3.5.2.1 Buttering the Mixer**

Before the raw materials were placed into the mixer, a buttering mixture was placed into the drum to coat the inside to help prevent clumping of component materials around the mixer's paddles. Each buttering mixture was comprised of two pounds of Type III portland cement and two pounds of fine aggregate. The mixer was then turned on and water was added until the mixture became fluid. The mixer continued to run until every surface inside was coated properly. With this procedure complete, the excess buttering mixture was discarded and the mixing process continued. The 12 ft<sup>3</sup> mixer used in this research project is pictured in Figure 3-3 below.



**Figure 3-3:** The 12-ft<sup>3</sup> mixer used for mixing operations

### **3.5.2.2 Mixing Sequence**

A mixing sequence was utilized when preparing each mixture to help promote procedural consistency. Since this study was part of larger research effort being conducted at Auburn University, it was possible to employ the sequence used in a prior phase of this project. This consistency helped to maintain a certain level of uniformity between all phases of the project. For this reason, the sequence used for this study was identical to that employed in Roberts (2005), which is as follows:

1. Add 80% of mixing water.
2. Add all the coarse and fine aggregates by alternating the five-gallon buckets containing each material.
3. Mix for one minute.
4. While mixing, add any air-entraining admixtures to the aggregates.
5. Stop mixing.
6. Add all powdered materials.
7. Add all remaining mixing water.
8. Cover the opening of the mixer.
9. Mix concrete for five minutes.
10. While mixing, add VMA if necessary.
11. While mixing, add water reducing admixtures if necessary.
12. Stop mixing and allow to rest for three minutes.
13. Run mixer for three minutes.
14. Stop mixer. Test the slump flow, VSI, and T-50. If the slump flow is too low, add more HRWR admixture. Run the mixer for one minute and test again. Continue the process until target slump flow is reached.
15. Once the desired slump flow has been achieved, perform the remaining fresh concrete QC tests: air, temperature, and unit weight.
16. Return all unused concrete to mixer and mix for one minute.
17. Make all specimens for testing hardened properties.

The procedure outlined above was followed for all the mixtures with one exception. When mixtures utilizing Grade 120 GGBF Slag were mixed, the rest time in Step 13 was increased to five minutes. This deviation from standard procedure allowed additional time for the high-range water-reducing (HRWR) admixtures to take effect. It was previously determined that if no increase in rest time was used, a significant reduction in the effect of HRWR admixture would occur.

### **3.5.3 METHODS FOR TESTING FRESH CONCRETE**

In order to determine the quality of each concrete mixture, several quality control tests were performed on the fresh concrete. These tests also allowed for an assessment of the consistency obtained between various batches. This section outlines those tests and describes the processes used to perform them.

#### **3.5.3.1 Slump Flow**

Due to the highly flowable nature of SCC, the traditional slump test is not applicable to SCC mixtures. As an answer to this problem, the slump flow test was created and its procedures are outlined in ASTM C 1611 (2006). This test provides a good indication of a mixture's ability to flow and fill crevices and provides some measure of a mixture's dynamic stability.

To conduct this test, the slump cone was placed in the inverted position and filled in a single lift with no external vibration applied. Then the slump cone was lifted in a smooth manner, allowing the concrete to flow across a smooth, horizontal surface. When the concrete patty came to rest, two orthogonal diameter measurements were made and the average of these two was deemed to be the slump flow of the concrete mixture.

For the purposes of this study, if the slump flow exceeded the maximum acceptable value of 30 in., the batch was discarded, and a new batch was proportioned and mixed. However, if the mixture failed to reach the minimum acceptable slump flow of 24 in., more HRWR was added to the mixture until the slump flow was 27 in.  $\pm$  3 in.. Figure 3-4 depicts the equipment used to conduct the test and Figure 3-5 provides a schematic of the testing apparatus.



**Figure 3-4:** Equipment used to conduct the slump flow test

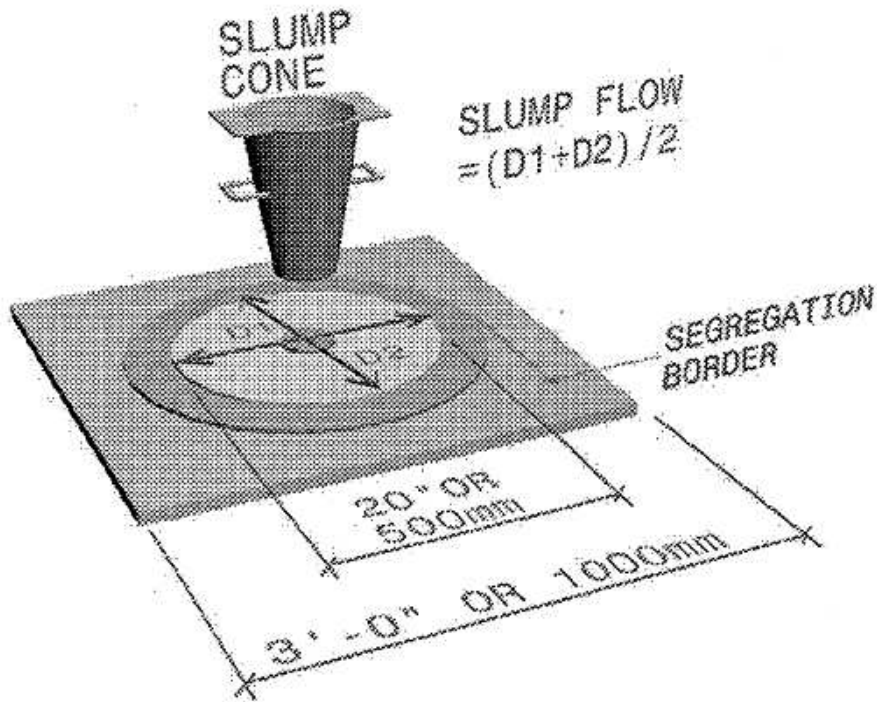


**Figure 3-5:** Schematic of slump flow apparatus (PCI 2003)

### 3.5.3.2 Visual Stability Index (VSI)

The Visual Stability Index (VSI) is a subjective measure of a mixture's dynamic stability. It is determined by visually inspecting and rating the degree of segregation of the fresh concrete patty obtained while performing the slump flow test. Table 3-4 describes VSI values and the criteria for assigning a VSI value to the concrete. This table is found in ASTM C 1611 (2006), the specification outlining the slump flow procedure.

**Table 3-4:** Appropriate VSI values (ASTM C 1611 2006)

VSI Value	Criteria
0 = Highly Stable	No evidence of segregation or bleeding.
1 = Stable	No evidence of segregation and slight bleeding observed as a sheen on the concrete mass.
2 = Unstable	A slight mortar halo $\leq 0.5$ in. ( $\leq 10$ mm) and/or aggregate pile in the of the concrete mass.
3 = Highly Unstable	Clearly segregating by evidence of a large mortar halo $> 0.5$ in. ( $> 10$ mm) and/or a large aggregate pile in the center of the concrete mass.

### 3.5.3.3 T-50

The T-50 is conducted simultaneously with the slump flow. It is measured using a stop watch and begins as the slump flow cone is raised and concrete begins to flow. The stop watch continues running until the concrete flow reaches a diameter of 20 in. This test is aimed at measuring the relative viscosity of a mixture.

### 3.5.3.4 Air Content and Unit Weight

The procedure described in AASHTO T 121 (2003) was used to determine the air content of all mixtures used in this research project, with a few exceptions. The following two modifications were made to this AASHTO specification only when SCC mixtures were being tested:

- The concrete was placed in 3 lifts but without rodding.
- After the placement of each layer, the container was lightly tamped 10 to 12 times around the entire circumference.

Slight tamping was used to expedite the removal of air pockets trapped along the side walls of the container rather than for consolidation purposes.



The range of air content values chosen for this study was 3% to 6%, as specified by ALDOT at the time the first phases of this project started. Mixtures not meeting the requisite air content requirements were discarded and remixed.

### **3.5.3.5 Fresh Concrete Temperature**

Fresh concrete temperatures were taken in accordance with the procedure outlined by AASHTO T 309 (2003) in an effort to record the environmental conditions in which mixing took place.

## **3.5.4 SPECIMEN PREPARATION AND CURING**

This study required the preparation of 29 - 6 in. x 12 in. molds for each mixture to be used for creep testing purposes, as well as 2 - 4 in. x 8 in. match cure molds and 2 - 4 in. x 8 in. cylinder molds. All the specimens mentioned above were prepared in accordance with AASHTO T 126 (2003); however, when SCC mixtures were being cast, a few modifications to the procedures were made. The sections that follow outline the changes made.

### **3.5.4.1 Specimen Preparation**

AASHTO T 126 (2003) specifications were followed precisely except when dealing with SCC mixtures. The following modifications were made:

- All 6 in. x 12 in. cylinder molds were cast using 3 lifts without rodding.
- After each lift was placed, each cylinder was tamped lightly 10 to 12 times to help remove entrapped air pockets along the sides of the cylinder mold.

All 4 in. x 8 in. cylinder and match-cure molds were also cast in accordance with AASHTO T 126 (2003). However, the following modifications had to be made when specimens for SCC mixtures were made:

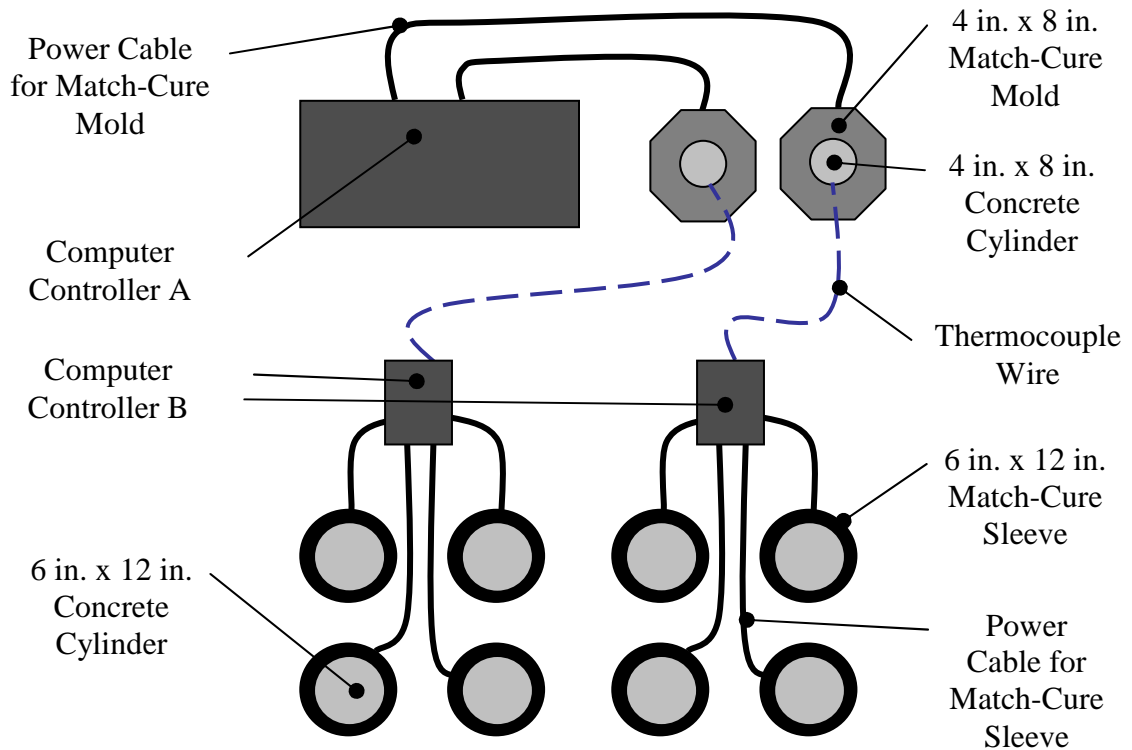
- Each 4 in. x 8 in. cylinder and match-cure mold was placed in 2 lifts without using any rodding.
- After the placement of each lift, the molds were tamped lightly 10 to 12 times to help remove the entrapped air pockets along the sides of each mold.

Figure 3-6 displays an example of one of the 4 in. x 8 in. match-cure molds used during this research project. They were used to allow the 6 in. x 12 in. match-cure system to be slaved to the computer controller, which forced the 18-hour specimens through a predetermined temperature cycle to accelerate the curing process.



**Figure 3-6:** Match-curing mold used in this study

Figure 3-7 illustrates the match-curing system that was used throughout this study. In this schematic the reader should notice Computer Controller A, which controlled the 4 in. x 8 in. match-cure system. This computer controlled the entire system by first forcing the 4 in. x 8 in. match-cure molds through the predetermined, elevated temperature cycle using the power cables at the top of the figure. Computer Controller B, which controlled the 6 in. x 12 in. match-cure system, was then able to duplicate the temperature profile of the 4 in. x 8 in. system because it was connected using thermocouple wires, which were embedded into the 4 in. x 8 in. concrete cylinders. These are the dashed lines in the figure. Computer Controller B then forced its match-curing sleeves through the same temperature profile using its power cables.



**Figure 3-7:** Schematic of match-curing system

### 3.5.4.2 Curing Regimes

This study required two types of curing regimes to be employed. The first involved a traditional moist-curing process which was governed by AASHTO T 126 (2003). The second was a heat-curing process that utilized a match-curing system to force each match-cured specimen through an elevated temperature cycle aimed at accelerating the maturity gain of the concrete.

The specimens which would undergo moist-curing were cast in their molds and sealed in accordance with the AASHTO T 126 (2003) guidelines. They were allowed to cure for 24 hours in a climate-controlled laboratory environment before being stripped and placed into a moist-curing room to mature for the required amount of time. The 2-day specimens then were non-accelerated-cured for 24 hours before being loaded. The 7-, 28-, and 90-day specimens were non-accelerated-cured for 7 days or until load application, whichever came first. After the prescribed amount of moist-curing time had passed, each specimen was removed from the curing room and placed into a climate-controlled room having a relative humidity of  $50\% \pm 10\%$ . Here the drying process began and creep testing was conducted.

The specimens chosen for match-curing were sealed, placed in the match-curing system, and forced through an elevated temperature cycle similar to that typically used in the prestressing industry in the Southeastern United States. Figure 3-8 shows a 6 in. x 12 in. cylinder in the match-curing sleeve. Eight cylinders were cured at a time by the system, which was slaved to the computer controller in the manner described in Section 3.4.4.1. When the system was activated, it followed the temperature profile in Figure 3-9

for a duration of 18 hours. Figure 3-9 also shows some typical temperature values which were measured from within a representative concrete cylinder.

The curing cycle began with a four-hour period of room-temperature curing before heating began. This allowed the concrete mixture to begin setting before any heat was applied. Heat was then gradually added until a maximum temperature of 150°F (65.6°C) was reached. This was maintained for the next nine hours at which time the cylinders were allowed to cool. The cooling process occurred gradually over the next several hours. The specimens were removed from the system when they were cool enough to touch. At this time the load application commenced.



**Figure 3-8:** A 6 in. x 12 in. concrete cylinder inside a match-curing sleeve

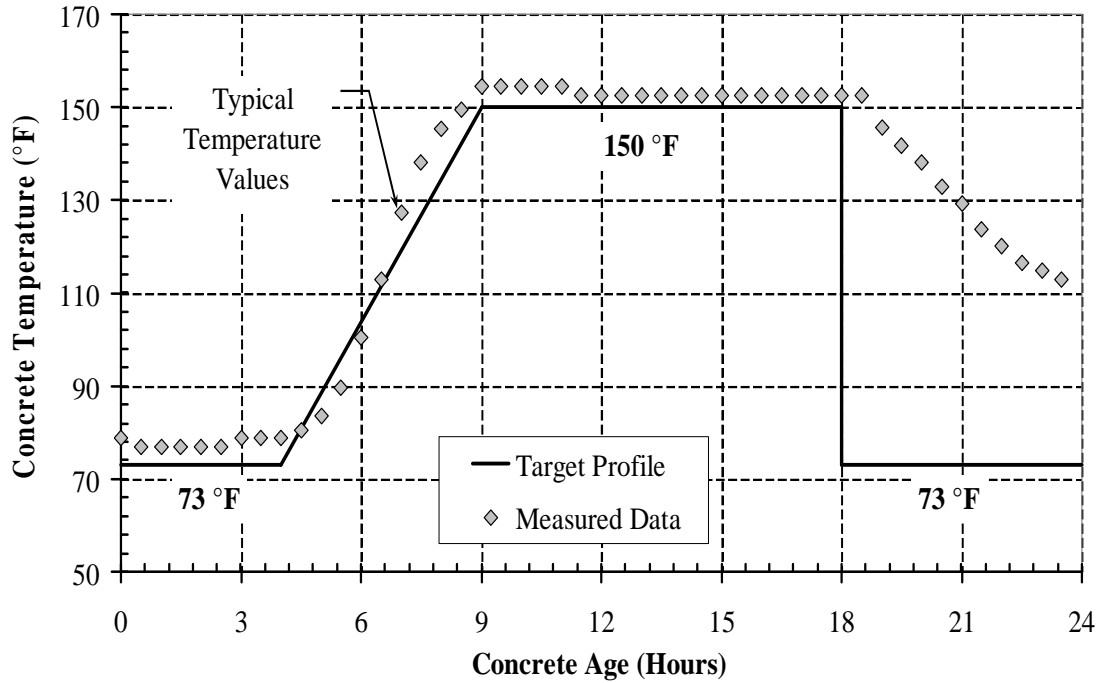


**Figure 3-9:** Temperature profile used by the match-curing system with typical measured temperatures

### 3.5.5 METHODS FOR TESTING HARDENED CONCRETE

The hardened properties of interest for this study included the compressive strength, drying shrinkage, and creep exhibited by each concrete mixture. This section outlines the procedures and equipment used to gather the data related to both compressive strength and drying shrinkage. The procedures and equipment used during the creep testing portion of this study are presented in Section 3.5.6.

#### 3.5.5.1 Compressive Strength

Before creep testing could commence, the compressive strength of each mixture and loading age had to be measured. All compressive strength testing was conducted in accordance with, and conducted on equipment meeting, the guidelines set forth by

AASHTO T 22 (2003). Each specimen was capped using a high-strength, sulfur-based capping compound in accordance with AASHTO T 231 (2003) before being placed into a Forney FX600 compressive testing machine. Each 6 in. x 12 in. cylinder was loaded at a target rate of 60,000 lbs/min. until failure on the 600-kip capacity compression machine shown in Figure 3-10 below.



**Figure 3-10:** The Forney compression testing machine used for this study

### **3.5.5.2 Drying Shrinkage**

Drying shrinkage must be determined and accounted for to accurately measure the strain associated with concrete creep. For the purposes of this study, measurement of drying shrinkage was accomplished by using a Demountable Mechanical (DEMEC) strain gauge

with DEMEC points to measure the shrinkage of a 6 in. x 12 in. concrete cylinder. Figures 3-11 and 3-12 show both the DEMEC points and DEMEC gauge, respectively. This type of test specimen and gauge were chosen because they were identical to those used in the creep testing portion of the study.

Drying shrinkage readings were taken at the time intervals specified in ASTM C 512 (2006), which is the specification that governs creep testing. These intervals included readings taken before the application of load onto the creep test specimens, immediately after load application, 2 to 6 hours after applying load, then once a day for the first week, once a week for the first month, and then every month for a full year. This schedule is detailed more thoroughly in Section 3.5.6.3. The procedures and equipment used for gathering the shrinkage data were identical to those used for gathering the creep strain data. This consistency was employed in an effort to establish uniformity across the study and to limit data gathering error.



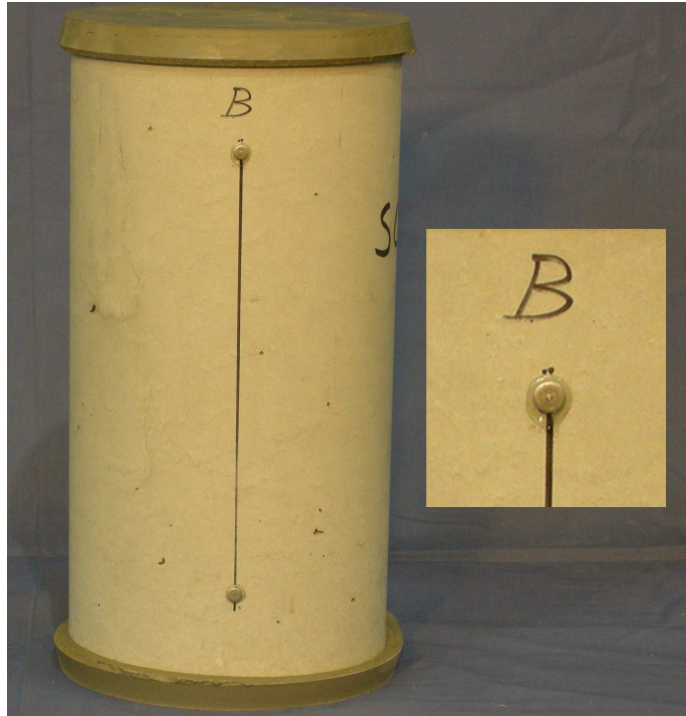


**Figure 3-11:** Concrete cylinder fitted with DEMEC points

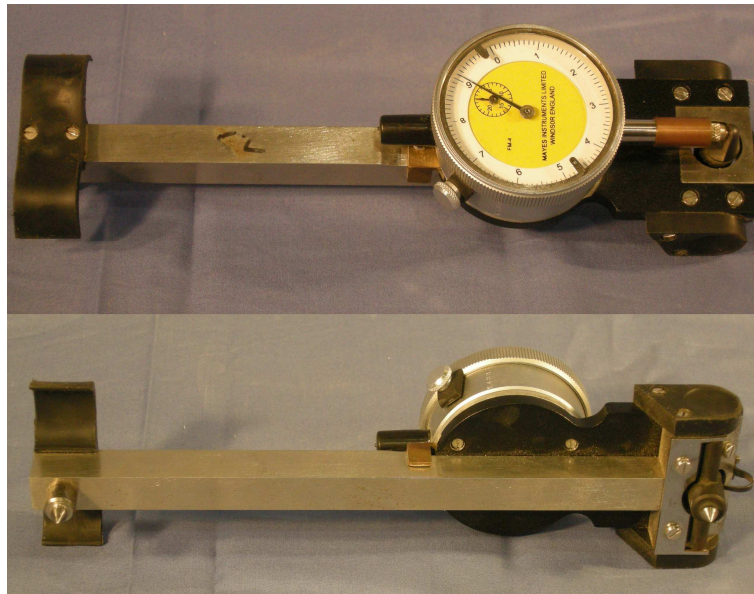


**Figure 3-12:** DEMEC gauge used for all strain measurements

### **3.5.6 CREEP TESTING**

In conducting this research project, all procedures and equipment used met the requirements set forth by ASTM C 512 (2006), which is the governing specification for creep testing in the United States. This section outlines the entire testing program and details the equipment and test methods used during the process.

#### **3.5.6.1 Creep Frames**

This study required the use of 25 creep testing frames in order to test the five loading ages for each of the five concrete mixtures of interest. ASTM C 512 (2006) provides a basic description of the layout of the required creep frame. In short, it specifies that the frame must be capable of maintaining the applied load within  $\pm 2\%$  of the target load even as length change occurs within the test specimens. To do this, the specification suggests the use of railroad car springs, which need to be flexible enough to allow reasonable amounts of length change to occur before any significant reduction in load occurs. The springs are sandwiched between two steel plates that transfer the applied load into the test specimens. A hydraulic ram was used to apply the load to the cylinders. Figure 3-13 and Figure 3-14 show schematics of one of the creep frames used in this project. Figure 3-15 is a picture of an actual frame used during the course of research.

### Elevation View

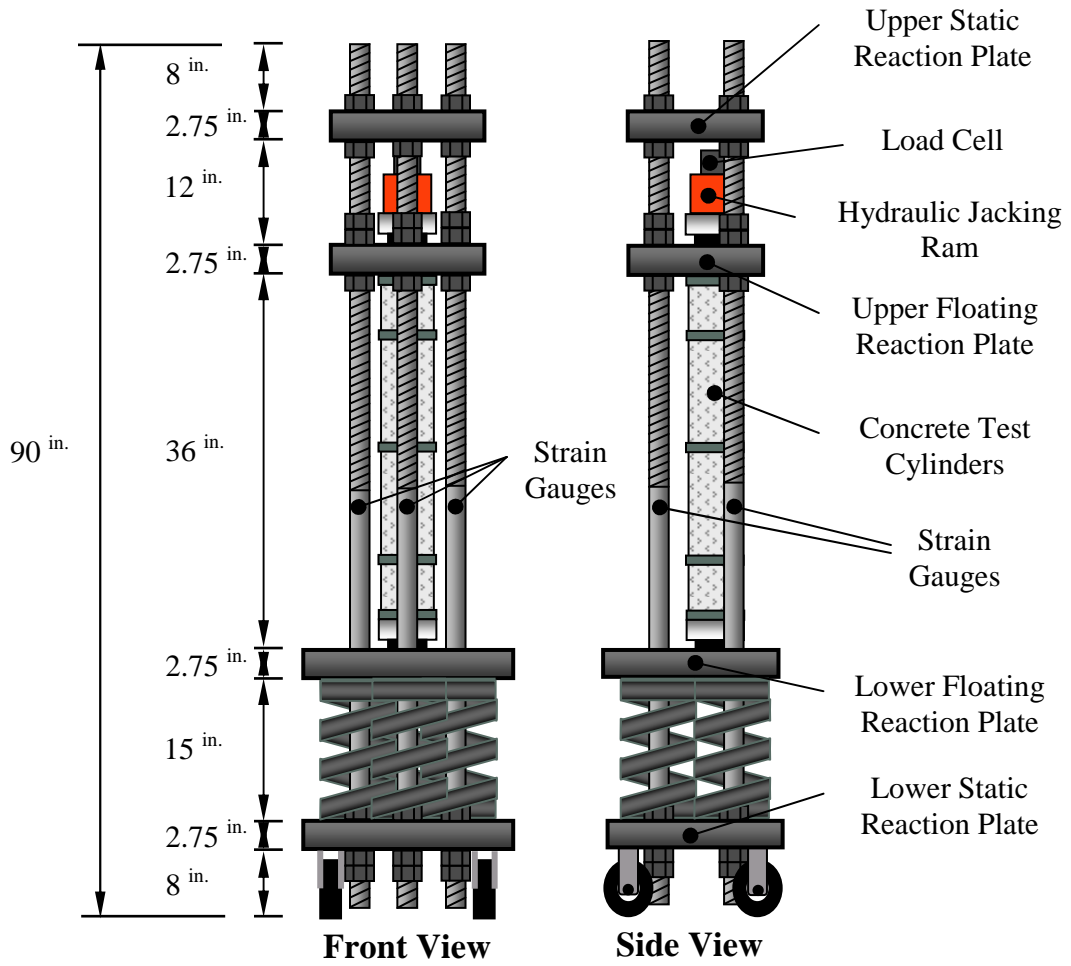


**Figure 3-13:** Elevation views of creep frame

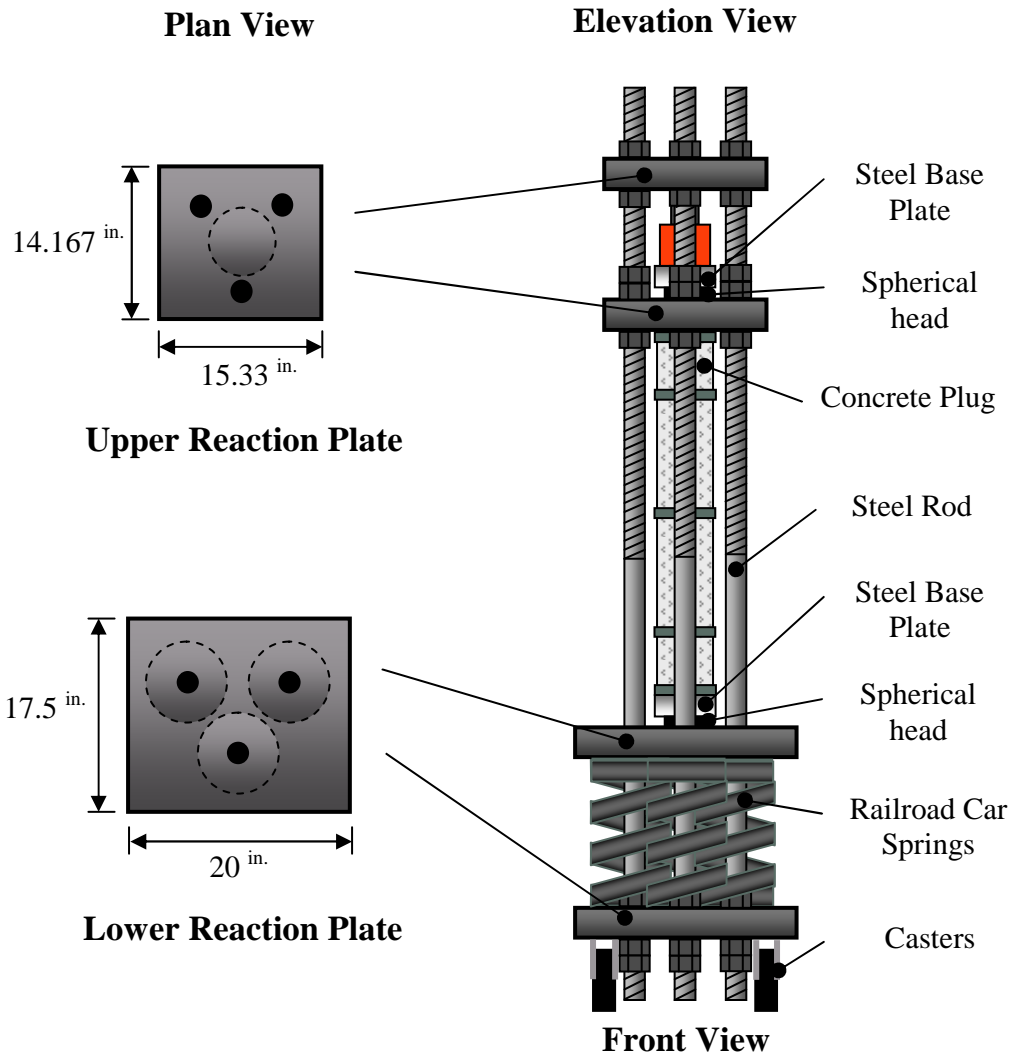


**Figure 3-14:** Plan views of reaction plates used in creep frame



**Figure 3-15:** Example of creep frame used during this research project

During the preliminary design phase, it was determined that each frame needed to be able to withstand the forces required to load 6 in. x 12 in., concrete cylinders having a compressive strength of 16,000 psi to 40% of their ultimate strength. This meant that that each frame needed to have a maximum service load capacity of approximately 180 kips.

All forces were considered to be dead loads because they were controllable and constant once the force was applied. This allowed for the use of a dead load factor of 1.4 to be used in determining the maximum required service load capacity.

Based on the load requirements established through the initial analysis, it was determined that 2¾ in.-thick Grade 50 steel plates were required. Their use would prevent excessive deflections under service loads and would allow for the most accurate creep strain measurements to be collected. As can be seen in Figure 3-13, four plates were needed. To assist with alignment during loading, 6 in. diameter scribe marks were etched into the underside of the upper floating reaction plate. This aided in aligning the cylinders into the required vertical position and minimized eccentricities associated with misalignment issues.

On the top side of the lower floating reaction plate a threaded hole was created to allow the proper alignment of a spherical head, which would again help reduce the chances of incurring eccentrically loaded specimens. To help align the springs, 3 - 8½ in. diameter scribe marks were engraved on the underside of the lower floating reaction plate. These can be seen in Figure 3-14, along with the positions of the steel restraining rods.

From Figure 3-14 it can be seen that three rods with nuts were used to hold the applied load once the jacking mechanism was released. Each rod needed to be able to safely hold 60 kips of force while experiencing minimal relaxation. This was accomplished by using 1¾ in. diameter steel rods which had a yield stress of 65 ksi and an ultimate stress of 80 ksi. Every rod was designed to be 90 in. in length and was threaded along the first 10 in. of the lower end of the bar and along the first 50 in. of the

top portion. This allowed for 1¾ in. Grade 8, heavy-duty hex nuts to be threaded onto the rods to hold the plates in the proper locations. Each frame required eight of these nuts, which were made from C 1045 steel having a minimum Rockwell hardness of C24 and a minimum ultimate tensile stress of 150 ksi. The nuts were machined reasonably well; however, due to tolerance issues, approximately 2% of the applied load was lost when the hydraulic ram was released, leaving the nuts to resist the applied force. This required the target load to be over applied by 2% to compensate for the seating action.

While the plates and rods acted to hold the applied loads once the hydraulic jack was removed, it was the springs that continued to apply the load even as the cylinders deformed under the compressive forces. Every frame required three of these springs, each of which had a spring constant of 25,000 lbs/in. They were designed and constructed specifically for Auburn University and this research project by Duer/Carolina Coil, Inc. of Reidville, SC. Each spring was made from ASTM-A-304, Grade 220 steel and was 15 in. in height and had an 8½ in. in outer diameter. These springs were highly flexible in comparison to previous springs used for this application, allowing for greater length change to occur in the test specimens before a 2% reduction in the total load occurred.

To help monitor the load, strain gauges were applied to the unthreaded portion of each bar at a distance of no less than two bar diameters away from the end of the threads. This location allowed the stress distribution in each bar to spread fully across the cross section and provided the most accurate strain reading possible. After the strain gauges were installed, each frame was calibrated to determine that the gauges were working properly. This calibration consisted of three loading runs in which each frame was loaded to 120 kips, taking strain measurements at 20 kip intervals along the way. After all three

runs were complete, the strain measurements were compared to ensure precision, and as necessary, a calibration factor was determined to guarantee the proper load was measured.

It should be noted that since each part of the frame was made of steel, they were all relatively heavy, which created challenges in relation to assembly. An overhead crane was a necessity as each frame was constructed on its side and then tilted into its final vertical position. To allow for movement once vertical, casters were placed on the underside of the lower static reaction plate, two of which were of the swivel type. These swivel casters allowed for greater mobility in the tight confines of the climate-controlled creep testing room.

#### **3.5.6.2 The Creep Room**

Creep is dependent on temperature and humidity conditions. ASTM C 512 thus requires that both temperature and relative humidity be controlled at  $73^{\circ}\text{F} \pm 2^{\circ}\text{F}$  and  $50\% \pm 4\%$ , respectively, during this test. A climate-controlled room was constructed with the sole purpose of providing an environment for conducting creep testing. This room had a dedicated air-conditioning unit and humidifier that were automatically controlled to meet the requirements of ASTM C 512. Figure 3-16 shows a plan view of the 18 ft x 11 ft room located within the Auburn University Structural Research Laboratory. Locations of the individual creep frames as they were positioned within the room are also indicated.



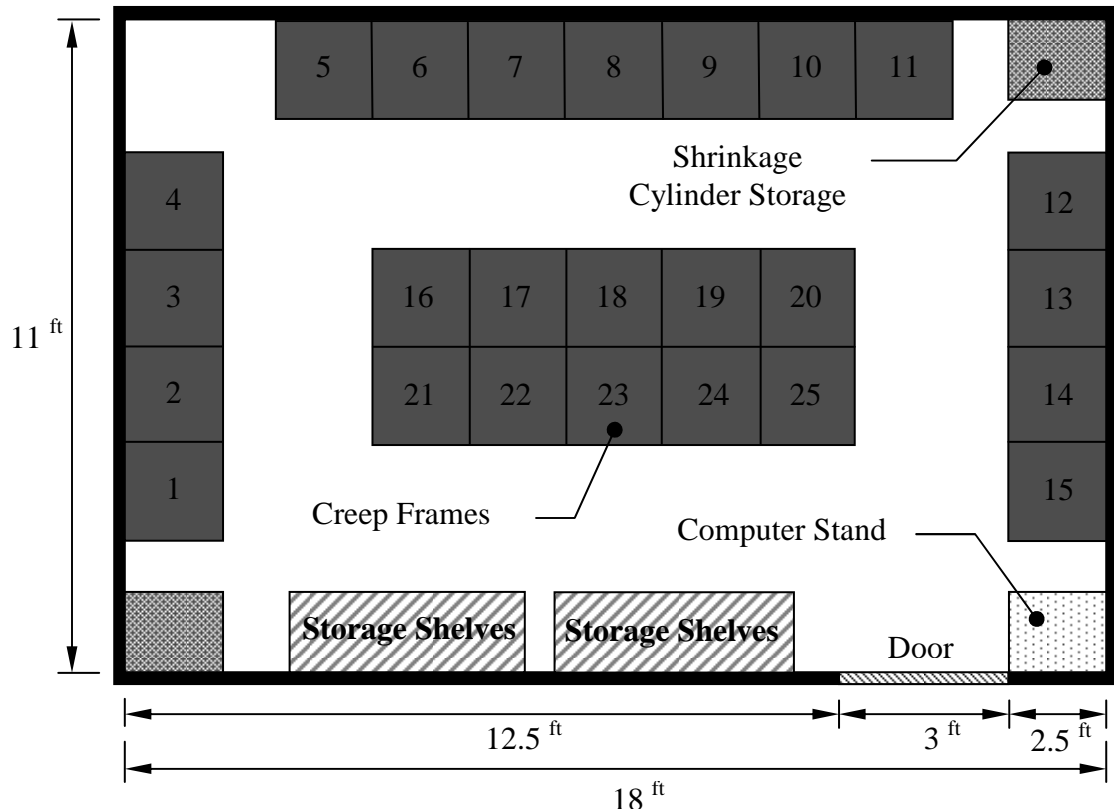


**Figure 3-16:** The layout of the environmentally-controlled creep testing room

The creation of this controlled environment allowed the test specimens to sustain relatively steady ambient conditions. In fact, the environmental conditions were recorded during the testing through the use of a data logger, and the temperature and relative humidity values consistently measured  $72^{\circ}\text{F} \pm 5^{\circ}\text{F}$  ( $22^{\circ}\text{C} \pm 5^{\circ}\text{C}$ ) and  $50 \pm 10\%$ , respectively. The climate-controlled nature of this room proved to be of further value as it provided a place to store specimens not yet ready for testing. ASTM C 512 (2006) requires each specimen to be stored in conditions similar to those described above upon the completion of moist-curing. Having samples stored and tested in the same environment adds another level of homogeneity to the study and provides uniformity in relation to test results.

### 3.5.6.3 Creep Testing Procedure

After the appropriate curing regime for each set of specimens was complete, all specimens were loaded in uniaxial constant compression. All creep testing procedures for this research project were conducted in as uniform a manner as possible, and as previously stated, in accordance with the specifications set forth by ASTM C 512 (2006). An outline of the procedure used throughout the creep testing program is presented below.

1. Remove creep, shrinkage, and strength specimens from curing conditions.
2. Sulfur-cap each specimen in accordance with AASHTO T 231 (2003) and allow caps to harden.
3. While cap is hardening, apply DEMEC points at 120-degree intervals around the perimeter of each creep and shrinkage test cylinder. Allow epoxy to fully harden before taking first reading.
4. Determine the ultimate compressive strength of two specimens.
5. Determine the best cylinder alignment to limit eccentricities.
6. Insert the test cylinders into the appropriate creep frame using the alignment determined in Step 5. The test cylinders should align with the scribe mark on the bottom of the upper floating reaction plate.
7. Lower the upper floating reaction plate onto the test cylinders.
8. Record initial strain measurements for test cylinders and drying shrinkage cylinders.

9. Position the hydraulic jacking mechanism on the top side of the upper floating reaction plate.
10. Position the load cell on top of the jacking mechanism and plumb the entire setup.
11. Attach the load cell and strain gauge wiring to the strain gauge indicator.
12. Begin slowly applying 40% of the ultimate compressive strength found in Step 4.
13. Continue slowly applying load until 102% of the desired load is reached.
14. Lock the load into place by hand-tightening all nuts on the top side of the upper floating reaction plate.
15. Gently retract the jacking mechanism.
16. Check the resulting specimen load by using the strains obtained from the steel bars to ensure it is within  $\pm 2\%$  of desired value. Reapply load as necessary.
17. Record concrete strain measurements resulting from load application and corresponding drying shrinkage strain as soon as possible after initial loading.

After this procedure was completed, strain readings were taken using the DEMEC strain reading gauge depicted in Figure 3-12, and were read in accordance with the time intervals required by ASTM C 512 (2006). These intervals included readings at 2 to 6

hours after loading, once a day for the first week, then once a week until the completion of the first month, and then once a month for the remainder of the testing period, which was one year for this project. The 2 to 6 hour reading was taken as close to the 2-hours-after-loading mark as possible. This was also true for all other readings. They were taken as close to their required time as possible, in an effort to provide uniform results.

As testing progressed and creep strain measurements were taken, ASTM C 512 (2006) required the applied load remain within  $\pm 2\%$  of the original load. To track changes in load, strain gauges were applied to all three bars of each frame. Using a strain indicator, bar strain readings were taken immediately prior to all creep strain readings. The measured bar strain was compared to initial bar strains taken prior to loading and the percent change in load was calculated. If the applied load was outside of the specified range, load was added as necessary, and then the creep strain measurements were taken.

In an effort to isolate the strain associated solely with creep, ASTM C 512 (2006) requires corresponding drying shrinkage strain readings to be taken. The readings were recorded at the same time intervals as the creep strain readings and were taken immediately following the creep measurements. As previously mentioned, 6 in. x 12 in. cylinders were chosen for the drying shrinkage specimens because they are identical to the creep specimens. The method used to measure the strain on these specimens was identical to that used for the creep specimens.

## **3.6 MATERIALS**

Over the course of this research project, numerous raw materials were used to produce the five concrete mixtures. This section outlines the specific details of each of these raw materials.

### **3.6.1 CEMENTITIOUS MATERIALS**

Three cementitious materials were used over the course of this study, including: Type III portland cement, Class C fly ash, and Grade 120 GGBF Slag. The incorporation of all of these cementitious materials allowed for the determination of the effect each has on creep of SCC. Two SCC mixtures were comprised of a combination of Type III portland cement and Class C fly ash. The remaining two SCC mixtures consisted of a combination of Type III portland cement and Grade 120 GGBF Slag.

#### **3.6.1.1 Type III Portland Cement**

The Type III portland cement used for this research project was manufactured in Demopolis, Alabama by Cemex. It was utilized because it is consistent with the materials used by the prestressing industry, which prefers it over other types of cement because of the high early-age strengths it provides. The chemical composition of the cement used for this study can be found in Table 3-5.

#### **3.6.1.2 Class C Fly Ash**

The Holcim (US), Inc. plant in Quinton, Alabama provided the Class C fly ash used for this project. It was chosen because it provides a more rapid strength gain than Class F fly ash, which is preferred by the prestressing industry. A more detailed description of Class

C fly ash can be found in Section 2.2.1.3, and the chemical composition of the Class C fly ash used during this study is shown in Table 3-5.

### 3.6.1.3 Ground-Granulated Blast-Furnace (GGBF) Slag

The GGBF Slag used in this study was Grade 120 and was procured from Buzzi Unicem in New Orleans, Louisiana. It was chosen for its ability to alter fresh concrete performance in a desirable way. In the case of this research project, the smaller fineness of the GGBF Slag particle relative to Class C fly ash particles provided greater viscosity to the fresh concrete mixture, which increased mixture stability. A more detailed discussion of GGBF Slag can be found in Section 2.2.1.3 of this report.

**Table 3-5:** Chemical composition of the powdered materials (Roberts 2005)

Parameter	Type III Portland Cement	Class C Fly Ash	Grade 120 GGBF Slag
Silicon dioxide, SiO <sub>2</sub> (%)	20.01	37.59	32.68
Aluminum oxide, Al <sub>2</sub> O <sub>3</sub> (%)	5.25	18.87	9.67
Iron oxide, Fe <sub>2</sub> O <sub>3</sub> (%)	3.88	6.06	1.12
Calcium oxide, CaO (%)	62.69	24.12	45.32
Magnesium oxide, MgO (%)	0.9	5.17	7.4
Alkalies (Na <sub>2</sub> O + 0.65K <sub>2</sub> O) (%)	0.27	2.29	----
Sulfur trioxide, SO <sub>3</sub> (%)	4.27	1.38	1.66
Loss on ignition, LOI (%)	2.02	0.31	0.84
Tricalcium silicate, C <sub>3</sub> S (%)	50.16	----	----
Dicalcium silicate, C <sub>2</sub> S (%)	19.52	----	----
Tricalcium aluminate, C <sub>3</sub> A (%)	7.34	----	----
Tetracalcium aluminoferrite, C <sub>4</sub> AF (%)	11.81	----	----
Specific surface area (m <sup>2</sup> /kg)	567	409	547
Specific gravity	3.15	2.63	2.91

### **3.6.2 CHEMICAL ADMIXTURES**

The three chemical admixtures used in the concrete mixtures for this research project are discussed in this section. The three admixtures include two types of water-reducing admixtures and a viscosity-modifying admixture. Their use allowed the desired fresh and hardened properties to be reached.

#### **3.6.2.1 High-Range Water-Reducing (HRWR) Admixture**

Glenium 3400 and Polyheed 1025 were used in this study to fulfill the roles of the HRWR admixtures, which make SCC possible. They both are based on polycarboxylate chemistry and were obtained from BASF Construction Chemicals, LLC. The Glenium 3400 admixture provides a greater water-reducing ability than the Polyheed 1025, which is more generally referred to as a mid-range water-reducer. However, both were used during this study to obtain the desired filling ability. More details on the behavior of HRWR admixtures is presented in Section 2.2.

#### **3.6.2.2 Viscosity Modifying Admixture (VMA)**

A VMA called Rheomac VMA 362 was used to help reduce each SCC mixture's sensitivity to fluctuations in free water content. It was obtained from BASF Construction Chemicals, LLC, which provided the HRWR admixture mentioned in the previous section. Section 2.2.1.4 gives a more in-depth description of the effects and usages of VMA.

### **3.6.3 COARSE AGGREGATE**

All mixtures used throughout the course of this research included No. 78 crushed limestone (AASHTO M 43) as their only coarse aggregate. It was obtained from a quarry in Calera, Alabama which is owned and operated by the Vulcan Materials Company. The limestone has a bulk specific gravity of 2.72, a saturated surface dry specific gravity of 2.73, and has an absorption capacity of 0.40%. It is apparent from looking at Table 3-6, which details the gradation of the No. 78 crushed limestone and the AASHTO M 43 requirements, that this coarse aggregate gradation meets the specification requirements.

### **3.6.4 FINE AGGREGATE**

The same fine aggregate was used in all the concrete mixtures for this research project. It was obtained from the Jemison, Alabama quarry operated by Superior Products, Inc. It is a siliceous sand that has a bulk specific gravity of 2.58, a saturated surface dry specific gravity of 2.60, and an absorption capacity of 1.00%. Refer to Table 3-7 for the sand's gradation and the specification requirements of AASHTO M 6. It should also be noted that the sand met the gradation requirements of AASHTO M 43.



**Table 3-6:** Gradation for the No. 78 crushed limestone (Roberts 2005)

<b>Sieve Size</b>	<b>Percent Passing</b>	<b>AASHTO M 43 Specification of Percent Passing (%)</b>
3/4"	100	100
1/2"	97	90-100
3/8"	73	40-75
No. 4	10	5-25
No. 8	0.9	0-10
No. 16	0.3	0-5

**Table 3-7:** Gradation for the fine aggregate (Roberts 2005)

<b>Sieve Size</b>	<b>Percent Passing</b>	<b>AASHTO M 6 Specification of Percent Passing (%)</b>
No. 4	97	95-100
No. 8	85	80-100
No. 16	76	50-85
No. 30	56	25-60
No. 50	19	10-30
No. 100	3	2-10

## **CHAPTER 4**

### **PRESENTATION AND ANALYSIS OF RESULTS**

#### **4.1 INTRODUCTION**

The fresh and hardened properties collected from mixing and testing four SCC mixtures and one conventional-slump concrete mixture are presented in this chapter. Fresh properties can be found in Section 4.2, while mechanical properties and creep results can be found in Sections 4.3 and 4.4, respectively. Additionally, suggestions derived from experience gained relative to ASTM C 512 creep testing procedures are detailed in Section 4.5. Information is included on lessons learned through designing and constructing the creep frames, as well as information regarding loading specimens and collecting data over the course of 365 days.

#### **4.2 FRESH PROPERTIES**

The results from the fresh property testing of all SCC mixtures and the conventional-slump mixture are presented in Table 4-1. It should be noted that the total number of specimens required from each mixture made it necessary to prepare 8.75 ft<sup>3</sup> of concrete for each mixture; however, the mixer used for this research project only had a 5.5 ft<sup>3</sup> useful service volume. Therefore, each mixture had to be prepared in at least two batches. Additionally, in some cases, three batches were used when some batches had to be repeated. For these reasons, Table 4-1 lists multiple batches for each mixture.

**Table 4-1: Summary of the fresh properties for all mixtures**

Mixture ID	Batch	Loadings Ages Produced	Fresh Properties					
			Slump Flow, in.	T-50, seconds	VSI	Total Air, %	Unit Weight, lb/ft <sup>3</sup>	Temp., °F
CTRL	A	18 hr, 2 & 90 day	7.75*	----	----	5.0	150.0	78
	B	7 & 28 day	7.25*	----	----	3.5	150.5	73
SCC-MS-FA	A	18 hr	27.0	1.9	1.5	2.5	148.0	74
	B	2, 7, 28, & 90 day	28.0	3.3	1.0	2.9	147.4	75
SCC-HS-FA	A	18 hr	27.0	4.3	1.0	2.0	152.6	75
	B	2 day	28.5	4.0	1.5	2.2	151.6	75
	C	7, 28, & 90 day	28.0	3.5	1.0	2.5	151.7	74
SCC-MS-SL	A	18 hr	27.0	5.8	1.5	2.0	152.1	75
	B	2, 7, & 90 day	26.0	4.9	1.0	2.0	150.8	74
	C	28 day	26.0	2.5	1.5	2.6	148.8	76
SCC-HS-SL	A	18 hr, 7, 28, & 90 day	27.0	6.3	1.0	2.3	153.4	74
	B	2 day	27.0	7.2	1.0	1.7	153.8	74

**Note:** \* indicates a conventional slump

## **4.2.1 SLUMP FLOW**

The values collected from performing the slump flow test for each SCC mixture are presented in this section. A brief discussion follows the presentation of results.

### **4.2.1.1 Slump Flow Test Results**

The slump flow values collected from testing fresh properties of each of the SCC mixtures all fell within the acceptable range ( $27 \pm 3$  inches) chosen in earlier phases of this study. In fact, after approximately 15 minutes of mixing, all slump flow values ranged from 26.0 to 28.5 in. (660 to 724 mm). Figure 4-1 depicts the slump flow values for each batch of all SCC mixtures.

### **4.2.1.2 Discussion of Slump Flow Test Results**

As previously stated, all slump flow values fell within the specified range chosen in earlier phases of this research effort. This conformance illustrated that each SCC mixture was highly flowable and that the flowability was easily attained. Additionally, no trends were noticed between changes in slump flow characteristics relative to changes in water-to-cementitious materials ( $w/cm$ ) ratios. Thus it can be reasoned that changes in the  $w/cm$  have little bearing on slump flow values if the mixtures are properly proportioned to account for this change.

A slight difference ( $< 4\%$ ) in the slump flow values was noticed between the fly ash and the slag mixtures. However, such a small difference is negligible and could be caused by a number of external variables which have no relation to the SCMs. Therefore it is reasoned that varying these two SCMs has no significant effect on the slump flow values.

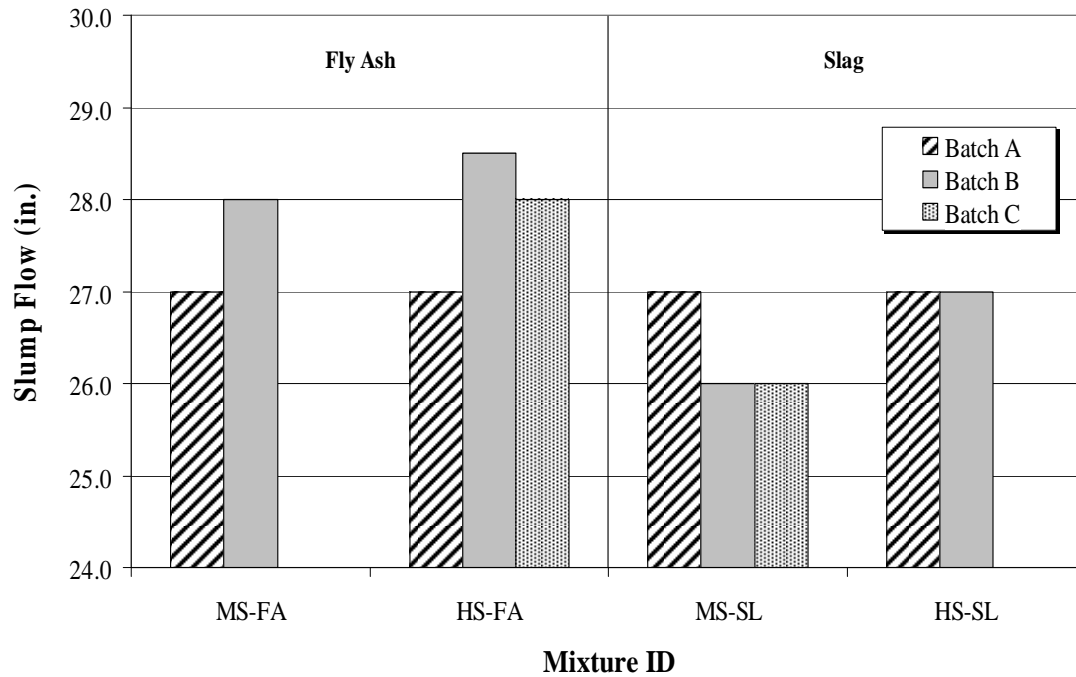


**Figure 4-1:** Slump flow values for each batch of every SCC mixture

#### 4.2.2 T-50

The T-50 values for each batch of every SCC mixture are plotted in Figure 4-2. They were collected as the slump flow test was run, which occurred after approximately 15 minutes of mixing. From Figure 4-2 it can be seen that the T-50 values increase as the  $w/cm$  decreases. This is consistent with findings from previous phases of this research project and can be attributed to the higher powder content of mixtures with lower  $w/cm$ , causing greater cohesiveness within the mixture (Roberts 2005). Furthermore, it can be seen that the mixtures containing a cement replacement of GGBF slag exhibit higher T-50 times than the fly ash mixtures of the same strength level. In fact, the slag mixtures demonstrated extremely high levels of cohesiveness, which is believed to be related to the

increased fineness of the slag particles. This too is consistent with findings from previous phases of this project (Roberts 2005).

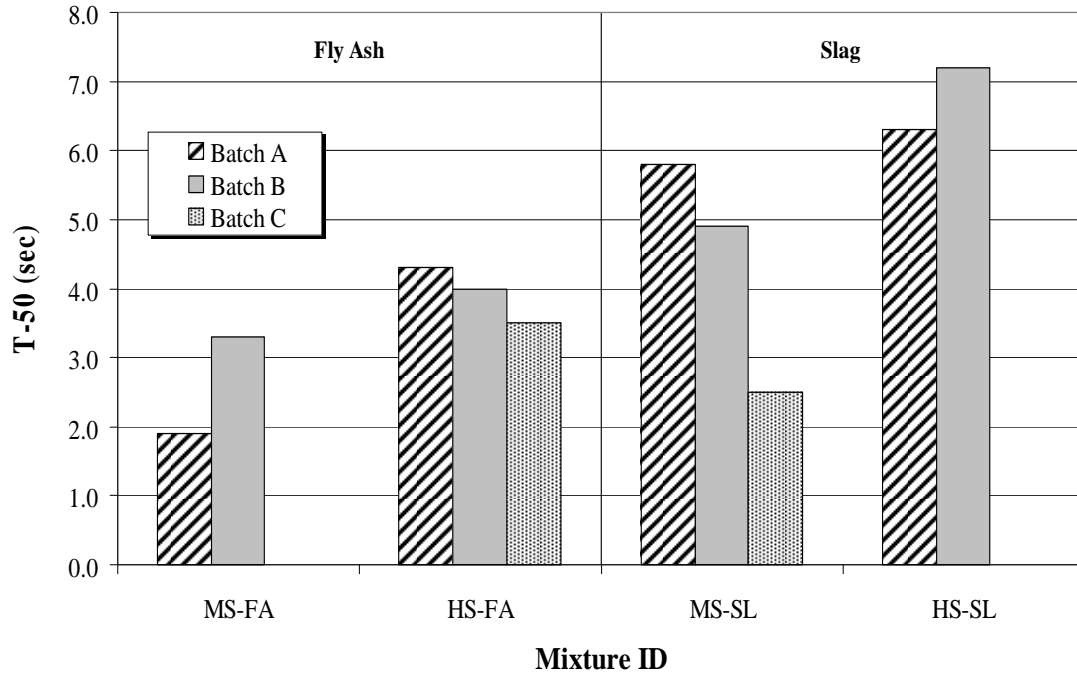


**Figure 4-2:** T-50 values for each batch of all SCC mixtures

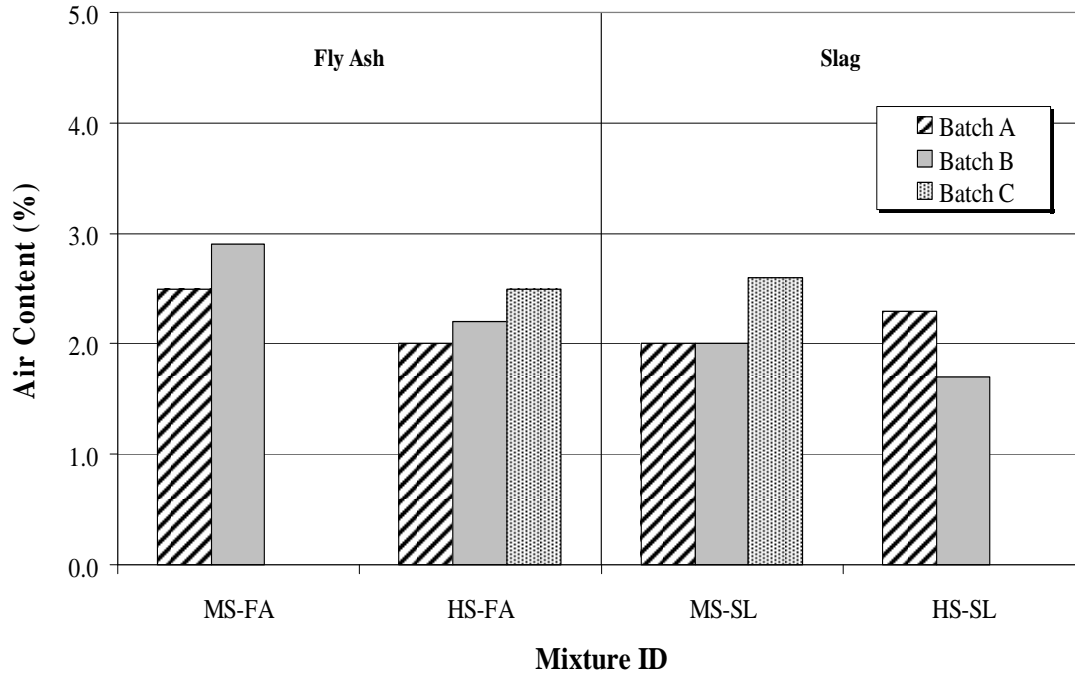
#### 4.2.3 VISUAL STABILITY INDEX (VSI)

Table 4-1 illustrates that all SCC mixtures had a VSI value between 1.0 and 1.5. The dynamic stability of all the SCC mixtures were considered adequate since all the collected VSI values ranged between 1.0 and 1.5. These values are consistent with the VSI results from previous phases of this project.

#### 4.2.4 AIR CONTENT

The values of air content measured ranged between 1.7% and 2.9% for all SCC mixtures. These values, which are plotted in Figure 4-3, are below the range (3% to 5%) specified

as adequate in earlier phases of this study (Roberts 2005). The measured air content values for all the batches were within  $\pm 1\%$  of each other.



**Figure 4-3:** Air content of every batch for all SCC mixtures

#### 4.2.5 UNIT WEIGHT

Table 4-1 contains the unit weight values of all four SCC mixtures and of the conventional-slump mixture. The average unit weight value of the SCC mixtures was  $151.0 \text{ lb/ft}^3$ , while the average value of both batches of the conventional-slump mixture were  $150.3 \text{ lb/ft}^3$ . The difference is only 0.5%, and as can be seen, all unit weight values are consistent with those commonly used in the design of concrete structures.

#### 4.3 MECHANICAL PROPERTIES

The results of the compressive strength testing are presented in this section. The results in Table 4-2 are organized according to the age of each concrete specimen at the time of

loading, which is termed the “loading age”. Creep and drying shrinkage results can be found in Section 4.4.

**Table 4-2:** Compressive strength values for all mixtures and loading ages

Mixture ID	Compressive Strength at Time of Loading, psi				
	18 hour	2 day	7 day	28 day	90 day
CTRL	5,430	5,850	7,660	9,090	8,330
SCC-MS-FA	5,800	5,700	7,570	9,570	9,830
SCC-HS-FA	9,190	9,100	11,110	12,800	13,630
SCC-MS-SL	6,250	4,620	6,840	10,610	11,580
SCC-HS-SL	9,600	8,830	10,580	12,880	13,670

#### 4.3.1 COMPRESSIVE STRENGTH

As shown in Table 4-2, the 18-hour compressive strengths ( $f'_{ci}$ ) for all SCC mixtures ranged from 5,800 to 9,600 psi (40 to 66 MPa), which is slightly higher than the target range of 5,000 to 9,000 psi (34 to 62 MPa) set forth in Roberts (2005). The conventional-slump mixture had an  $f'_{ci}$  value of 5,430 psi (37 MPa).

##### 4.3.1.1 Effects of Water-to-Cementitious Materials Ratio

Figures 4-4 and 4-5 illustrate, for all loading ages, the changes in compressive strength as the  $w/cm$  changes. From these graphs it can be seen that the compressive strength increases as the  $w/cm$  decreases, which is congruent with known trends associated with conventional-slump concrete. The compressive strength values were determined through destructive testing conducted immediately prior to the application of load.



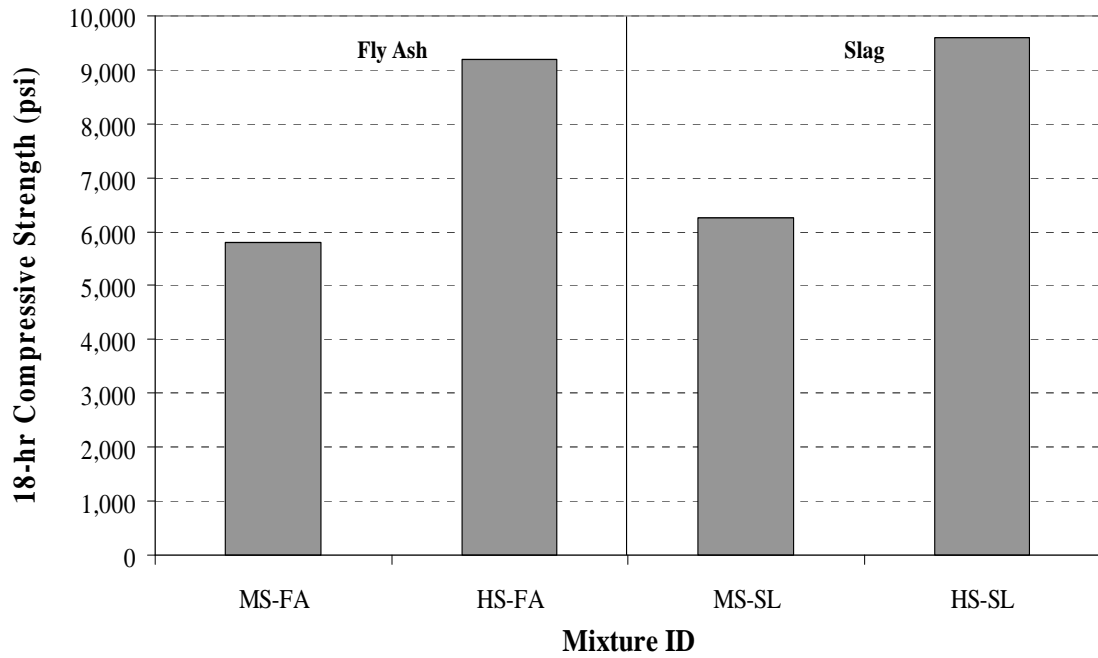


**Figure 4-4:** 18-hr compressive strengths for all SCC mixtures

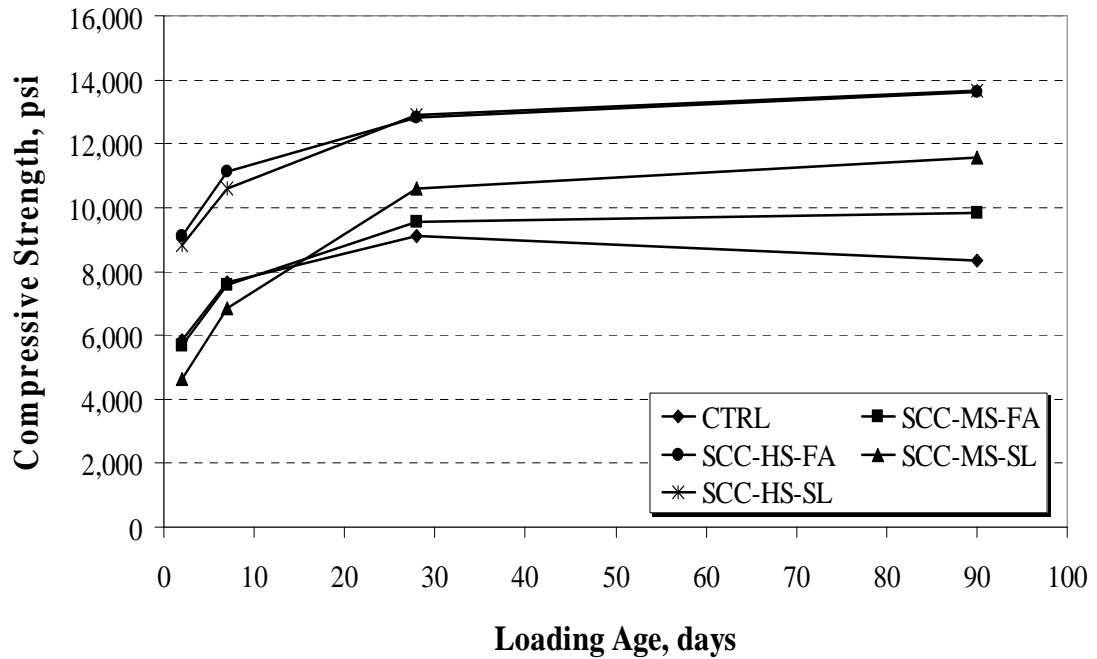


**Figure 4-5:** Change in compressive strength of each mixture with time

#### **4.3.1.2 Effects of Cementitious Material System**

The effects of the different cementitious materials systems on compressive strength can be seen in Figures 4-4 and 4-5. Both the moderate- and high-strength slag mixtures exhibited lower compressive strengths at the 2- and 7-day loading ages than the corresponding fly ash mixtures. This is most likely brought on by the slag itself, which initially tends to gain strength more slowly than fly ash does. However, at later ages, the GGBF slag mixtures exhibited different compressive strength trends. The moderate-strength GGBF slag mixture had a higher compressive strength than the moderate-strength fly ash mixture at the 28- and 90-day loading age. Additionally, the high-strength GGBF slag mixture had compressive strengths that were of the same magnitude as the high-strength fly ash mixture at the 28- and 90-day loading age.

#### **4.3.1.3 Behavior of SCC versus Conventional-Slump Concrete**

A plot of the compressive strength values for all SCC mixtures versus those of the conventional-slush mixture can be seen in Figure 4-6. With three exceptions, all SCC mixtures exhibited higher compressive strengths than the conventional-slush mixture at every level of maturity by an average of 27%. At the 2-day mark, both the moderate-strength slag and fly ash mixtures were slightly below (21% below and 3% below, respectively) the strength level achieved by the conventional-slush mixture.

Additionally, the strength of the moderate-strength slag mixture was below (11%) the conventional-slush mixture at the 7-day mark. The lower strengths exhibited by the early-age slag specimens is caused by slag's tendency to gain strength more slowly, as discussed earlier. It should be noted that the moderate-strength slag mixture has higher

strengths than the conventional-slump mixture at later ages. As for the moderate-strength fly ash mixture, it displayed compressive strengths which were very similar to the conventional-slump mixture at both the 2- and 7-day loading, but had slightly higher compressive strengths at the 28- and 90-day loading ages.

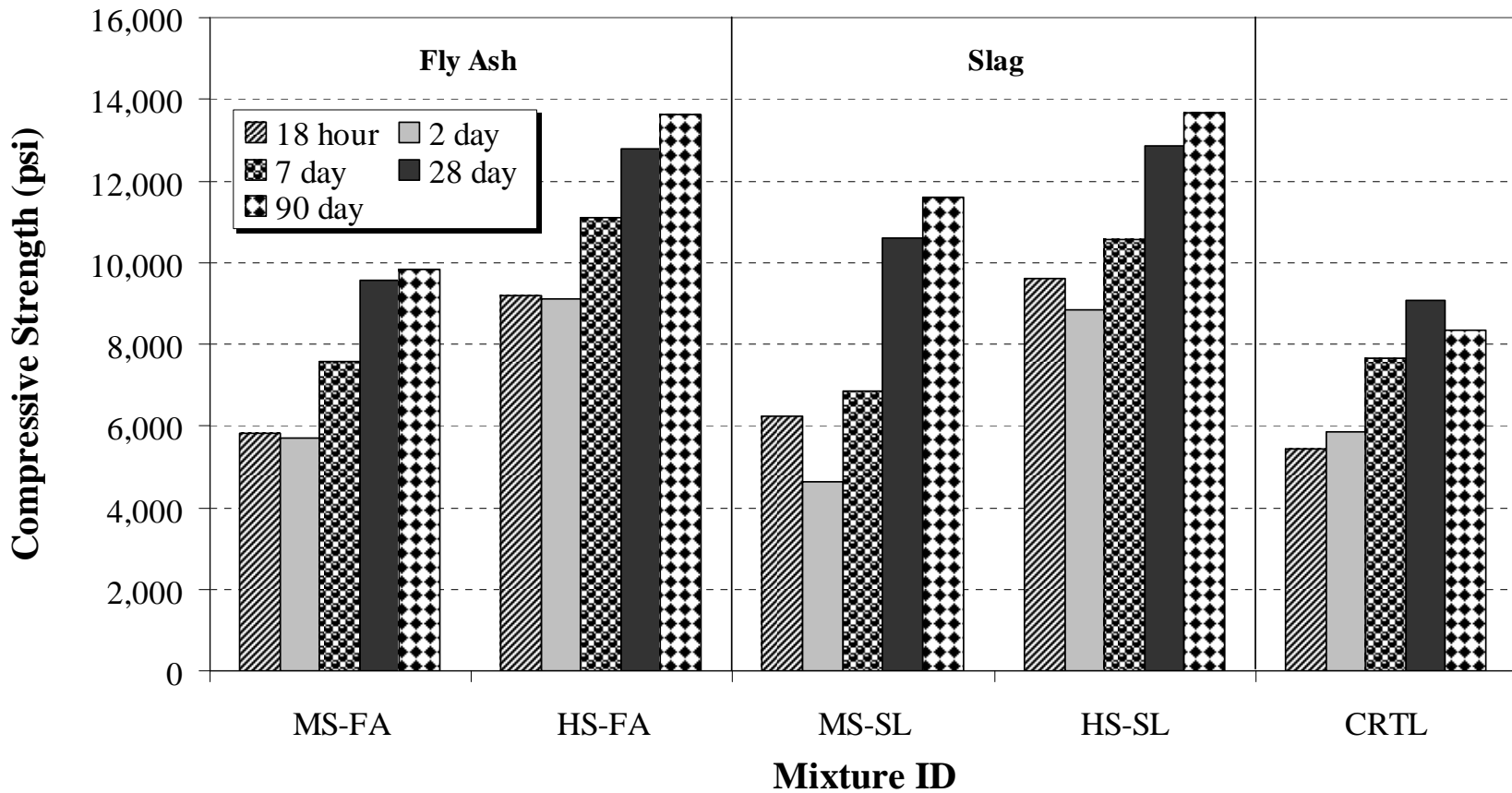


**Figure 4-6:** Compressive strength of all SCC mixtures compared to the conventional-slump mixture at all ages

#### **4.4 RESULTS FROM CREEP TESTING**

The results from creep testing are presented in the section. Creep results, drying shrinkage results, data on the environmental conditions in which creep testing was performed, and data obtained while tracking the applied load are included. Table 4-3 contains the 365-day creep and drying shrinkage strain results for each loading age of the concrete mixtures investigated in this study.

**Table 4-3:** 365-day creep and drying shrinkage strains for all loading ages and mixtures

Mixture ID	365-Day Creep Strain (in./in. x 10 <sup>-6</sup> )					365-Day Drying Shrinkage Strain (in./in. x 10 <sup>-6</sup> )				
	Loading Age					Loading Age				
	18 hour	2 day	7 day	28 day	90 day	18 hour	2 day	7 day	28 day	90 day
<b>CTRL</b>	-687	-965	-983	-951	-806	-276	-317	-335	-200	-87
<b>SCC-MS-FA</b>	-592	-847	-941	-1106	-746	-301	-329	-287	-174	-87
<b>SCC-HS-FA</b>	-615	-769	-802	-682	-575	-267	-255	-271	-125	-71
<b>SCC-MS-SL</b>	-512	-513	-616	-616	-539	-293	-273	-301	-113	-101
<b>SCC-HS-SL</b>	-529	-817	-505	-545	-424	-223	-260	-225	-87	-75

## 4.4.1 CREEP AND COMPLIANCE RESULTS

### 4.4.1.1 Creep Strain Results

Creep strain results due to creep effects only are detailed in this section. The drying shrinkage and instantaneous elastic deformation have been subtracted from the raw data that were collected. From Table 4-3 it can be seen that the 365-day creep strain values for the 18-hr match-cured SCC specimens ranged between -512 and -615 microstrain. The 365-day creep strain values for 2-, 7-, 28-, and 90-day SCC specimens varied between -513 and -847 microstrain, -505 and -941 microstrain, -545 and -1106 microstrain, and -424 and -746 microstrain, respectively. The measured creep for each mixture can be seen in Figures 4-7 through 4-11. Each figure contains all loading ages tested for one mixture.

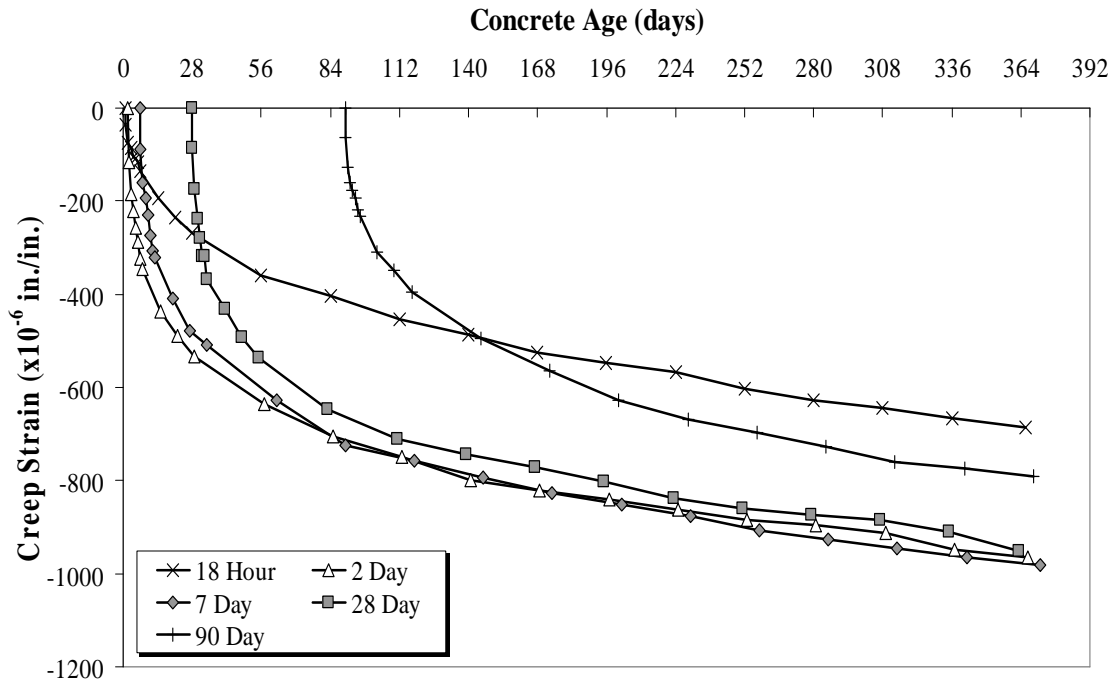
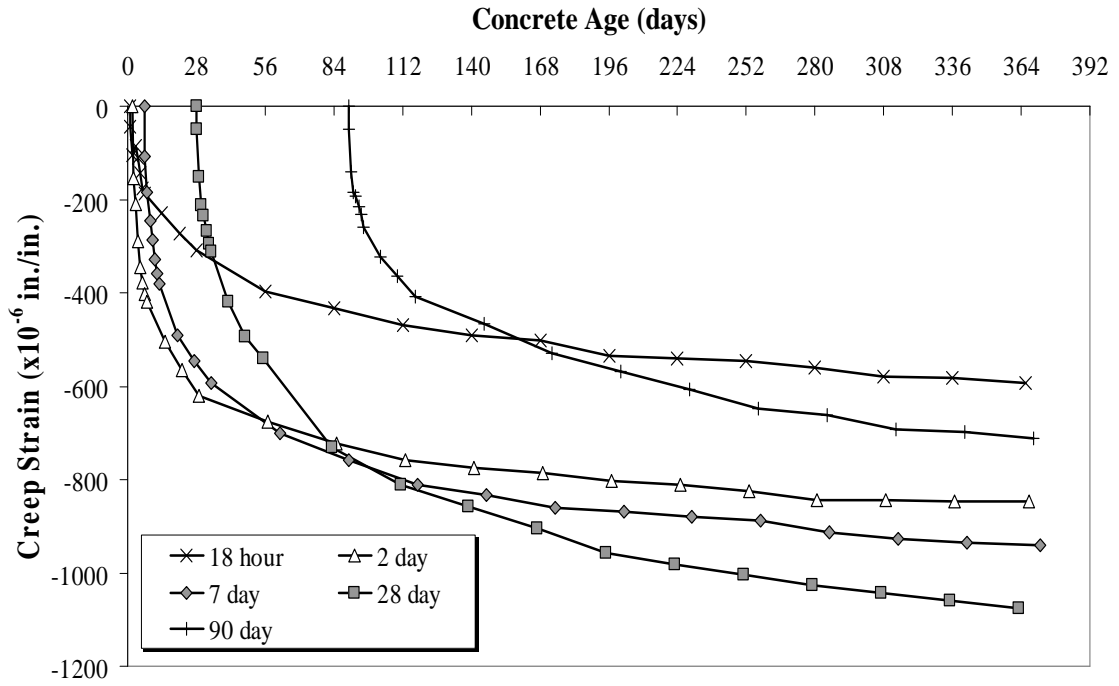
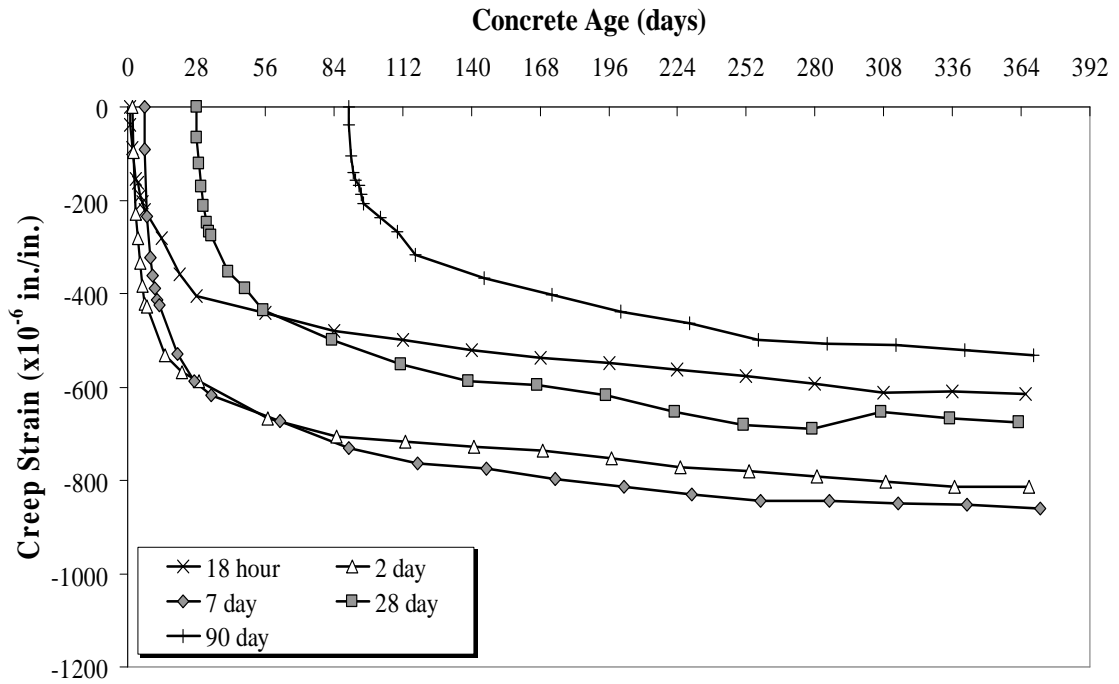


Figure 4-7: Creep strain development for the conventional-slump mixture



**Figure 4-8:** Creep strain development for SCC-MS-FA



**Figure 4-9:** Creep strain development for SCC-HS-FA



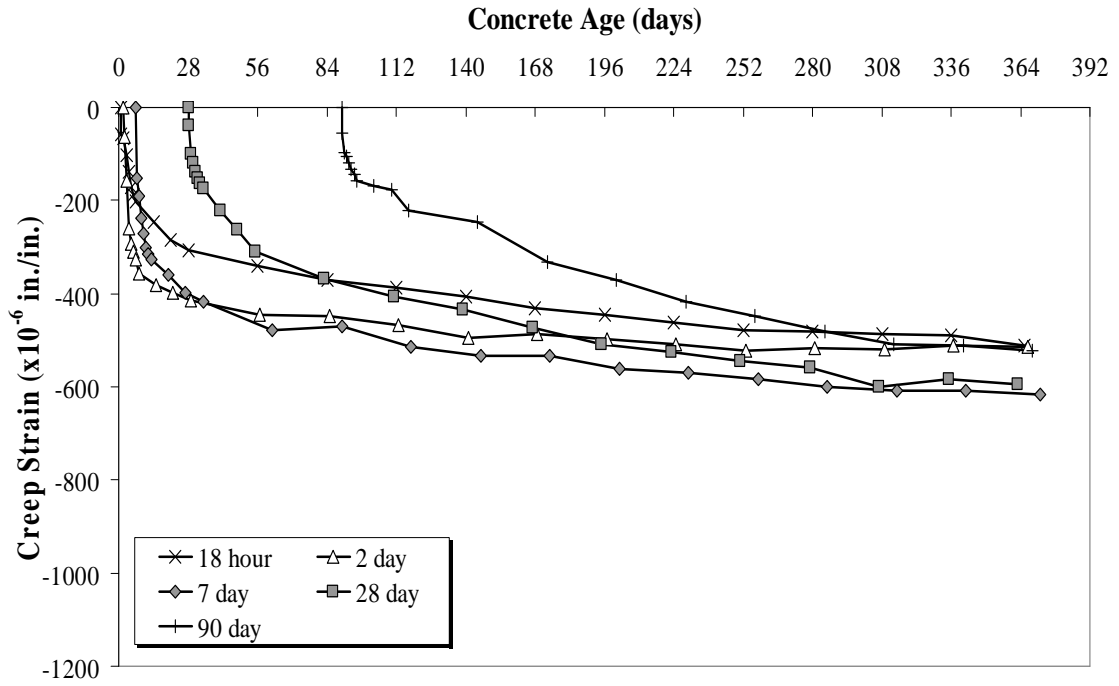


**Figure 4-10:** Creep strain development for SCC-MS-SL

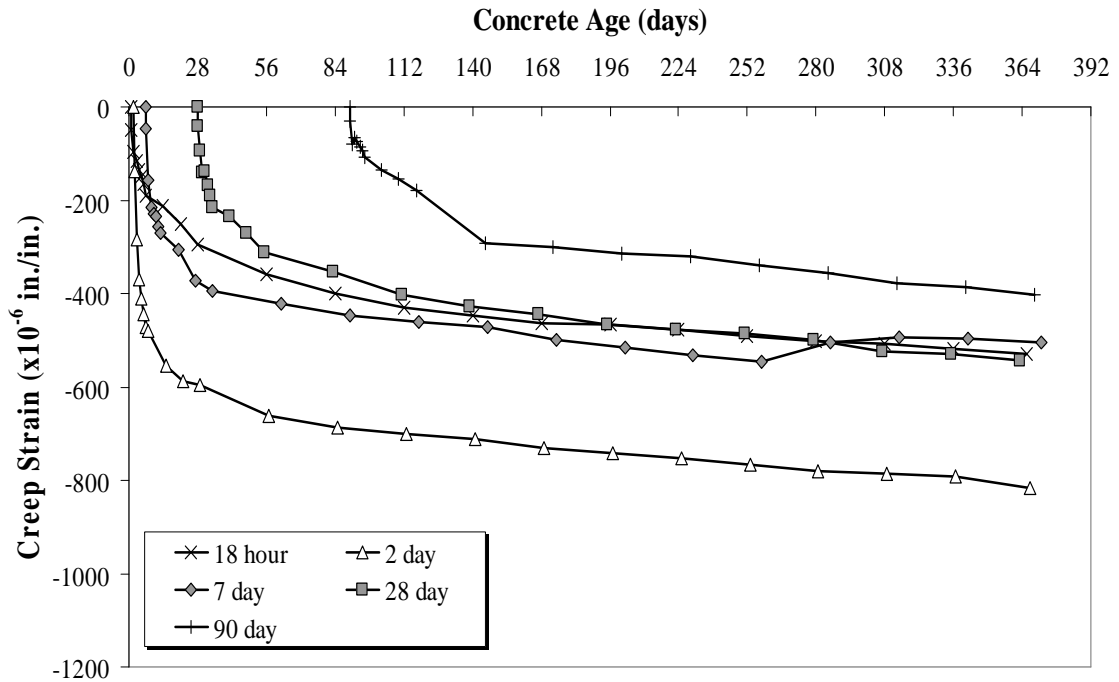


**Figure 4-11:** Creep strain development for SCC-HS-SL

#### 4.4.1.2 Compliance Results

ACI Committee 209 (1997) defines compliance as follows:

$$J(t, t') = \frac{\text{Total strain} - \text{drying shrinkage strain} - \text{autogenous shrinkage strain}}{\text{stress}}$$

where,

$J(t, t')$  = creep compliance at age  $t$  caused by a unit uniaxial sustained load applied at age  $t'$  ( $1 \times 10^{-6}$ /psi)

$t$  = age of the concrete

$t'$  = age of the concrete at loading.

Compliance values allow for a more accurate comparison of creep results because they are normalized for applied load levels and for concrete stiffness (ACI 209 1997). The 365-day measured compliance values for each loading age of each mixture can be seen in Table 4-4. The compliance behavior for each mixture can be seen in Figures 4-12 through 4-16. They are presented slightly different than the creep strain graphs in that they are organized according to loading age and each figure contains the behavior for all five mixtures. Additionally, they show the compliance values versus the concrete age after loading.

**Table 4-4:** 365-day measured compliance values for all loading ages of every mixture

Mixture ID	365-Day Compliance Results ( $1 \times 10^{-6}$ /psi)				
	18 hour	2 day	7 day	28 day	90 day
CTRL	0.55	0.63	0.52	0.43	0.42
SCC-MS-FA	0.44	0.61	0.51	0.48	0.37
SCC-HS-FA	0.35	0.42	0.34	0.29	0.27
SCC-MS-SL	0.39	0.50	0.37	0.31	0.28
SCC-HS-SL	0.32	0.41	0.30	0.27	0.22

#### 4.4.1.2.1 Effects of Water-to-Cementitious Materials Ratio

The effect of the  $w/cm$  on compliance is illustrated in Figures 4-12 through 4-16, where it is evident that compliance decreases as the  $w/cm$  decreases. This is especially evident in Figure 4-12, which depicts the 18-hour loading age compliance values. It can be seen that the compliance values decrease with a decrease in the  $w/cm$  for all specimens cured at elevated temperatures. This trend continues for all of the other loading ages too, with one exception. The MS-SL and HS-FA exhibit similar compliance values for the 2-, 7-, 28-, and 90-day loading ages, even though the HS-FA has a lower  $w/cm$  than the MS-SL mixture. The author believes this to be a function of the slag itself; further discussion on this topic will be presented in a later section.

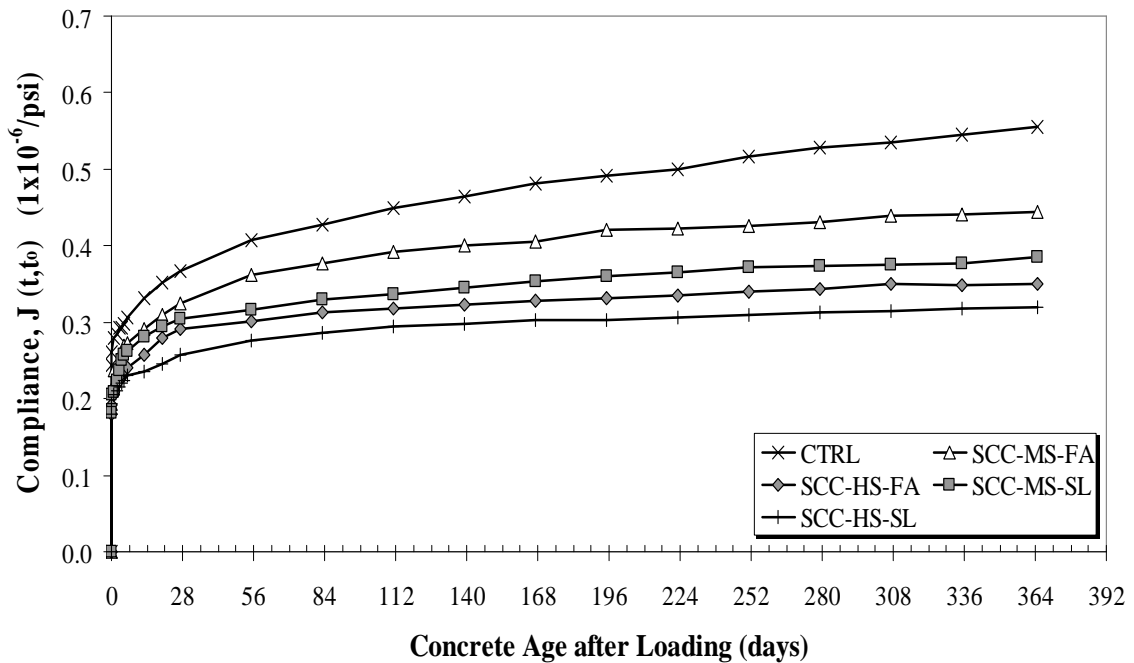


Figure 4-12: 18-hr compliance for all mixtures

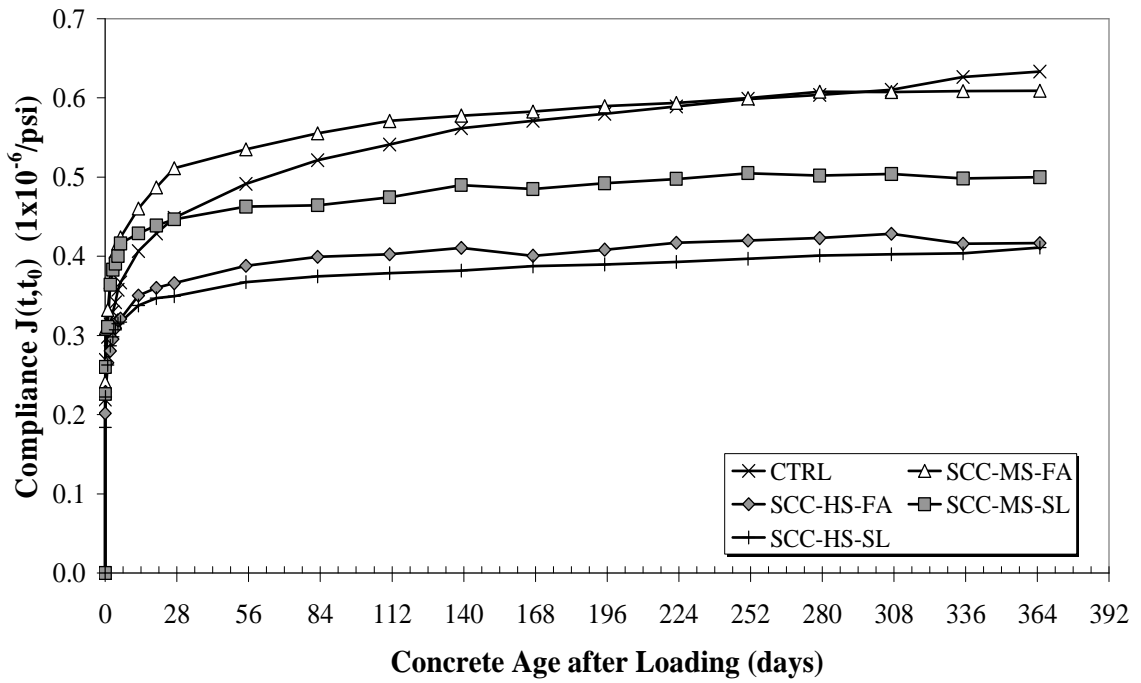


Figure 4-13: 2-day compliance for all mixtures

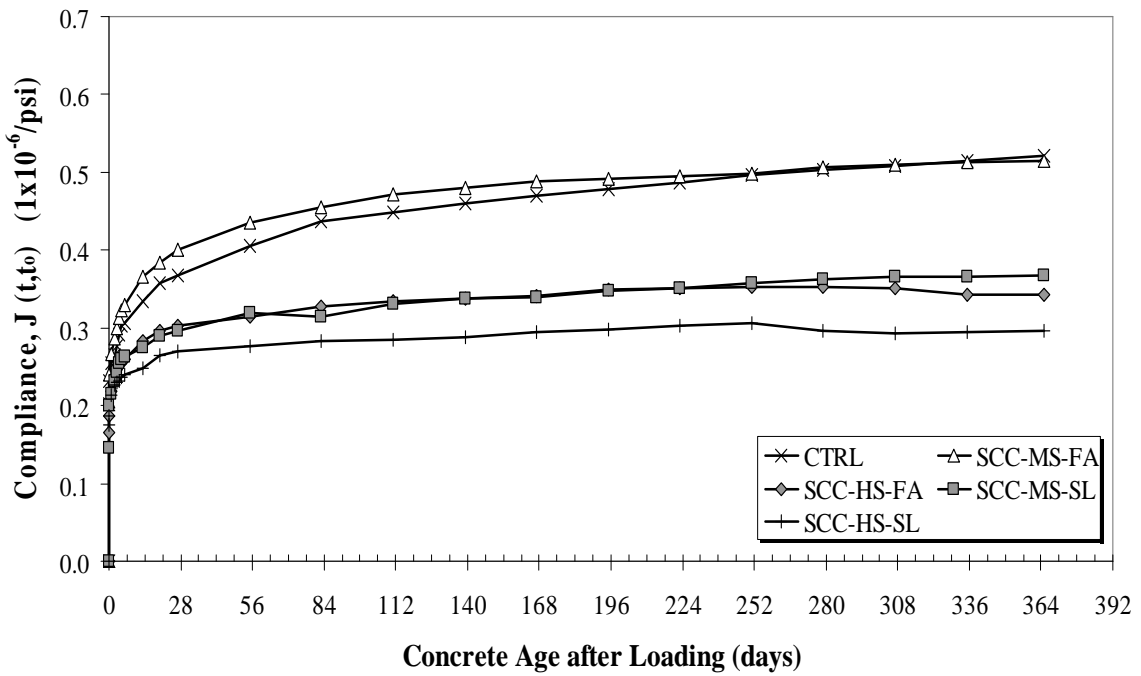


Figure 4-14: 7-day compliance for all mixtures

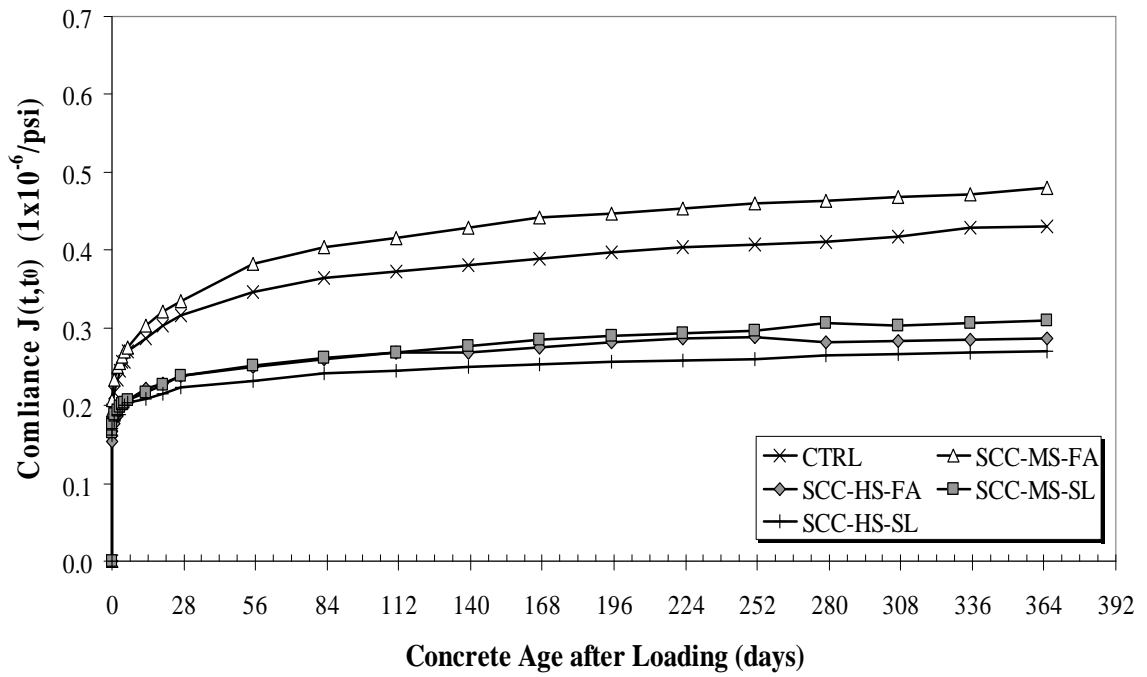


Figure 4-15: 28-day compliance for all mixtures

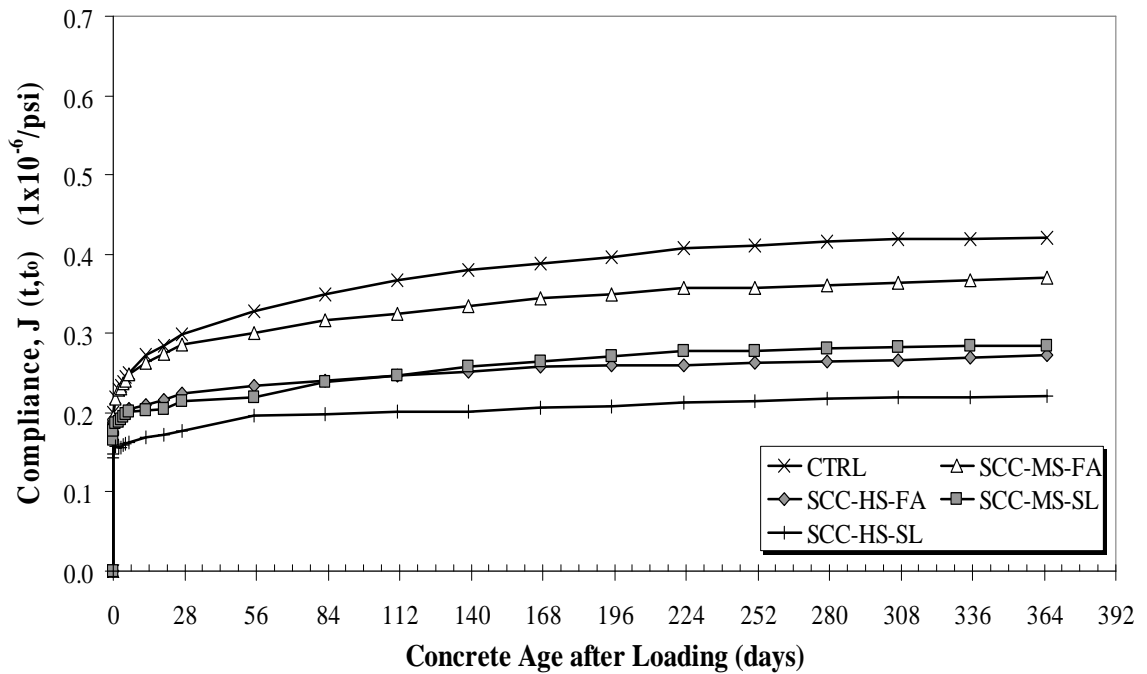


Figure 4-16: 90-day compliance for all mixtures

#### **4.4.1.2.2 Effects of Cementitious Materials System**

The effects different cementitious materials systems have on the compliance values can be evaluated from the results shown in Figures 4-12 through 4-16. On the whole, the compliance values associated with the slag mixtures are lower than those measured for the fly ash mixtures when only mixtures of similar strengths are compared.

The most surprising trend that was noted related to the moderate-strength slag mixture. This mixture exhibited far lower compliance values (on average, 31% lower) than its contemporary in the fly ash category. Furthermore, as previously stated, the moderate-strength slag mixture exhibited similar compliance values to the high-strength fly ash mixture at the 7-, 28-, and 90-day loading ages. The reasoning behind this trend is believed to be related to the dense micropore structure and low permeability commonly associated with concrete comprised of a cement replacement of GGBF slag.

#### **4.4.1.2.3 Behavior of SCC versus Conventional-Slump Concrete**

Figure 4-17 shows the compliance results of all loading ages for all SCC mixtures relative to the compliance results of the conventional-slump mixture. For the 18-hour loading age (i.e. the accelerated curing condition), the compliance values of all the SCC mixtures are less than the conventional-slump mixture. The compliance values for all loading ages shown are also less for the moderate-strength GGBF slag mixture, and for both high-strength SCC mixtures as compared to the corresponding control mixture compliance values. At loading ages of 28 and 90 days, the 365-day compliance is approximately 18% greater and 13% less, respectively, for Mixture SCC-MS-FA than for the control mixture. These differences are not very large. Thus, for practical purposes,

the creep behavior is similar for the moderate-strength fly ash SCC and conventional-slump concrete.

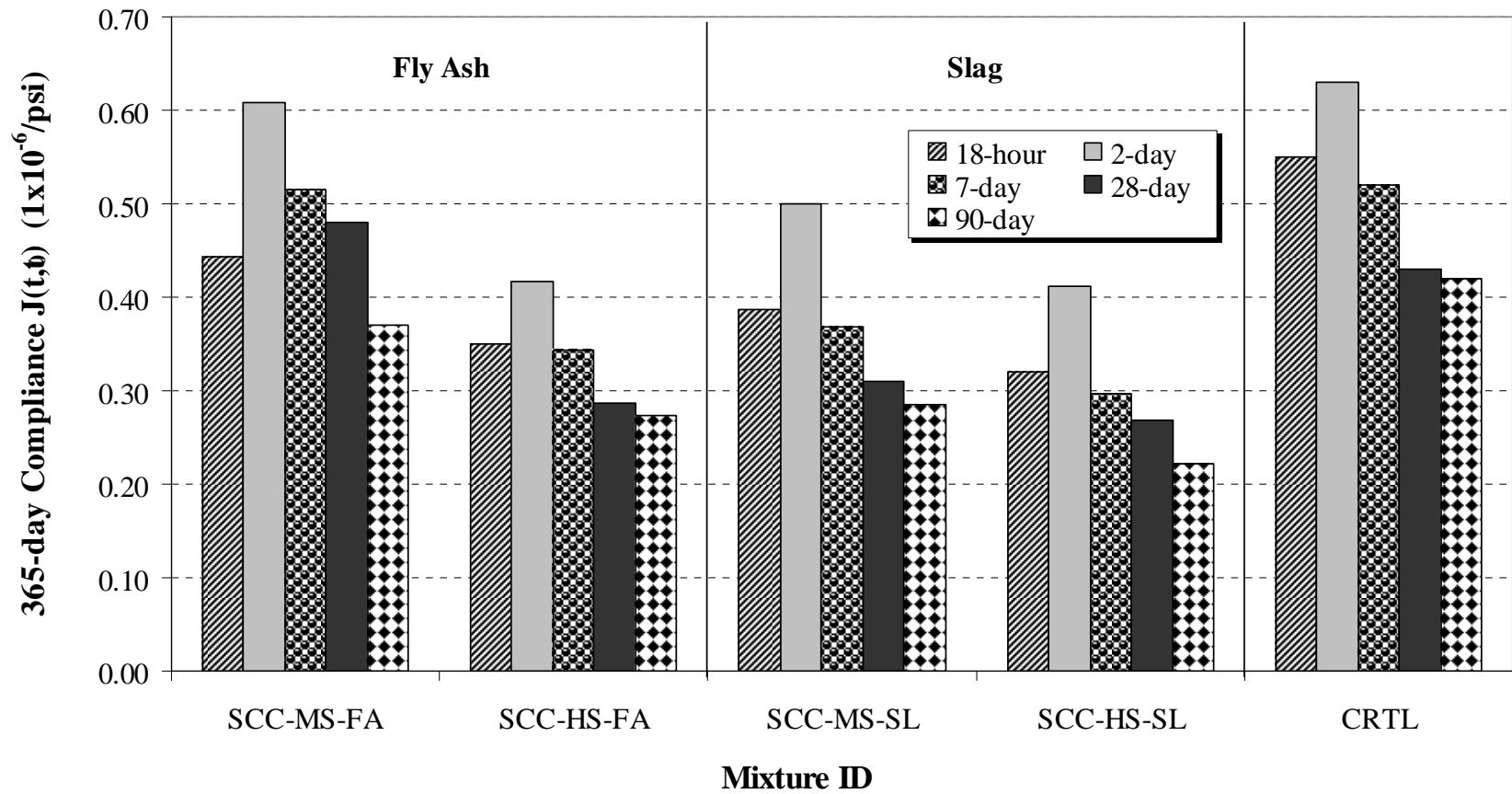


**Figure 4-17:** 365-day compliance values for all SCC mixtures and the conventional-slump mixture



#### 4.4.2 DRYING SHRINKAGE

The results for the drying shrinkage data are presented in this section; however, the 365-day drying shrinkage values for all loading ages of all mixtures are presented in summary form in Table 4-3 in the previous section. The 18-hr match-cured SCC samples exhibited 365-day drying shrinkage values ranging between -223 and -301 microstrain. The 2-, 7-, 28-, and 90-day SCC samples experienced 365-day drying shrinkage values ranging between -255 and -329 microstrain, -225 and -301 microstrain, -87 and -174 microstrain, and -71 and -101 microstrain, respectively. The drying shrinkage strain development data are presented in Figures 4-18 through 4-22 and include all loading ages for one mixture within each chart.

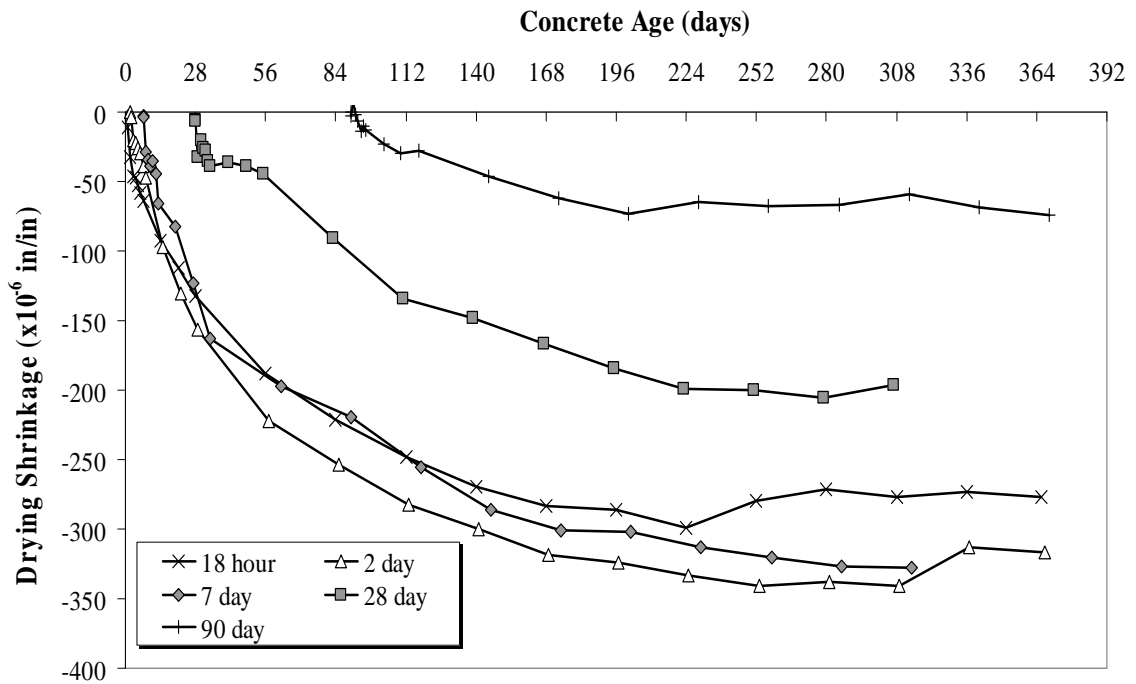


**Figure 4-18:** Drying shrinkage strain development for the conventional-slump mixture

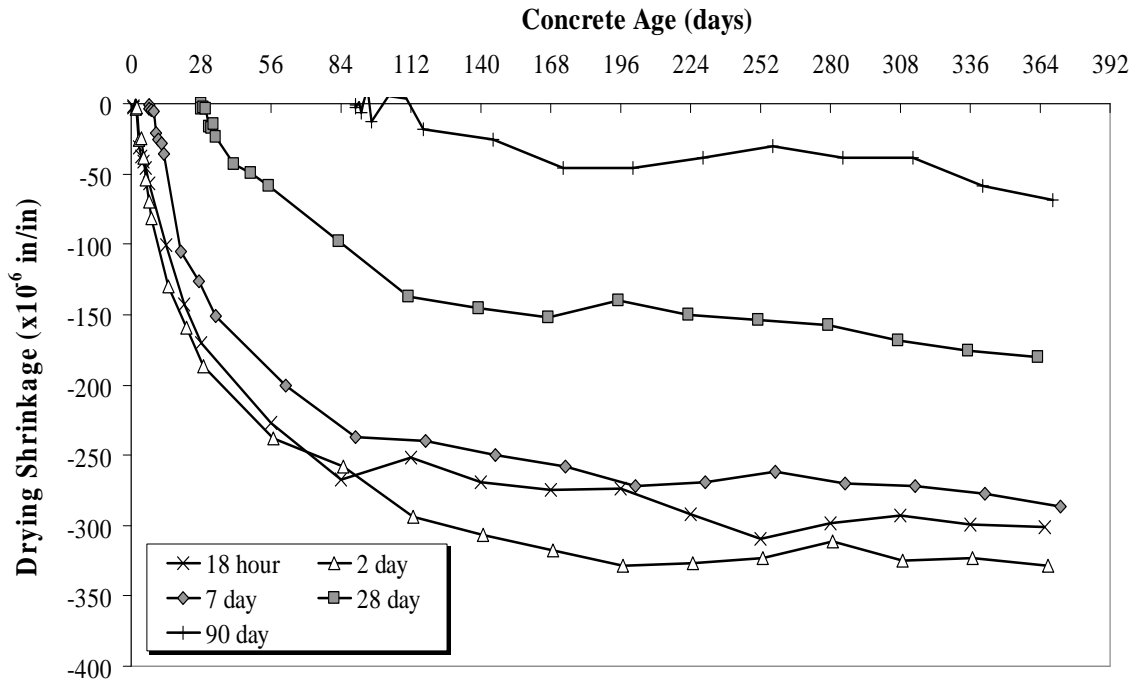


**Figure 4-19:** Drying shrinkage strain development for the SCC-MS-FA mixture

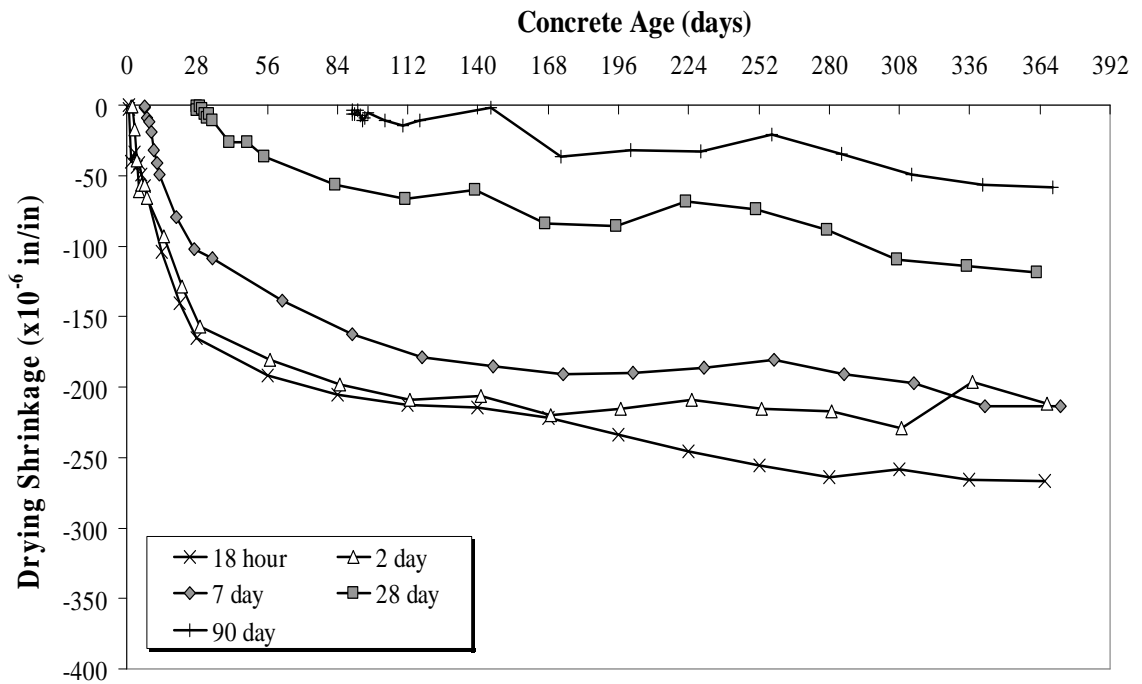


**Figure 4-20:** Drying shrinkage strain development for the SCC-HS-FA mixture

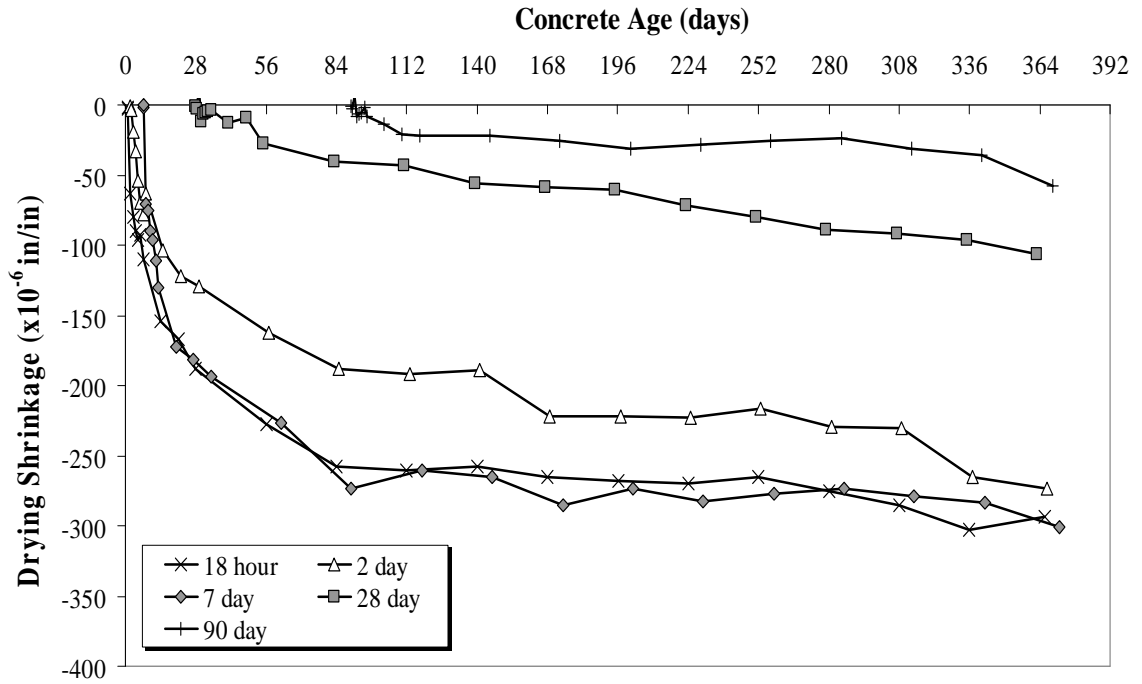


**Figure 4-21:** Drying shrinkage strain curve for the SCC-MS-SL mixture

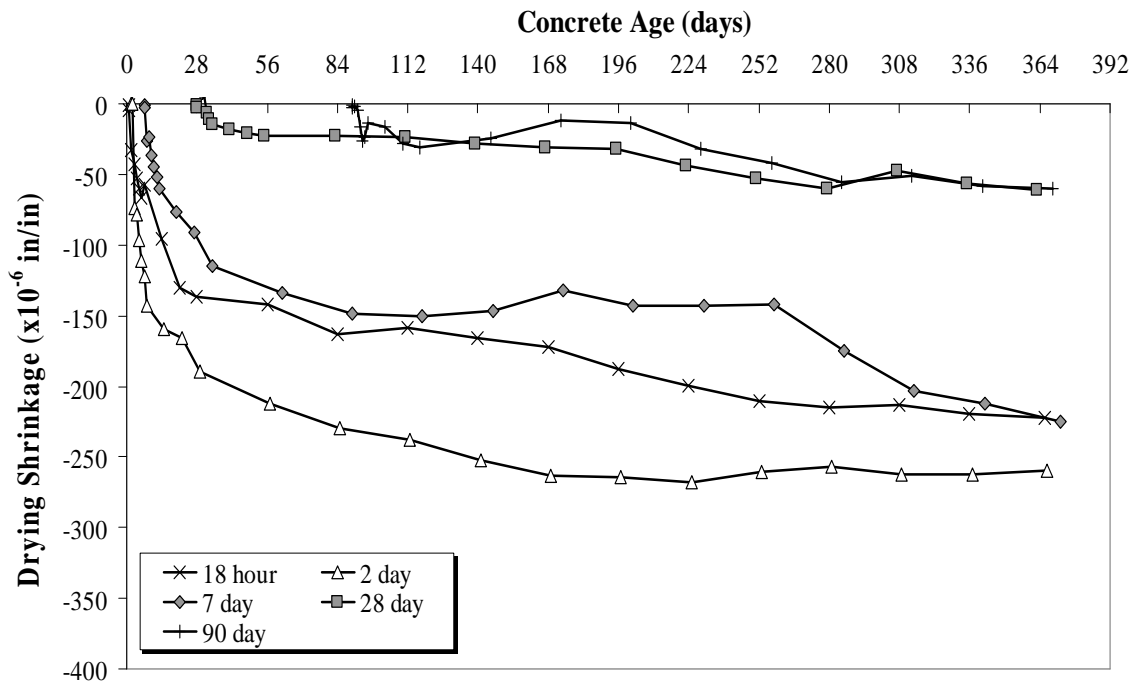


**Figure 4-22:** Drying shrinkage strain curve for the SCC-HS-SL mixture

#### 4.4.2.1 Effects of Water-to-Cementitious Materials Ratio

The effects of changes in  $w/cm$  can be seen for both SCM categories in Figures 4-23 through 4-27, which are organized according to loading age. For the 18-hr specimens, as the  $w/cm$  reduced, the fly ash mixtures exhibited an 11% reduction in the 365-day  $\epsilon_{SH}$ , while the slag mixtures exhibited a 24% reduction. This trend continued for the other ages as well. The 2-day specimens saw a 5% and 22% decrease, respectively, for the slag and fly ash mixtures as the  $w/cm$  decreased, and the 7-, 28-, and 90-day specimens exhibited a 6% and 25%, a 28% and 22%, and an 18% and 26% decrease in  $\epsilon_{SH}$  as the  $w/cm$  decreased.

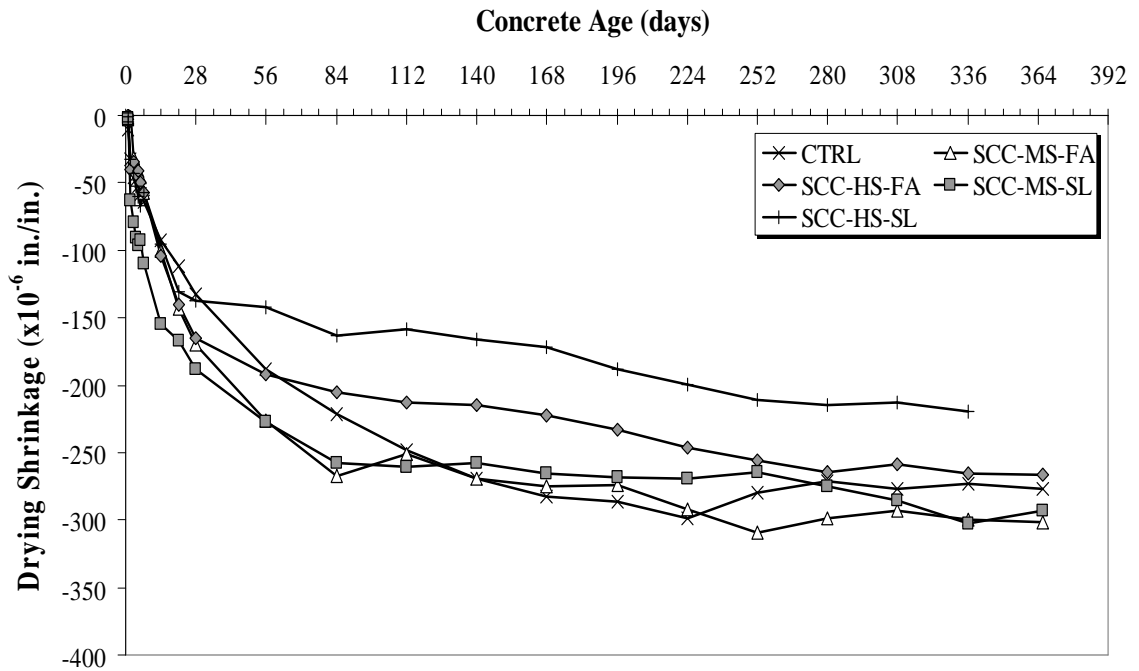


Figure 4-23: 18-hr drying shrinkage strains for all SCC mixtures

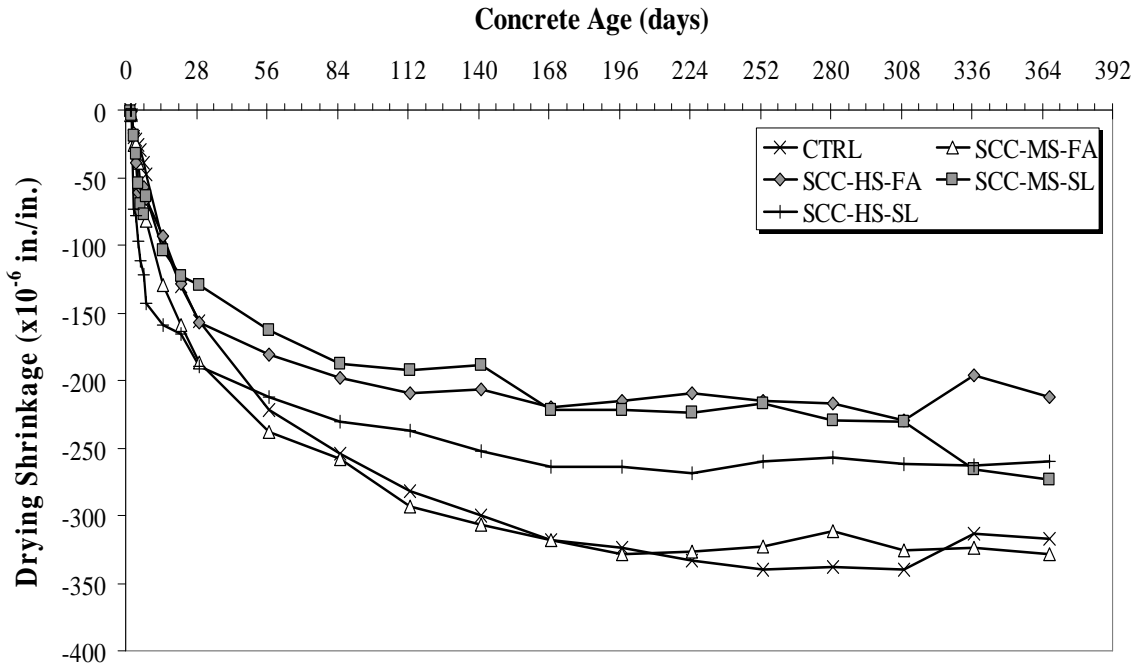


Figure 4-24: 2-day drying shrinkage strains for all SCC mixtures

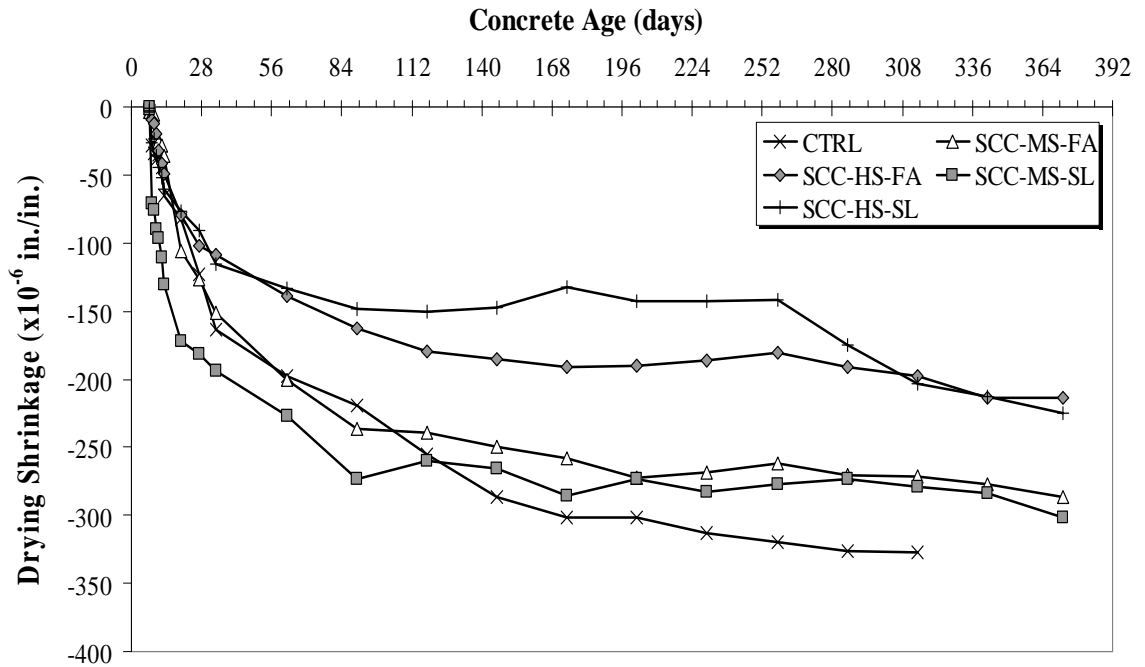


Figure 4-25: 7-day drying shrinkage strains for all SCC mixtures

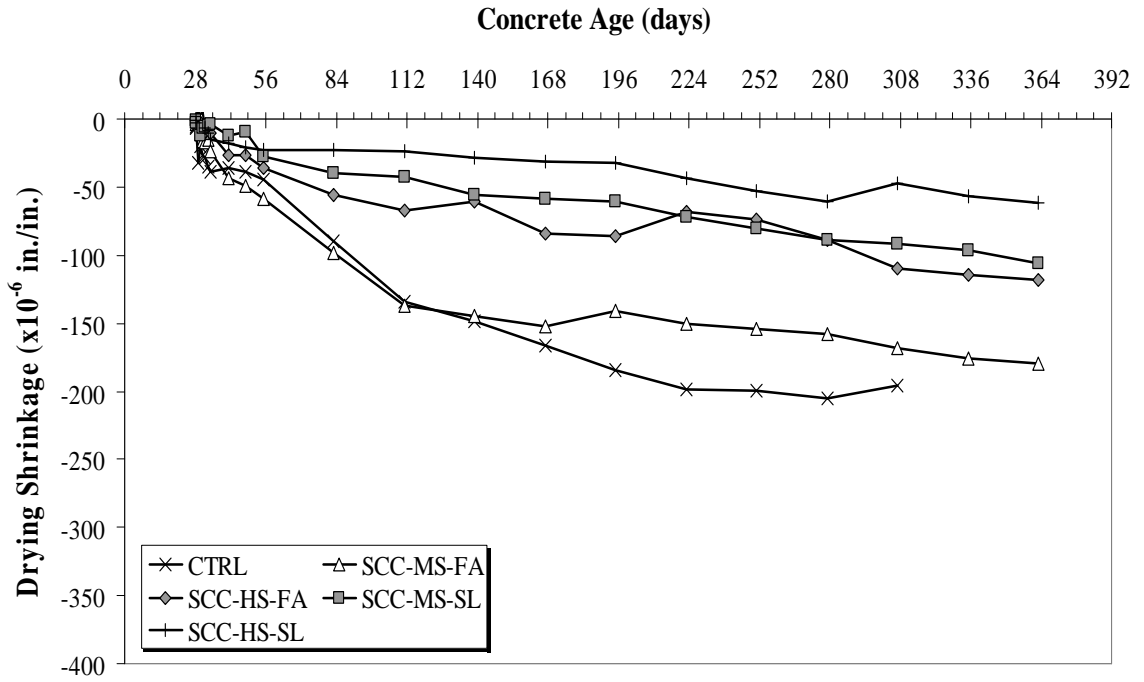


Figure 4-26: 28-day drying shrinkage strains for all SCC mixtures

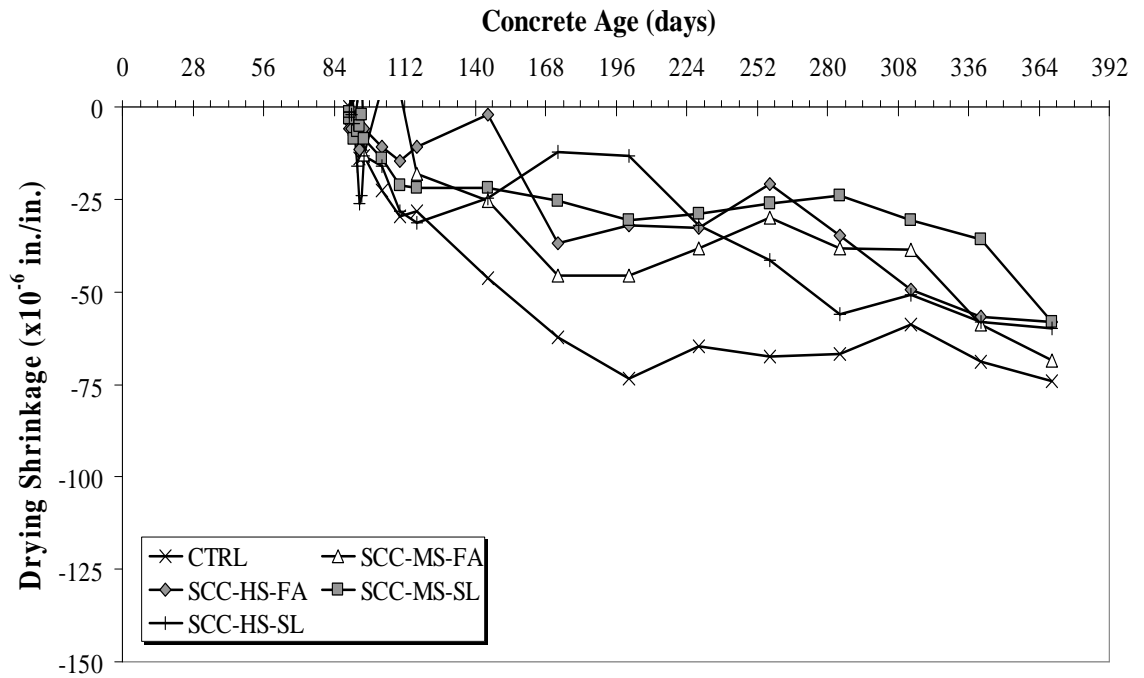


Figure 4-27: 90-day drying shrinkage strains for all SCC mixtures

#### **4.4.2.2 Effects of Cementitious Materials System**

The effects both slag and fly ash had on  $\epsilon_{SH}$  can be seen in Figures 4-23 through 4-27, which are arranged according to the loading age of the test specimens. From those figures, no definitive trend can be seen that occurs over all loading ages. On average, there is less than an 8% difference in  $\epsilon_{SH}$  between the fly ash and slag mixtures at all loading ages. The only outlier is in the 28-day specimens of SCC-HS-SL, where the 365-day drying shrinkage strain value is -87 microstrain. Aside from this data point, all other specimens exhibited  $\epsilon_{SH}$  values within 10% of each other. It can thus be concluded that no appreciable difference in drying shrinkage exists between the SCC mixture containing slag and the one containing fly ash.

#### **4.4.2.3 Behavior of SCC versus Conventional-Slump Concrete**

The analysis that follows is illustrated in Figure 4-28, which shows the 365-day drying shrinkage strain values for all loading ages of all SCC mixtures against those of the conventional-slump mixture. No obvious trends present themselves here either, except one. All SCC mixtures share comparable drying shrinkage traits with the conventional-slump mixture. For this reason, it is believed that members constructed from the SCC mixtures tested in this study should behave similarly to those built using conventional-slump concrete, with no abnormally large drying shrinkage strains expected.

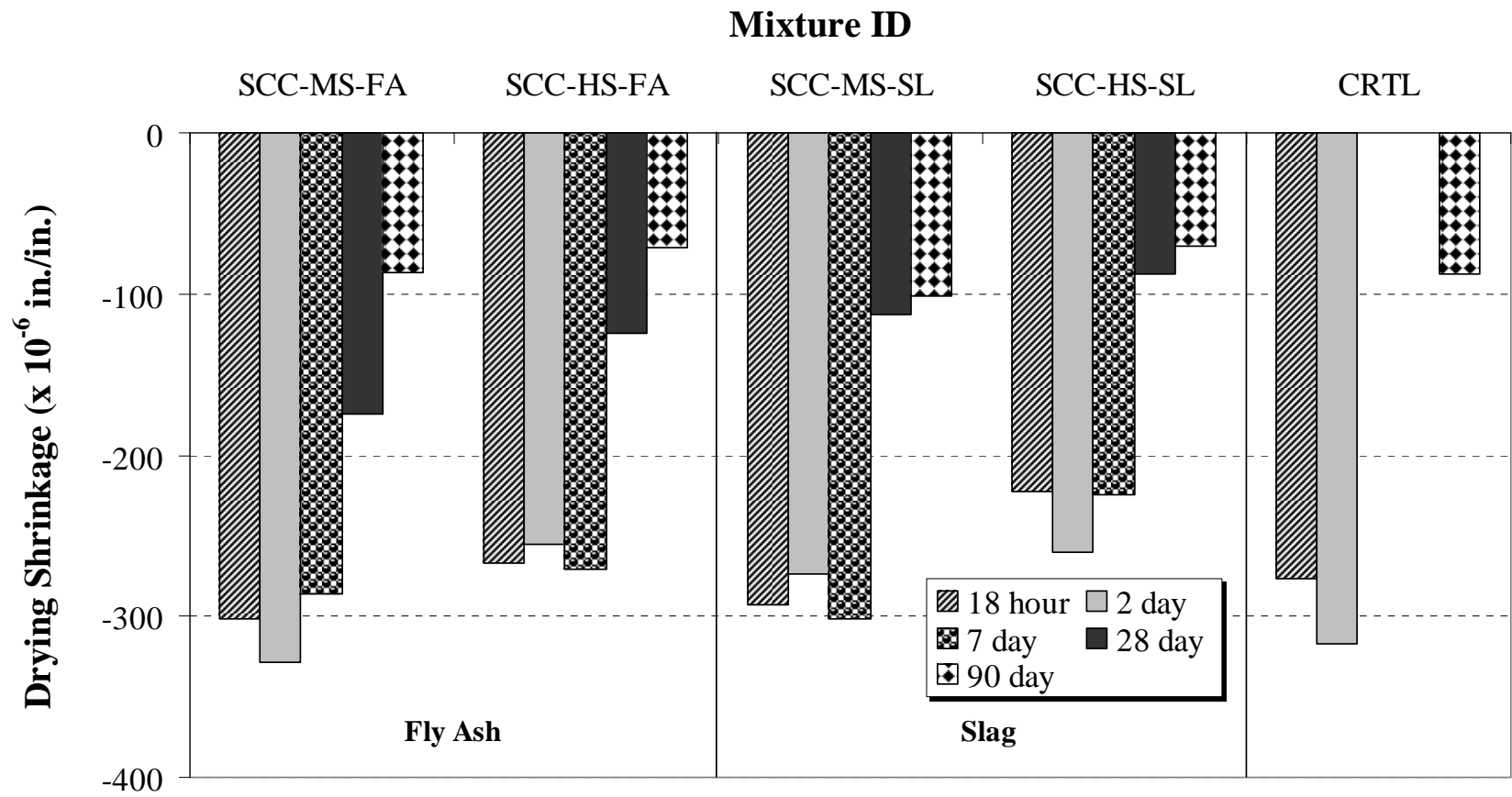


**Figure 4-28:** 365-day drying shrinkage strains for all SCC mixtures and the conventional-slump mixture



#### **4.4.3 ENVIRONMENTAL CONDITIONS**

All testing (creep and drying shrinkage) was performed in a climate-controlled room, which is described in detail in Section 3.4.6.2. The ambient conditions within this room were monitored using a data collection unit. The average temperature was 71.9°F (22.2°C), while the minimum and maximum temperatures were 70.0°F (21.1°C) and 74.2°F (23.4°C), respectively. Additionally, 93% of the collected temperature data were within the range specified by ASTM C 512, which was  $73.4 \pm 2^\circ\text{F}$  ( $23.0^\circ\text{C}$ ).

The relative humidity was also measured over the entire duration of testing. The average was 48.7%, while the minimum and maximum relative humidity values were 40.7 and 61.6%, respectively. In addition, 96% of the relative humidity data were within the range specified by ASTM C 512, which was  $50 \pm 4\%$ .

#### **4.4.4 TRACKING AND MAINTAINING THE APPLIED LOAD**

ASTM C 512 requires the applied load placed on test specimens to be maintained within  $\pm 2\%$  of the target load for the duration of testing. If a change in applied load occurs that is outside this range, the load must be adjusted before creep measurements are taken. This stipulation required that the applied load be tracked and maintained.

The frames that were designed and built for this study are described thoroughly in Section 3.5.6.1. Unlike many creep frames, these employed flexible springs which allowed for greater displacement to occur before an unwanted drop in applied load occurred. The design worked well and only required load to be reapplied during the early periods of data collection. A chart which tracks the applied load of the creep frame that

contained the 18-hour specimen of the control mixture is shown in Figure 4-29. One of these charts was created for each of the 25 frames used during testing.

As stated above, all creep frames were maintained within  $\pm 2\%$ , except one. The frame containing the 90-day test specimen for SCC-HS-FA was allowed to exceed the specified range because cracks were noticed on the specimens themselves. To avoid increasing crack widths, it was decided that the applied load would be allowed to decrease. The largest difference recorded for the concrete specimens was  $-4.69\%$ .

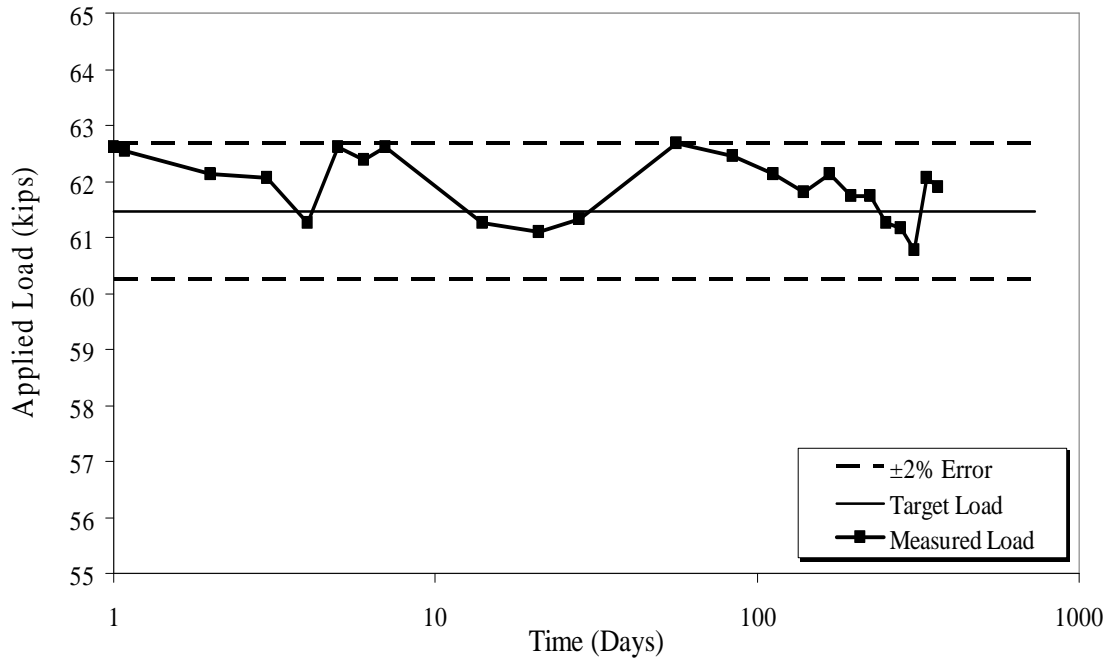


**Figure 4-29:** The applied load on the 18-hour specimen of the control mixture

Table 4-5 contains the maximum positive and negative percent error values for all 25 mixtures. From this table, it can be seen that all mixtures stayed within the  $\pm 2\%$  applied load range specified in ASTM C 512, except for the one SCC-HS-FA case noted above.

**Table 4-5:** Maximum positive and negative percent errors in applied load

<b>Mixture ID</b>	<b>Maximum Negative Error in Applied Load, (%)</b>	<b>Maximum Positive Error in Applied Load, (%)</b>
<b>CTRL-18</b>	-1.13	2.00
<b>CTRL-2</b>	-0.53	2.00
<b>CTRL-7</b>	-1.86	1.76
<b>CTRL-28</b>	-1.77	1.57
<b>CTRL-90</b>	-1.95	2.00
<b>SCC-MS-FA-18</b>	-1.81	2.00
<b>SCC-MS-FA-2</b>	-1.88	1.70
<b>SCC-MS-FA-7</b>	-0.37	2.00
<b>SCC-MS-FA-28</b>	-1.94	1.06
<b>SCC-MS-FA-90</b>	-1.06	2.00
<b>SCC-HS-FA-18</b>	-1.95	0.15
<b>SCC-HS-FA-2</b>	-1.64	2.00
<b>SCC-HS-FA-7</b>	-1.99	2.00
<b>SCC-HS-FA-28</b>	-1.64	1.69
<b>SCC-HS-FA-90</b>	-4.69*	0.00
<b>SCC-MS-SL-18</b>	-1.87	1.27
<b>SCC-MS-SL-2</b>	-1.83	1.60
<b>SCC-MS-SL-7</b>	-1.79	1.91
<b>SCC-MS-SL-28</b>	-1.64	0.59
<b>SCC-MS-SL-90</b>	-1.99	0.00
<b>SCC-HS-SL-18</b>	-1.92	0.00
<b>SCC-HS-SL-2</b>	-1.26	1.93
<b>SCC-HS-SL-7</b>	-1.86	1.94
<b>SCC-HS-SL-28</b>	-1.97	0.26
<b>SCC-HS-SL-90</b>	-1.96	0.00

Note: \* denotes the one frame that was allowed to go beyond the  $\pm 2\%$  range specified in ASTM C 512.

#### 4.5 RAPID CHLORIDE ION PENETRATION TEST

To determine the resistance of each concrete mixture to the rapid penetration of chloride ions, tests were conducted in accordance with ASTM C 1202 (2005). Table 4-6, which indicates the chloride ion penetration of concrete based on the charge passed, was taken directly from ASTM C 1202 (2005). It indicates the penetrability of concrete based on the range of measured charge. Table 4-7 shows the average values that were measured for each mixture in this study. There it may be seen that all of the SCC mixtures registered average charges that were in the very low range. Even the conventional-slump mixture registered an average value that was low.

**Table 4-6:** Chloride ion penetrability based on charge passed (ASTM C 1202 2005)

Charge Passed (coulombs)	Chloride Ion Penetrability
>4,000	High
2,000-4,000	Moderate
1,000-2,000	Low
100-1,000	Very Low
<100	Negligible

**Table 4-7:** Average 91-day total charge measured and resulting penetrability

Mixture ID	Average Total Charge, coulombs	Chloride Ion Penetrability
CTRL	1866	Low
SCC-MS-FA	530	Very Low
SCC-HS-FA	224	Very Low
SCC-MA-SL	558	Very Low
SCC-HS-SL	503	Very Low

## **4.6 LESSONS LEARNED THROUGH TESTING**

This section details experienced gained over the course of performing the tests outlined in ASTM C 512. Here the reader will find information regarding lessons learned while designing and building the creep frames, preparing the test specimens, and conducting creep testing.

### **4.6.1 DESIGNING AND BUILDING CREEP FRAMES**

This section outlines lessons learned through the design-build process of this study.

#### **4.6.1.1 Creep Frame Design**

For the most part, the creep frames that were designed for this study performed very well, and the material choices were well thought-out. One portion of the frame design that worked quite well was the spring assembly. As stated earlier in this report, the springs allowed relatively large displacements to occur before requiring the reapplication of applied load. In fact, the only time load needed to be reapplied was in the early phases of testing when relatively large amounts of creep occurred. Beyond the one month time point, no frame needed to have load reapplied.

In contrast to the superb performance of the springs, the caster arrangement was less satisfactory; however, it should be noted that the casters themselves were a good idea. They just needed to be rearranged to allow for greater mobility in tight areas. The two swivel casters, which were the only casters that were able to turn and promote mobility, were placed on the wrong side of the lower static reaction plate. In their present location, they were unable to swivel a full 360 degrees due to interference with two of the steel bars that protruded through the plate and restricted rotation. For future frame designs it

would be best if the swivel casters were placed on the side of the lower static reaction plate that contains only one protruding steel bar.

The addition of more alignment marks would also be a design improvement. These marks were used to help align the springs on the lower static reaction plate and the test specimens onto the upper floating reaction plate; however, they would also be helpful in other locations. For instance, alignment marks should be placed on top of the upper floating reaction plate to help align the bottom of the jacking mechanism and on the underside of the upper static reaction plate to help align the jack vertically. Both of these improvements would help to further limit the possibilities of having eccentrically loaded specimens.

#### **4.6.1.2 Creep Frame Construction**

The construction process became easier as more frames were built and more knowledge was gained in the area. It became clear after building one or two frames that the easiest way to construct these frames was in the horizontal position due to the heavy nature of all the pieces.

The process began by attaching all casters to the lower static reaction plate and then locking the swivel casters so they were inline with the non-rotating casters. At this point, the steel rods were inserted into the lower static reaction plate and nuts were tightened down on the top and bottom of the plate to secure the rod firmly to the plate. Next the springs were slid into place. With the springs in place, the lower floating reaction plate was aligned on the steel rods and slid into place. Then all the necessary nuts were threaded on to the rods and the upper floating reaction plate was moved into place. This

process was repeated for the upper static reaction plate. When all plates were in place, the frame was lifted upright using an overhead gantry-crane. With the frame in the upright position, the strain gauges were installed and were coated with a protective coating.

After completing the construction process, each frame was load tested to determine the accuracy of the strain measuring instrumentation. This process entailed loading test specimens into the frames and applying load up to 120 kips and then releasing the load. This was done three times and the measured load was recorded at 20 kips intervals on each run and checked against the known applied load. After the completion of the final run, a calibration factor was assigned to the frame in order to improve the accuracy of the applied load measurement. When this was complete, the frame was ready for service.

#### **4.6.2 PREPARING SPECIMENS**

Many lessons were learned while preparing the test specimens for testing. This section outlines that experience and includes information on casting and final specimen preparation.

##### **4.6.2.1 Mixing and Casting Specimens**

During the mixing and casting phase of this study, it was determined that batch size was critical. Too large of a batch required extra time to homogenize the mixture constituents. This reduced the time available for fresh properties testing and actual casting. Therefore, as previously stated, it was decided that no batch be larger than  $5.5 \text{ ft}^3$ . This meant that multiple batches were mixed, which was not the ideal condition, but the quality of the finished specimens greatly improved by following this guideline.

Furthermore, as was previously stated, the air-entraining admixture (AEA) was left out of the final mixtures. This was decided upon after preliminary mixing revealed erratic air-content values between different batches of the same mixture. By leaving the AEA out, this problem was circumvented and all batches were much more uniform.

#### **4.6.2.2 Final Specimen Preparation**

After curing was complete, all specimens were capped with a sulfur-based compound. This compound needed to harden properly before any load was applied. For this reason, all specimens were capped before attaching the Demountable Mechanical (DEMEC) points. This allowed all specimens extra time to harden before any testing took place. This also proved to be a more efficient use of time.

After the proper amount of time was allowed for hardening, the strength specimens were tested and the ultimate strength of the test specimens determined. At this point, the creep test specimens were loaded into the frames and the load was applied.

#### **4.6.3 CONDUCTING CREEP TESTING**

ASTM C 512 is not a test that is run with any great regularity. For this reason, there is a certain level of uncertainty involved; however, after going through the process several times, many of the “kinks” were worked out and the best procedure was determined. This section outlines lessons learned regarding this test procedure.

The first lesson learned was with regard to data collection. This test requires that many data points be collected, which makes collecting and properly tracking all of the information very important. The use of good data collection methods and information



storage is paramount. Furthermore, the timely gathering of this information is of great importance because there are so many times at which it must be collected.

The second lesson learned pertains to specimen alignment, which is crucial when performing creep testing. If eccentricities are allowed, erratic strain measurements will ensue. For this reason, properly determining the best alignment of the test specimens is of the utmost importance. During this study, specimens were stacked on a level surface, in their test configuration, prior to being placed into the creep frame. A level was then placed on top of the upper concrete plug and the specimens were rotated until the best alignment was found. In this case, that meant a level reading was observed all along the top of the upper concrete plug.

Alignment also is important within the frames. For this reason, it is crucial that the specimens be in good alignment with the frame itself. Otherwise, the possibility of eccentricity increases. This is where the alignment marks mentioned in Sections 3.4.6.1 and 4.5.1.1 come into play. These marks make this process easier and the alignment more uniform for all frames. In addition to these alignment tools, other tools would also be beneficial. For instance, a jig to help align the test cylinders properly amongst themselves and the creep frame would greatly help to efficiently achieve proper alignment.

## **4.7 SUMMARY OF RESULTS**

### **4.7.1 FRESH PROPERTIES**

From this research, the following conclusions can be drawn about the fresh properties of SCC:

- For a given SCM, as the  $w/cm$  decreases, the T-50 time increases, which indicates that the viscosity increases with a decrease in  $w/cm$ .
- GGBF slag mixtures exhibited larger T-50 times than fly ash mixtures proportioned to provide similar 18-hour strengths.

#### **4.7.2 HARDENED PROPERTIES**

From this research, the following conclusions can be drawn about the hardened properties of SCC:

- Mixtures containing GGBF slag gained compressive strength at a slower rate than those containing a cement replacement of Class C fly ash.
- When curing is accelerated and the load is applied at 18 hours, the creep of all the SCC mixtures is less than the creep of the conventional-slump mixture.
- Since the accelerated curing condition simulates plant conditions, excessive creep is not expected for full-scale members constructed with these SCC mixtures.
- All SCC mixtures cured under elevated or standard laboratory temperature exhibited creep values similar to, or less than, that of the conventional-slump concrete mixture.
- When curing is *not* accelerated, the creep behavior of the moderate-strength fly ash SCC and the conventional-slump mixture is similar.
- The high-strength mixtures had the highest paste content, but exhibited less creep than any of the moderate-strength mixtures. This is attributed to

the increased strength and decreased permeability of the hydrated cement paste of these low- $w/cm$  mixtures.

- At a fixed  $w/cm$ , SCC mixtures made with GGBF slag creep less than those made with fly ash, regardless of the age at loading.
- All SCC mixtures exhibited lower drying shrinkage as the  $w/cm$  decreased.
- All SCC mixtures exhibited drying shrinkage strains that were similar in magnitude to the conventional-slump mixture. For this reason, full-scale members constructed with SCC are not expected to experience excessive drying shrinkage.

## **CHAPTER 5**

### **EVALUATION OF CREEP PREDICTION METHODS**

#### **5.1 INTRODUCTION**

As previously stated, one of the main objectives of this study was to evaluate the five creep prediction methods detailed in Section 2.4 in order to determine their effectiveness in estimating creep of SCC. This was accomplished by comparing the measured creep strain ( $\epsilon_{CR}$ ) from each mixture with the  $\epsilon_{CR}$  estimated by the following methods:

- ACI 209 (ACI Committee 209 1997)
- AASHTO (2007)
- CEB 90 (CEB 1990)
- GL 2000 (Gardner and Lockman 2001), and
- B3 (Bazant and Baweja 2000).

The results from that analysis are presented in this chapter and it is organized according to creep prediction methods. The first section of this chapter provides an overview of the statistical methods used to calculate the error associated with each prediction method. A discussion of the accuracy of each method follows in later sections and a summary of all conclusions is located at the end of the chapter. Furthermore, the method found to give the most accurate prediction is calibrated to improve estimations of the creep response for the concrete mixtures used in this study.

## 5.2 STATISTICAL ANALYSIS OF CREEP PREDICTION METHODS

Once all the creep data were collected and the prediction analysis was performed, a statistical comparison of the results of all the methods was performed to determine which method provides the most accurate results. The accuracy of all methods was determined by evaluating the percent error, absolute average error, and the absolute average percent error.

### 5.2.1 COMPARISON STATISTICS

To calculate the percent error, the measured creep strain was subtracted from the estimated creep strain. This difference was divided by the measured creep strain, and the resulting value was multiplied by 100. This calculation can be seen in the equation that follows:

$$\% \text{ Error} = \left( \frac{\hat{y} - \bar{y}}{\bar{y}} \right) \times 100$$

where,

$\hat{y}$  = predicted creep strain, and

$\bar{y}$  = measured creep strain.

The acceptable error range for the creep prediction methods evaluated in this study was chosen to be  $\pm 20\%$ . This was based on literature published by Gardner and Lockman (2001), which stated that predictions for “shrinkage within 15% would be excellent, and a prediction within 20% would be adequate.” Since creep strain is obtained

after subtracting measured shrinkage strains from the total strain, creep prediction within 20% of the measured values should be considered to be excellent.

The absolute average error is not a true statistical value; however, it does provide a single parameter by which the estimated creep strain may be compared to the measured value. A report co-authored by Carino and Tank (1992) provides the following equation, which was used to calculate the absolute average error:

$$AAE = \frac{\sum |\hat{y} - \bar{y}|}{n}$$

where,

$AAE$  = absolute average error, and

$n$  = number of creep strain values in a data set.

The absolute average percent error provides another single-parameter comparison tool to evaluate the accuracy of the predicted creep strain to the measured value. The following equation was used to determine the absolute average percent error:

$$AA\%E = \frac{\sum \left| \left( \frac{\hat{y} - \bar{y}}{\bar{y}} \right) \times 100 \right|}{n}$$

where,

$AA\%E$  = absolute average percent error.

### **5.2.2 RESULTS FROM STATISTICAL ANALYSIS**

Using the error calculations described above, results from each of the prediction methods was compared to the others to evaluate their performance. Tables 5-1 and 5-2 show all of the error values for the non-accelerated-cured and accelerated-cured specimens, respectively. Each table is broken into three areas, each of which contains the results from one of the error calculation types. At the bottom of areas two and three is a section that summarizes which method performed the best for each of the mixtures. This summary is not shown for area one, which is the area showing the maximum positive and negative percent error results; however, the maximum positive and negative error values are listed. Positive error means the predicted creep strain value was larger than the measured value and negative error means the predicted value was less than the measured value.

**Table 5-1 : Error calculation results for the non-accelerated-cured specimens for all mixtures**

<b>Non-Accelerated-Cured Samples</b>					
	<b>Mixtures</b>				
	<b>CTRL</b>	<b>MS-FA</b>	<b>MS-SL</b>	<b>HS-FA</b>	<b>HS-SL</b>
<b>1. Percent Error (%)</b>					
<b>ACI 209</b>					
Positive Range	----	86	115	72	147
Negative Range	-81	-84	-89	-67	-79
<b>AASHTO</b>					
Positive Range	33	41	112	38	84
Negative Range	-98	-98	-99	-96	-97
<b>CEB 90</b>					
Positive Range	20	55	80	70	121
Negative Range	-35	-39	-66	-30	-32
<b>GL 2000</b>					
Positive Range	124	109	217	171	351
Negative Range	-20	-12	-35	----	----
<b>B3</b>					
Positive Range	233	95	118	224	266
Negative Range	-271	-308	-279	-687	-360
<b>2. Absolute Average Error (<math>\mu\epsilon</math>)</b>					
ACI 209	105	150	125	151	211
AASHTO	133	144	163	118	157
CEB 90	80	97	84	59	120
GL 2000	284	436	470	660	806
B3	284	195	252	467	520
<b>Best Method</b>	<b>CEB 90</b>	<b>CEB 90</b>	<b>CEB 90</b>	<b>CEB 90</b>	<b>CEB 90</b>
<b>3. Absolute Average Percent Error</b>					
ACI 209	24	30	37	31	58
AASHTO	35	34	48	31	44
CEB 90	15	16	27	13	38
GL 2000	53	72	124	122	211
B3	64	41	62	94	122
<b>Best Method</b>	<b>CEB 90</b>	<b>CEB 90</b>	<b>CEB 90</b>	<b>CEB 90</b>	<b>CEB 90</b>



**Table 5-2:** Error calculation results for the accelerated-cured specimens for all mixtures

<b>Accelerated-Cured Samples</b>					
	<b>Mixtures</b>				
	<b>CTRL</b>	<b>MS-FA</b>	<b>MS-SL</b>	<b>HS-FA</b>	<b>HS-SL</b>
<b>1. Percent Error (%)</b>					
<b>ACI 209</b>					
Positive Range	102	55	56	75	110
Negative Range	-34	-52	-63	----	-37
<b>AASHTO</b>					
Positive Range	104	----	78	52	83
Negative Range	-93	-95	-96	-92	-93
<b>CEB 90</b>					
Positive Range	179	122	126	123	110
Negative Range	----	----	----	----	----
<b>GL 2000</b>					
Positive Range	616	378	331	808	551
Negative Range	----	----	----	190	----
<b>B3</b>					
Positive Range	162	147	147	218	284
Negative Range	----	-6	-16	----	-77
<b>2. Absolute Average Error (<math>\mu\epsilon</math>)</b>					
ACI 209	160	96	133	244	319
AASHTO	257	165	185	155	211
CEB 90	203	91	106	156	239
GL 2000	559	387	400	853	775
B3	356	350	343	685	765
<b>Best Method</b>	<b>ACI 209</b>	<b>CEB 90</b>	<b>CEB 90</b>	<b>AASHTO</b>	<b>AASHTO</b>
<b>3. Absolute Average Percent Error</b>					
ACI 209	55	28	38	55	89
AASHTO	62	44	54	39	57
CEB 90	86	36	36	47	77
GL 2000	228	140	142	257	265
B3	103	90	95	159	208
<b>Best Method</b>	<b>ACI 209</b>	<b>ACI 209</b>	<b>CEB 90</b>	<b>AASHTO</b>	<b>AASHTO</b>

### 5.3 ACI 209 CREEP PREDICTION METHOD

The ACI 209 creep prediction method was developed before the advent of water-reducing admixtures. Therefore, changes had to be made to account for the high admixture-induced slumps which occur in SCC mixtures. For this reason, the slump correction factor used in the ACI 209 method was computed using the wet slump before any chemical admixtures were added. Additionally, an assumption was made with regards to the interpretation of the meaning of cement content, which in this analysis, was taken to be the total cementitious material content (cement plus SCMs). With these decisions made, the prediction analysis was conducted according to the method outlined in Section 2.4.1.

Figures 5-1 through 5-5 show comparisons of the measured  $\epsilon_{CR}$  to the estimated  $\epsilon_{CR}$  that was calculated using the ACI 209 prediction method. The figures are organized according to mixture, and each figure contains all loading ages for one individual mixture. From Figure 5-1, it may be seen that ACI 209 predicts the  $\epsilon_{CR}$  for conventional-slump concrete with relatively good accuracy; however, it does tend to underestimate the  $\epsilon_{CR}$  values by nearly 20%, with one exception. ACI 209's prediction algorithm does not estimate the 18-hour accelerated curing specimens very well. In fact, according to Table 5-2, the *AA%E* for the 18-hour creep values estimated by the ACI 209 method is 55%.

Figure 5-2, which depicts the comparison for the MS-FA mixture, reveals similar results to Figure 5-1. Here it is clear that ACI 209 estimates values that correspond reasonably well to the measured values for the 18-hour, 2-, 7-, and 28-day specimens. In fact, they are all within reasonable proximity of the 20% error line. In contrast to these findings, the 90-day loading ages were not well estimated by this prediction method.

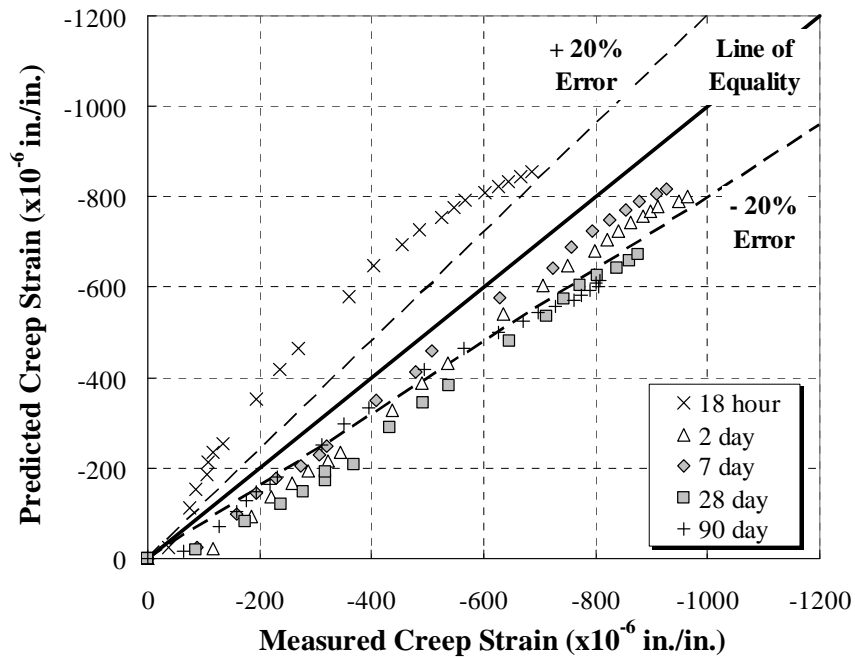
According to Table 5-1, the *AAE* values for the estimated creep of the 90-day specimens was 150 microstrain, which indicates the poor accuracy of this method for this loading age.

Figure 5-3 illustrates the comparison for the HS-FA mixture, which has a lower *w/cm* than both the conventional-slump and MS-FA mixtures. From this figure it can be seen that as the strength level rises, the accuracy of the method diminishes slightly. This is especially evident with the later ages, which consequently are higher in strength. In fact, the creep of the 18-hr, 28-, and 90-day specimens are all overestimated at nearly all ages. While the creep of the 2- and 7-day specimens are underestimated at early ages and overestimated later, as their strength levels rise. It should also be noted that most of the estimated creep values fall outside of the preferable  $\pm 20\%$  error range.

Figure 5-4, which shows the comparison for the MS-SL mixture, illustrates that ACI 209 underestimates the  $\epsilon_{CR}$  values for the 2- and 7- day specimens at early ages. However, the creep estimates for the later ages of the 2-day specimens are overestimated, while prediction error for the 7-day specimens is within the  $\pm 20\%$  criteria. In contrast to these trends, this method significantly overpredicts creep values at all ages for the 18-hr, 28-, and 90-day specimens. This is in agreement with the trends from the comparison of both the moderate- and high-strength fly ash mixtures, which showed that as strength levels increased, prediction accuracy diminished.

Finally, Figure 5-5 illustrates the comparison for the HS-SL mixture, and from this figure it can be seen that ACI 209, in general, does not accurately predict the  $\epsilon_{CR}$  values for mixtures of this strength level. Only some of creep values of the 2-day specimens are ever underestimated and even those are overestimated at later concrete ages.

In Tables 5-1 and 5-2, it can be seen that the ACI 209 method was one of the better performing methods that was investigated; however, it was not the top performer overall. It did provide the most accurate results for the accelerated-cured, conventional-slump mixture, according to both the *AAE* and *AA%E* calculations. Additionally, it provided the most accurate results for the MS-FA mixture according to the *AA%E* statistic.



**Figure 5-1:** Measured versus estimated creep strain for the conventional-slump mixture using the ACI 209 procedure

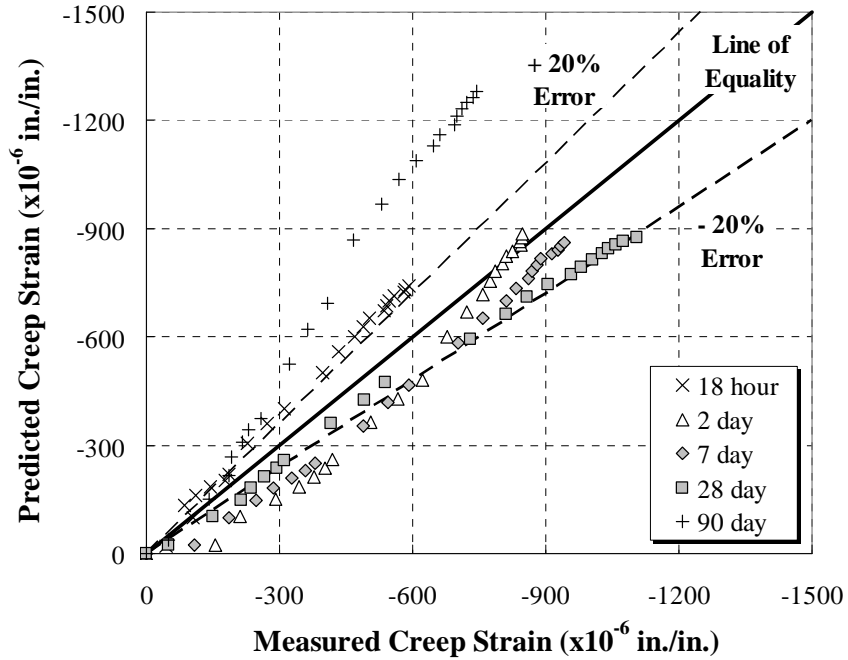


**Figure 5-2:** Measured versus estimated creep strain for the MS-FA mixture using the ACI 209 procedure

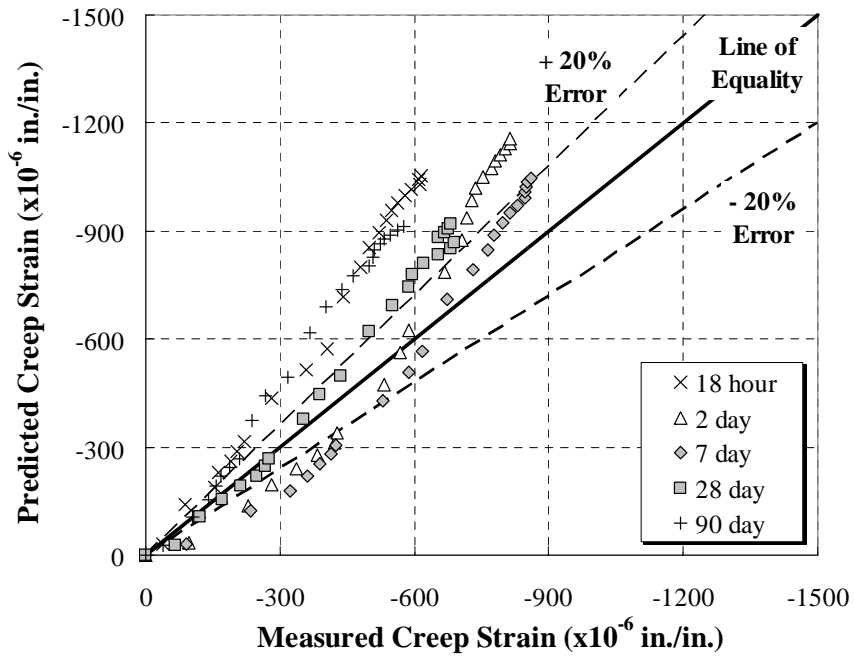


**Figure 5-3:** Measured versus estimated creep strain for the HS-FA mixture using the ACI 209 procedure

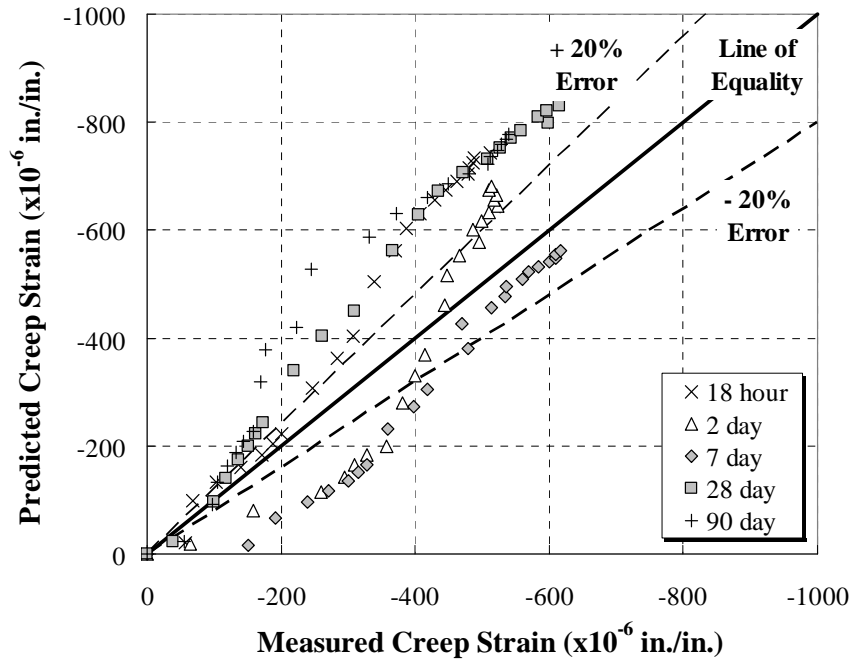


**Figure 5-4:** Measured versus estimated creep strain for the MS-SL mixture using the ACI 209 procedure

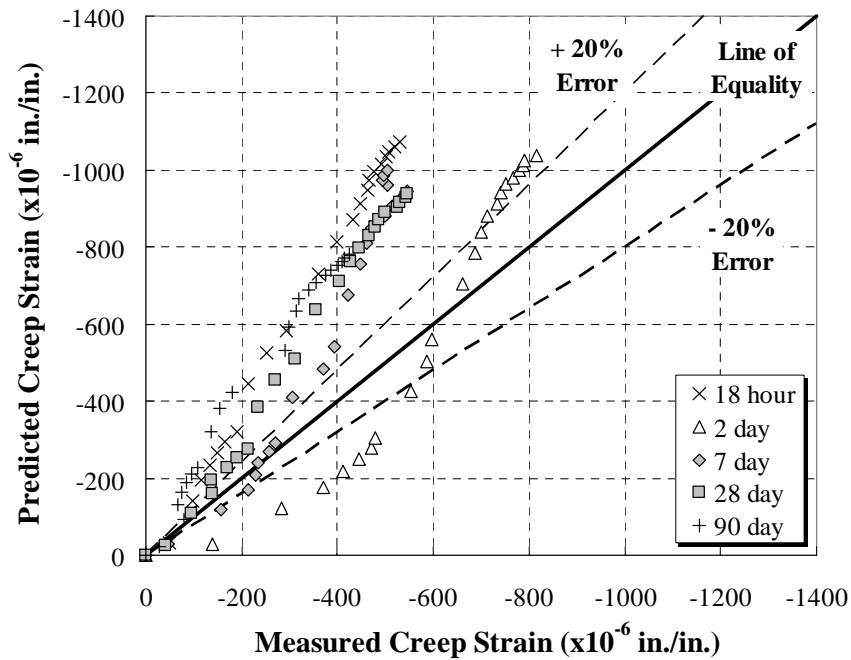


**Figure 5-5:** Measured versus estimated creep strain for the HS-SL mixture using the ACI 209 procedure

## 5.4 AASHTO CREEP PREDICTION METHOD

Unlike the ACI 209 method that was developed in the 1990's, the AASHTO 2007 method was developed with high-strength concrete in mind. Furthermore, unlike ACI 209, no corrections or assumptions had to be made in order to use this method to predict the creep associated with SCC mixtures. The procedure for this method was completed in the manner described in Section 2.4.2.

Figures 5-6 through 5-10 depict the AASHTO estimated  $\epsilon_{CR}$  values versus the  $\epsilon_{CR}$  values collect during the research phase of this study. Like the ACI 209 results, they show all loading ages for all mixtures and are organized according to mixture. From Figure 5-6, it can be seen that this method underestimates the  $\epsilon_{CR}$  values for all loading ages except the 18-hour accelerated-curing specimens. However, AASHTO 2007 does correct the estimations for the 28- and 90-day loading ages as the concrete ages, but the 2- and 7-day ages are overcorrected at later concrete ages, which results in an overestimation of  $\epsilon_{CR}$  values.

Figure 5-7 illustrates the comparison of AASHTO 2007 predicted creep versus measured creep and depicts similar trends to that of the conventional-slump mixture's comparison. From Figure 5-7, it may be seen that this method underestimates the  $\epsilon_{CR}$  values at all early ages and tends to over predict  $\epsilon_{CR}$  values at the later ages. Here again, the 18-hour loading age  $\epsilon_{CR}$  values are overestimated; however, from Table 5-2, it can be seen that the *AA%E* value for this loading age and method is 44%, which is an improvement from the conventional-slump mixture. In addition, the 2- and 7-day loading ages are overestimated at later concrete ages, much like they were for the control mixture.

Finally, the creep for the 28- and 90-day specimens are more closely estimated than any other ages for this mixture, as most of the estimates are within the  $\pm 20\%$  error tolerance.

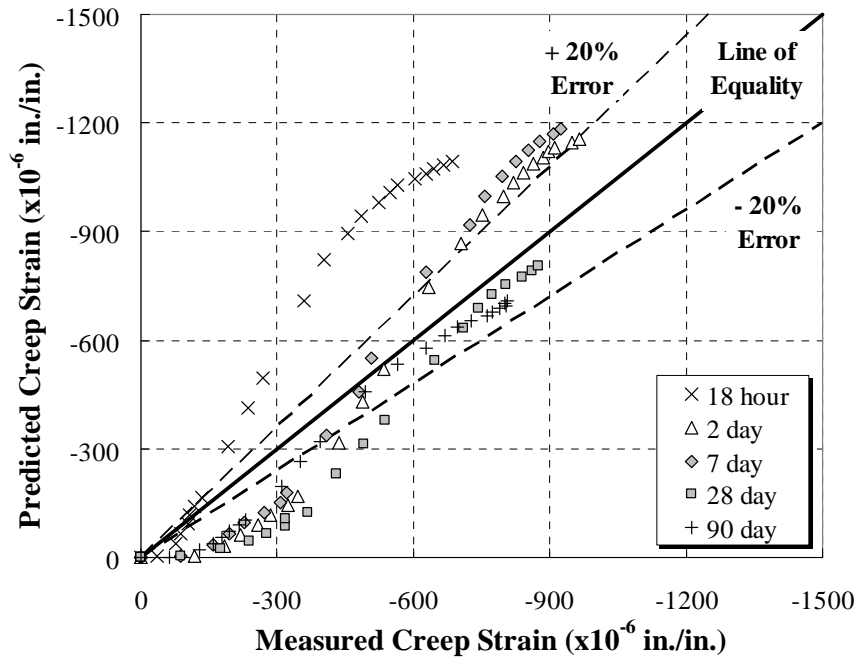
From Figure 5-8, which shows the comparison for the HS-FA mixture, it is evident that this method continues to underestimate the  $\epsilon_{CR}$  values at early concrete ages. Moreover, it then overestimates the 18-hour  $\epsilon_{CR}$  values at later concrete ages. Here again, the 2- and 7-day  $\epsilon_{CR}$  values are overestimated at later ages and the 28-day  $\epsilon_{CR}$  values tend to be very accurate. The estimated creep values for the 90-day specimens are within reasonable proximity to the  $\pm 20\%$  error tolerance, indicating tolerable accuracy for this loading age.

Figure 5-9 illustrates the same comparison for the MS-SL mixture. From this figure, it is again evident that early-age  $\epsilon_{CR}$  values are underestimated; however, this method overestimates the later concrete age  $\epsilon_{CR}$  values for this mixture. In fact, only the 7-day  $\epsilon_{CR}$  values are within the preferred  $\pm 20\%$  range at later concrete ages. This method proves especially inaccurate for estimating the creep values for the 18-hour accelerated-cured specimens. In fact, according to Table 5-2, the  $AA\%E$  value for this loading age and method is 54%, which is among the highest error values of all five mixtures.

Figure 5-10 shows the same trends that were identified for the creep estimated for previous mixtures using this method. This method underestimates the early-age  $\epsilon_{CR}$  values for the 2-, 7-, and 28-day loading ages, but then overestimates the later-age  $\epsilon_{CR}$  values for the 7-, 28, and 90-day specimens. The biggest difference here is the improved accuracy of the later-age 2-day  $\epsilon_{CR}$  values, which are the only ones within the  $\pm 20\%$  range. It is evident from looking at this figure that this method does not accurately estimate the  $\epsilon_{CR}$  values for concrete mixture of this SCM type and strength level.



It is clear from Tables 5-1 and 5-2 that the AASHTO 2007 method is among the top three prediction methods evaluated in this investigation; however, like the ACI 209 method, it is not the best method overall. It is the most accurate of all the methods for estimating the creep for the high-strength SCC mixtures according to the results from the *AAE* and *AA%E* calculations. Additionally, it is among the top three methods for estimating the creep of the non-accelerated-cured specimens used in this study.



**Figure 5-6:** Measured versus estimated creep strain for the conventional-slump mixture using the AASHTO 2007 procedure

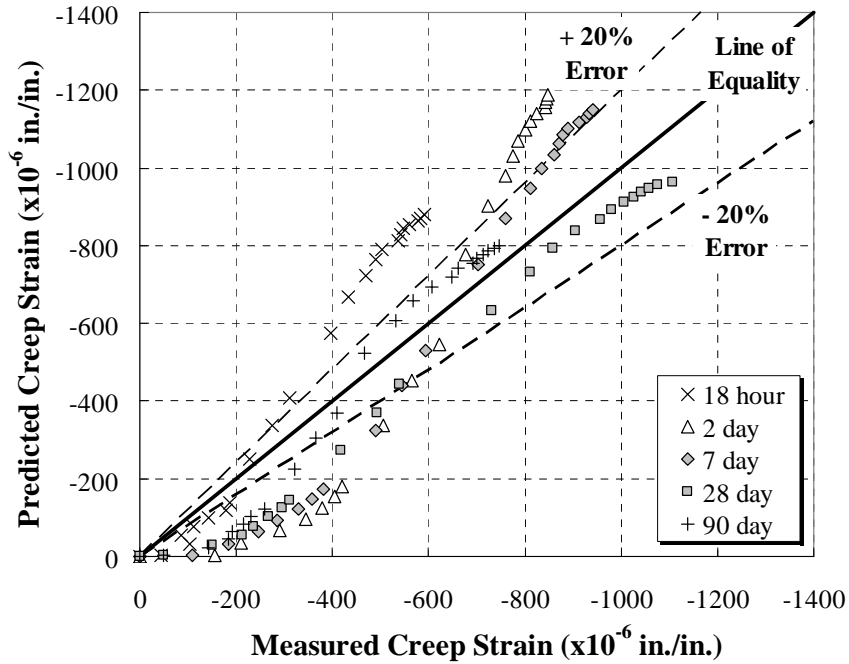


**Figure 5-7:** Measured versus estimated creep strain for the MS-FA mixture using the AASHTO 2007 procedure

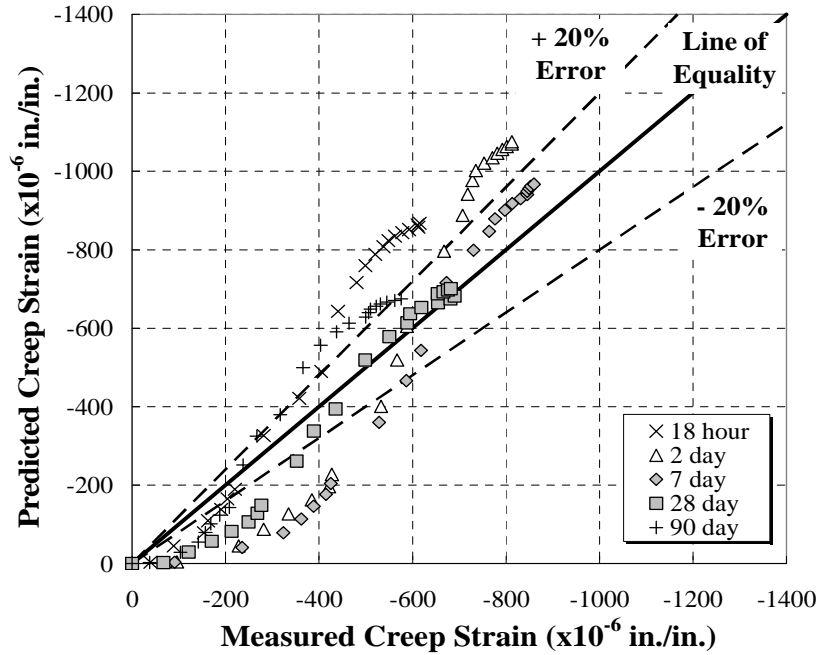


**Figure 5-8:** Measured versus estimated creep strain for the HS-FA mixture using the AASHTO 2007 procedure

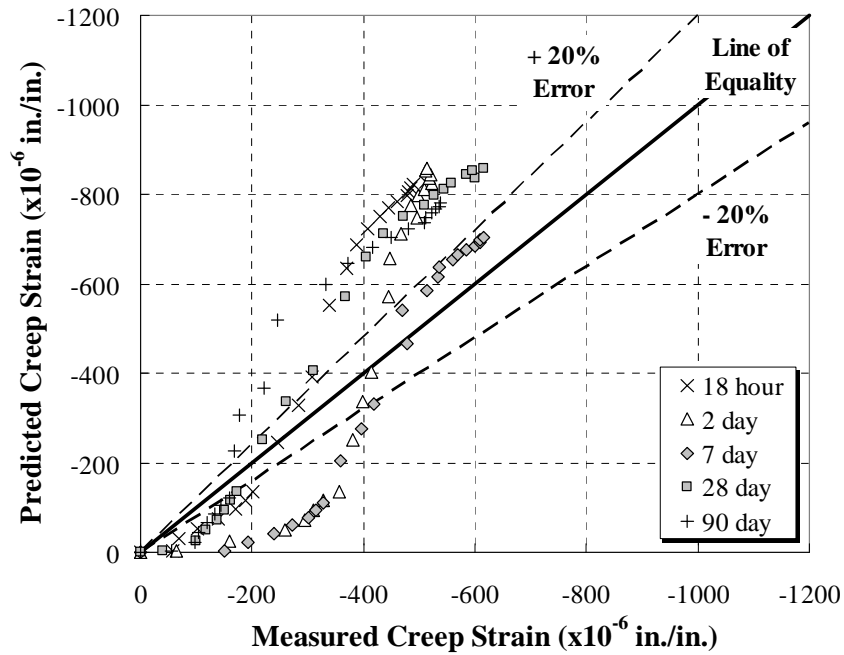


**Figure 5-9:** Measured versus estimated creep strain for the MS-SL mixture using the AASHTO 2007 procedure

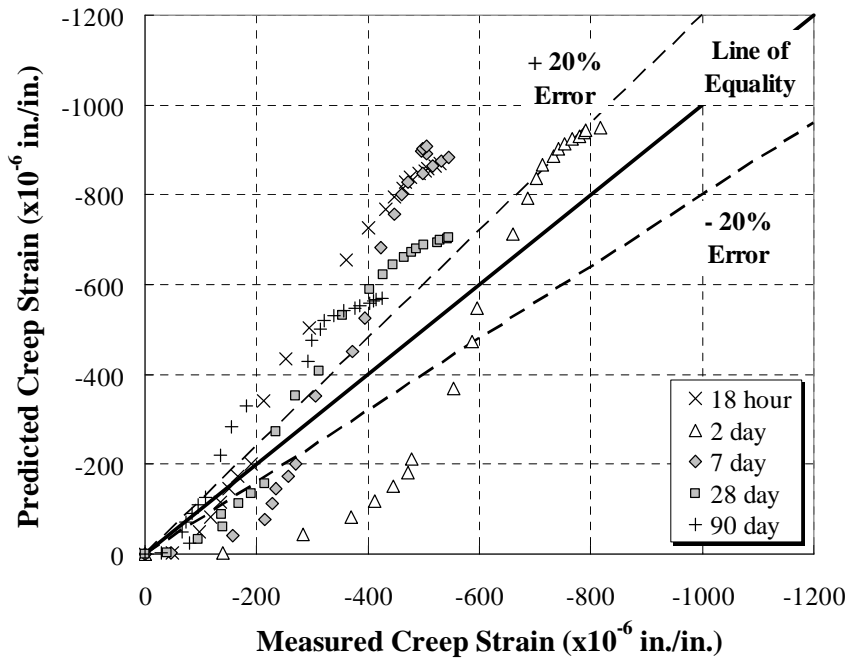


**Figure 5-10:** Measured versus estimated creep strain for the HS-SL mixture using the AASHTO 2007 procedure

## 5.5 CEB 90 CREEP PREDICTION METHOD

The CEB 90 creep prediction method, like the AASHTO 2007 method, required no assumptions or corrections be made in order for it to be used to estimate  $\epsilon_{CR}$  values for any of the mixtures. All analysis associated with this method was completed according to the procedures outlined in Section 2.4.3 of this report.

Figures 5-11 through 5-15 illustrate the comparison made between the predicted  $\epsilon_{CR}$  values from the CEB 90 method and the measured  $\epsilon_{CR}$  values recorded during testing. In Figure 5-11 and in Tables 5-1 and 5-2, it can be seen that this method provides better  $\epsilon_{CR}$  estimates for the conventional-s slump mixture than both the ACI 209 and AASHTO 2007 methods. The early-age  $\epsilon_{CR}$  values for all non-accelerated-cured samples are all reasonably well estimated. The only noticeably underestimated  $\epsilon_{CR}$  values are the ones associated with the 28- and 90-day specimens; however, these are within reasonable proximity to the  $\pm 20\%$  range, which is preferred. The only overestimated values are those associated with the 18-hour accelerated-cured specimens. The creep for the 18-hour loading age is grossly overestimated at all concrete ages.

Figure 5-12 shows the  $\epsilon_{CR}$  comparison for the MS-FA mixture. Here it can be seen that this method provided accurate estimates of the  $\epsilon_{CR}$  values for this mixture. The creep for all loading ages, including the 18-hour loading age, is accurately estimated. In fact, the only creep estimates that fall outside of the  $\pm 20\%$  range are those of the 28-day loading age, and even those are only slightly more than 20% underestimated.

Figure 5-13, which shows the HS-FA mixture's creep comparison, illustrates again that this method provides reasonably accurate estimations of the measured  $\epsilon_{CR}$  values for SCC mixtures. Most of the estimated  $\epsilon_{CR}$  values fall within the preferred  $\pm 20\%$  error

range. In fact, only the 18-hour loading age has  $\epsilon_{CR}$  values that stay outside of this range for an appreciable amount of time. In all, this method provides accurate creep estimates for all loading ages and at all concrete ages.

In Figure 5-14, it is evident that the estimated  $\epsilon_{CR}$  values are within close proximity of the line of equality, which means that this method accurately predicts  $\epsilon_{CR}$  values at all concrete ages. Only the creep of the 2- and 7-day specimens are ever underestimated at earlier ages; however, at later ages, their creep estimates are improved. In contrast, all other loading ages are always overestimated; however, these overestimated creep values are predominantly in close proximity of the  $\pm 20\%$  error envelope.

Finally, Figure 5-15, which depicts this comparison for the HS-SL mixture, shows slightly different trends. Here the creep for all the loading ages except the 2-day loading age are over predicted at all concrete ages. Even though the 2-day  $\epsilon_{CR}$  values are overestimated, they are still within close proximity of the  $\pm 20\%$  error range. In all, this method provides the most accurately predicted  $\epsilon_{CR}$  values for all the SCC mixtures in this study.

The last statement is reinforced by the results from the statistical analysis, which are found in Tables 5-1 and 5-2. From those tables it is clear that the CEB 90 method provided the most accurate results for all non-accelerated-cured specimens according to both the *AAE* and *AA%E* calculations. In addition, it was among the top three methods used to predict the creep strain for the accelerated-cured specimens.

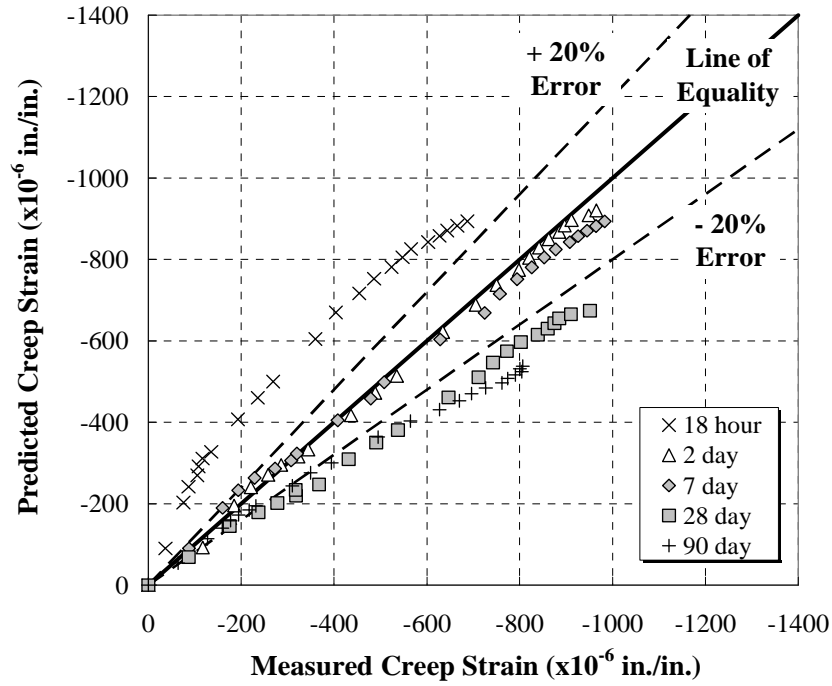


**Figure 5-11:** Measured versus estimated creep strain for the conventional-s slump mixture using the CEB 90 procedure

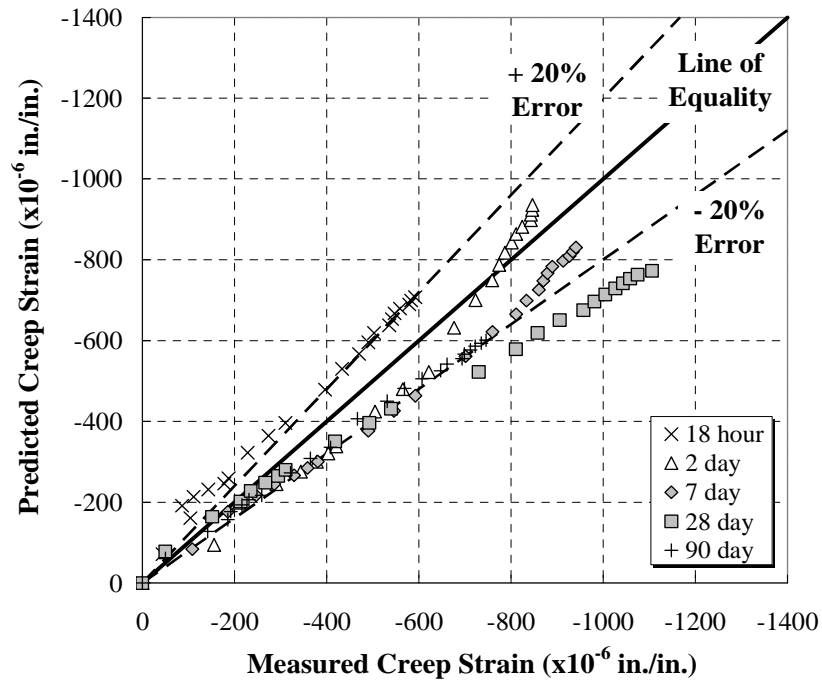


**Figure 5-12:** Measured versus estimated creep strain for the MS-FA mixture using the CEB 90 procedure

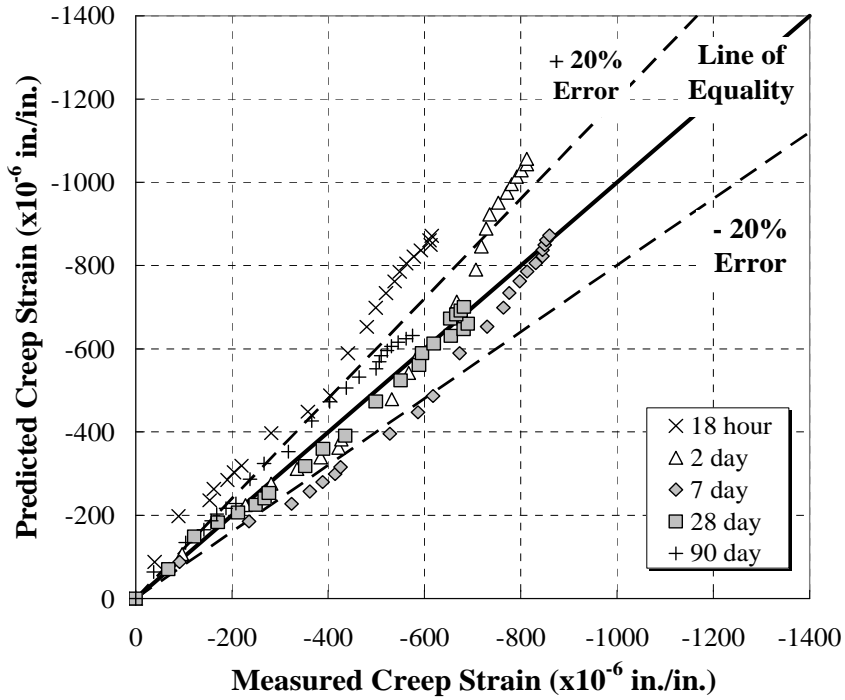


**Figure 5-13:** Measured versus estimated creep strain for the HS-FA mixture using the CEB 90 procedure

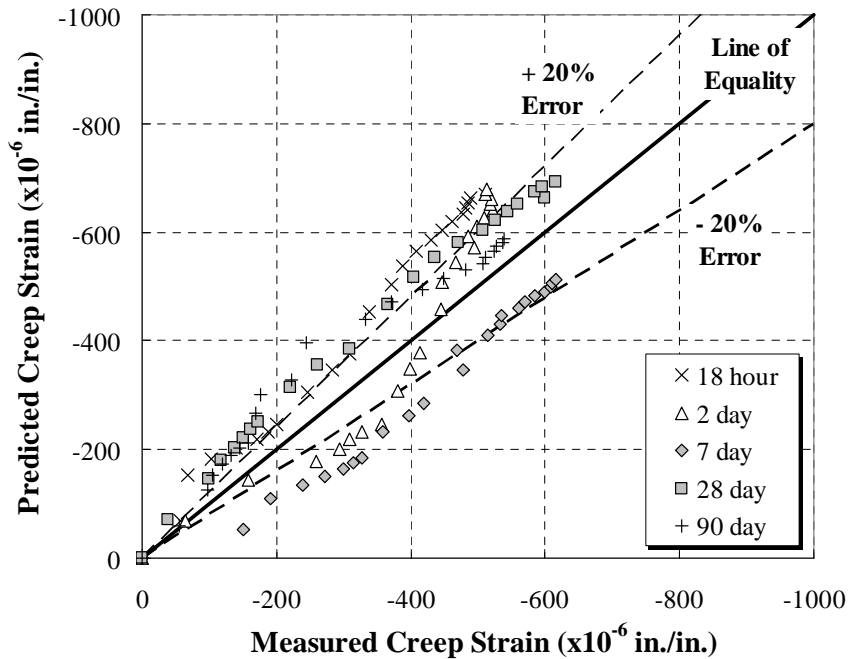


**Figure 5-14:** Measured versus estimated creep strain for the MS-SL mixture using the CEB 90 procedure

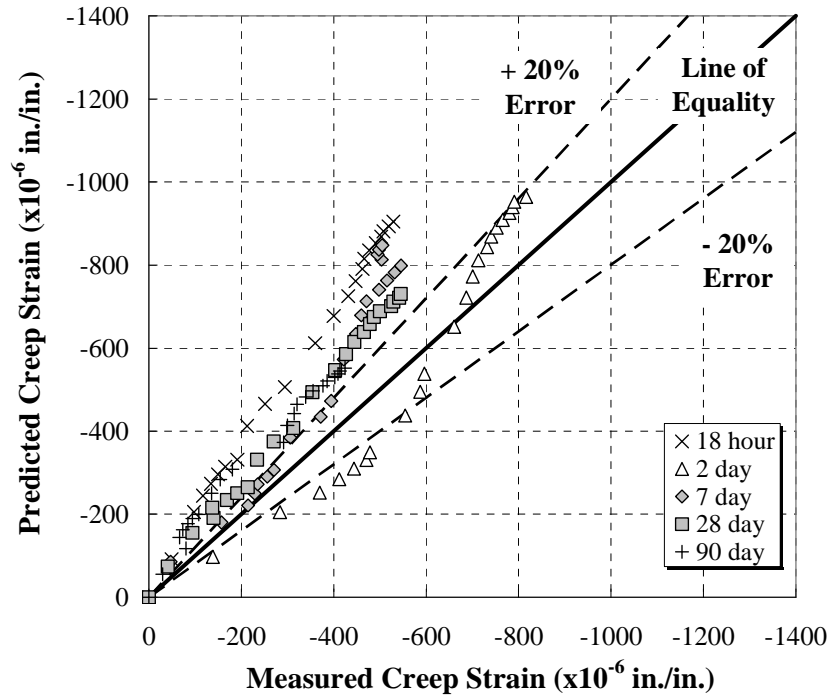


**Figure 5-15:** Measured versus estimated creep strain for the HS-SL mixture using the CEB 90 procedure

## 5.6 GL 2000 CREEP PREDICTION METHOD

Like both the AASHTO 2007 and CEB 90 methods, this creep prediction method required no assumptions or modifications in order for it to be used with SCC mixtures. However, the equivalent age maturity of the 18-hour specimens was calculated in accordance with ASTM C 1074 (2004) using an activation energy of 45,000 J/mol. Aside from this change, all analysis associated with this method was completed in accordance with the procedures outlined in Section 2.4.4.

Figures 5-16 through 5-20 show the creep comparisons made for all mixtures using the  $\epsilon_{CR}$  values predicted by the GL 2000 method. Starting with Figure 5-16, the reader will notice that this method overestimated all  $\epsilon_{CR}$  data for all loading ages, regardless of



mixture type, concrete age, or the curing regime used. It was especially inaccurate when estimating the  $\epsilon_{CR}$  values for the 18-hour loading age. Only the  $\epsilon_{CR}$  values for the 90-day loading age were within the  $\pm 20\%$  error range.

In Figure 5-17, which depicts the comparison for the MS-FA mixture, the same trends are evident. The 18-hour accelerated curing specimens were grossly overestimated. In a similar fashion, but to a lesser degree, all other loading ages were overestimated. Not even the 90-day  $\epsilon_{CR}$  values were within the preferred range.

This trend continues in Figures 5-18 through 5-20, becoming more pronounced as the strength levels increase. This is especially evident in Figure 5-20, which shows the comparison for the HS-SL mixture. In this figure, the  $\epsilon_{CR}$  values are severely overestimated and the trends for all loading ages are much steeper than any of the other mixtures. It is clear by looking at these figures, that this method does not provide accurate estimates of the  $\epsilon_{CR}$  values for any of the concrete mixtures used in this study.

These conclusions are reaffirmed through the results in Tables 5-1 and 5-2, which clearly show that the GL 2000 method provided results among the least accurate of all the methods in this study. According to all three comparison statistics, the estimation errors associated with this method grow as the concrete strength level rises, which agrees with the visual information provided in Figures 5-16 through 5-20.

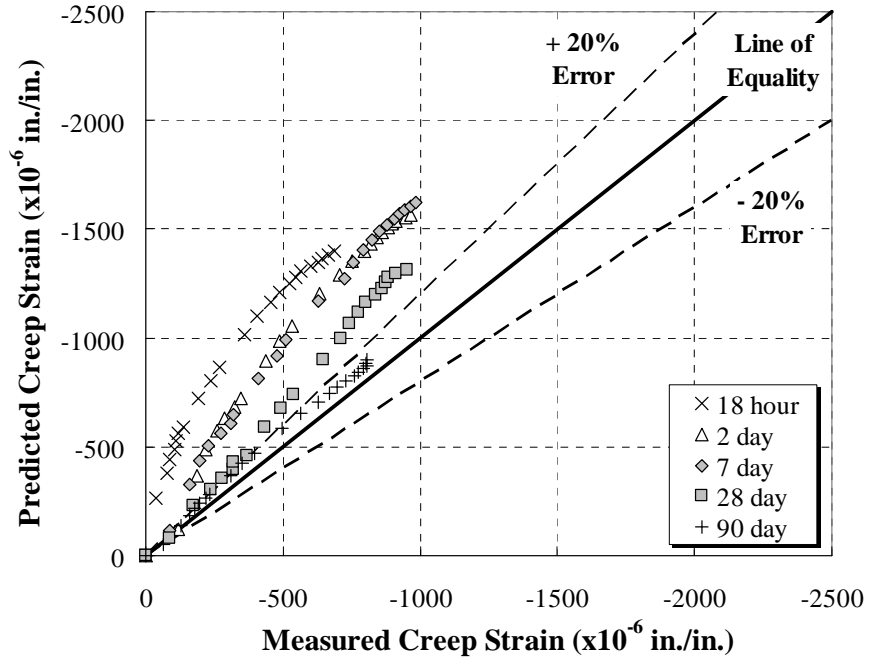


**Figure 5-16:** Measured versus estimated creep strain for the conventional-s slump mixture using the GL 2000 procedure

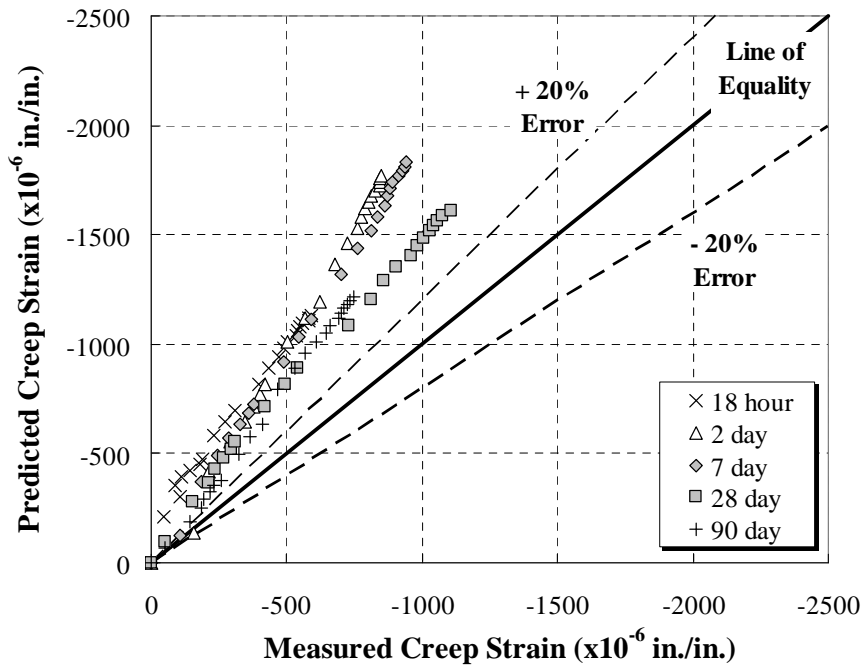


**Figure 5-17:** Measured versus estimated creep strain for the MS-FA mixture using the GL 2000 procedure

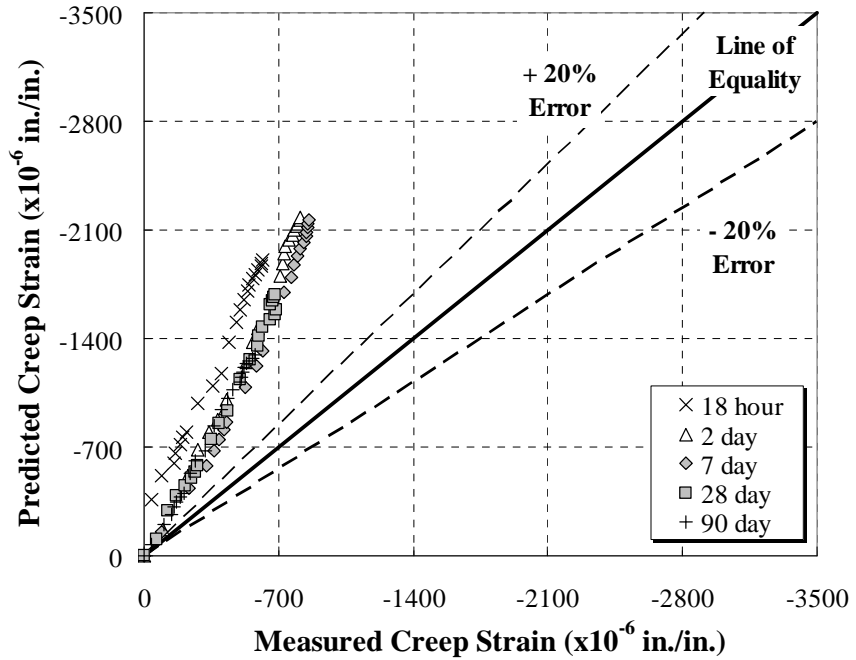


**Figure 5-18:** Measured versus estimated creep strain for the HS-FA mixture using the GL 2000 procedure

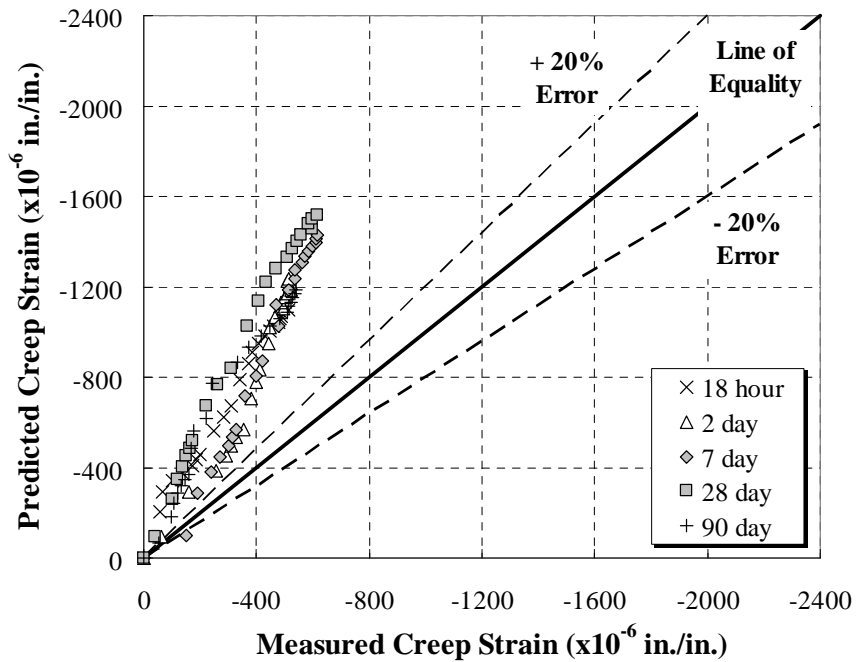


**Figure 5-19:** Measured versus estimated creep strain for the MS-SL mixture using the GL 2000 procedure

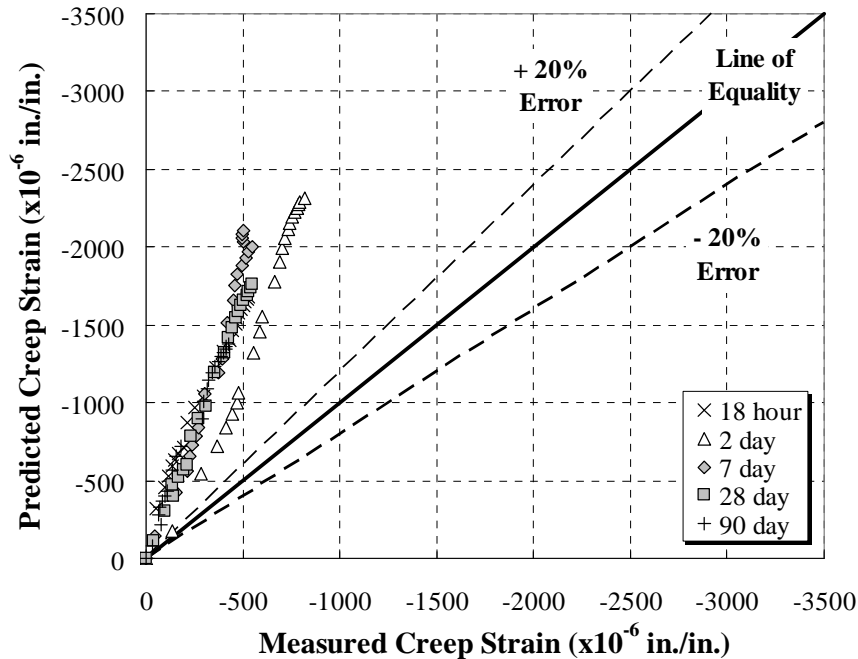


**Figure 5-20:** Measured versus estimated creep strain for the HS-SL mixture using the GL 2000 procedure

### 5.7 B3 CREEP PREDICTION METHOD

The B3 creep prediction method required an intricate procedure to be followed in order to estimate  $\epsilon_{CR}$  values and one assumption had to be made in the process. As in the ACI 209 method, the cement content was taken to be the total cementitious material content (cement plus SCMs). Aside from this assumption, the procedures outlined in Section 2.4.5 were used, and the results are presented below.

Figures 5-21 through 5-25 depict the creep comparisons for all mixtures and loading ages. In Figure 5-21, the reader will notice that this method tends to overestimate the  $\epsilon_{CR}$  values for all loading ages at both early and late concrete ages. The only exceptions to this are the 28- and 90-day specimens. For these loading ages, this method

underestimated the  $\epsilon_{CR}$  values for the early concrete ages and then overestimates them at later concrete ages.

Figure 5-22 shows the creep comparison for the MS-FA mixture. This method tends to overestimate all  $\epsilon_{CR}$  values for the early ages of the 18-hour, 2-, and 7-day specimens, which are overestimated for all concrete ages. The 28- and 90-day specimens are underestimated early on, but then overestimated at later concrete ages; however, the 28-day estimated  $\epsilon_{CR}$  values do, for the most part, stay within the  $\pm 20\%$  error range at all times.

Figures 5-23 through 5-25 also reveal that the  $\epsilon_{CR}$  values are overestimated at later concrete ages for all five loading ages. From the trends seen in these three figures, it appears that this method is unable to accurately predict creep strain in high-strength concrete mixtures.

This argument is further strengthened by the results from the statistical comparison found in Tables 5-1 and 5-2. From these tables, it can be seen that, statistically, the B3 method is among the least accurate of all the methods in this study, especially with the high-strength concrete mixtures. This can be seen with the increasing values from both the  $AAE$  and  $AA\%E$  calculations for the non-accelerated- and accelerated-cured specimens. It is only surpassed in inaccuracy by the GL 2000 method.

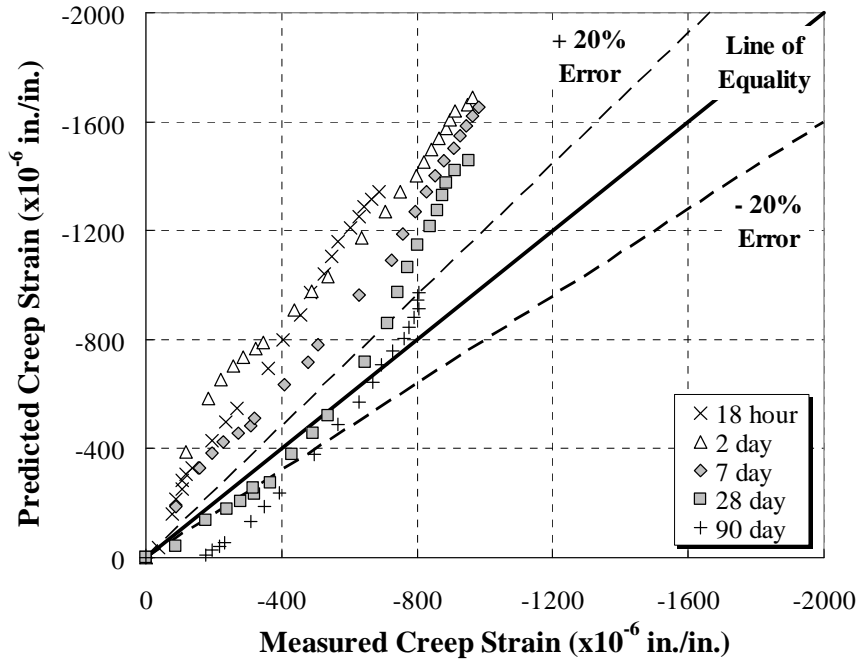


**Figure 5-21:** Measured versus estimated creep strain for the conventional-slump mixture using the B3 procedure

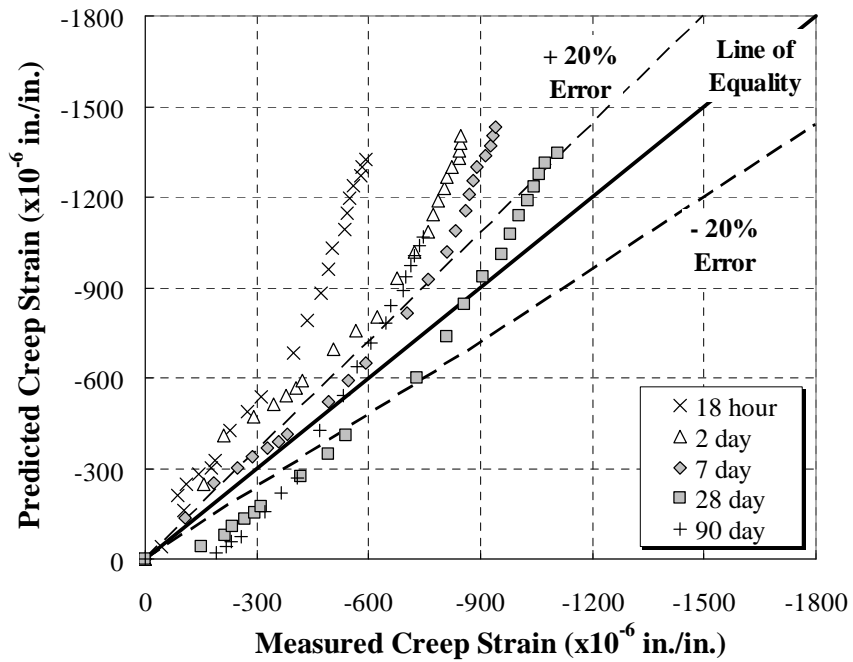


**Figure 5-22:** Measured versus estimated creep strain for the MS-FA mixture using the B3 procedure

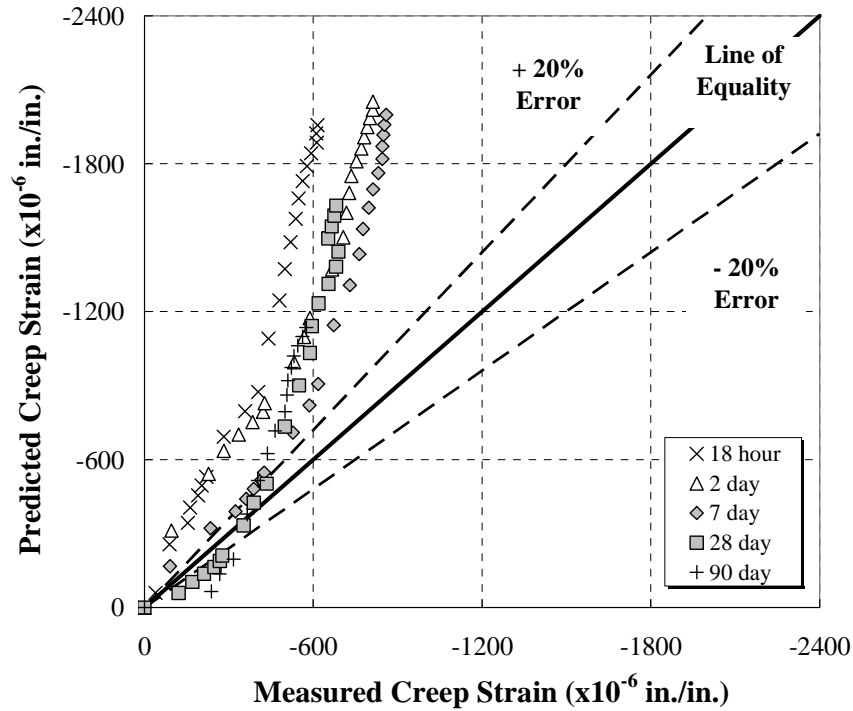


**Figure 5-23:** Measured versus estimated creep strain for the HS-FA mixture using the B3 procedure

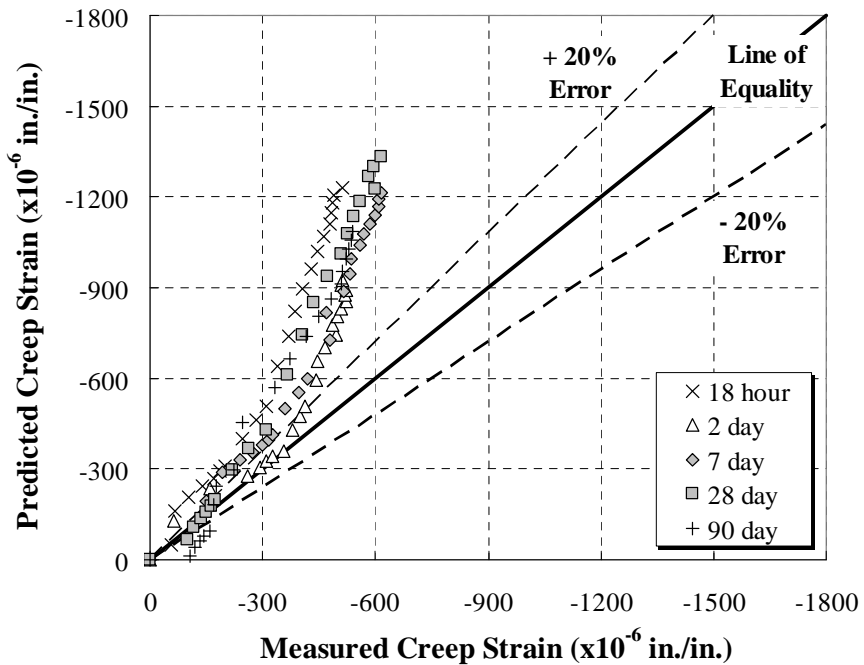


**Figure 5-24:** Measured versus estimated creep strain for the MS-SL mixture using the B3 procedure

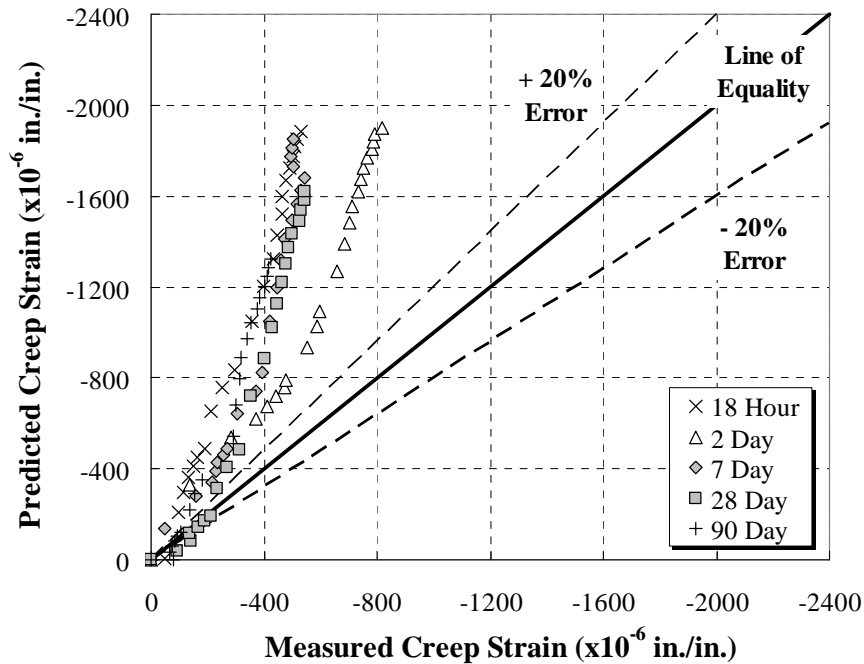


**Figure 5-25:** Measured versus estimated creep strain for the HS-SL mixture using the B3 procedure

## 5.8 CALIBRATION OF THE CEB 90 CREEP PREDICTION METHOD

After performing all the analyses, the CEB 90 model, which is detailed in Section 2.4.3, was determined to provide the most accurate creep estimates of the five models investigated in this study; however, it was determined that improvement could be made. To this end, a process was undertaken by which the CEB 90 method was calibrated to provide accurate creep predictions for each of the five mixtures used in this study. During the calibration process, the parameters in Table 5-3 were modified:



**Table 5-3: Parameters used in the Modified CEB 90 method**

Parameter	Original Formulation	Non-Accelerated-Cured Formulation	Accelerated-Cured Formulation
$\beta(f_{cm})$	$\frac{5.3}{(f_{cm} / f_{cmo})^{(0.5)}}$	$\frac{5.3}{(f_{cm} / f_{cmo})^{(0.5)}}$	$\frac{4.65}{(f_{cm} / f_{cmo})^{(0.5)}}$
$\beta(t_0)$	$\frac{1}{0.1 + (t_0 / t_1)^{(0.2)}}$	$\frac{1}{0.26 + (t_0 / t_1)^{(0.18)}}$	$\frac{1}{0.26 + (t_0 / t_1)^{(0.18)}}$
$\beta(t_0)$	$\left[ \frac{(t - t_0) / t_1}{\beta_H + (t - t_0) / t_1} \right]^{(0.3)}$	$\left[ \frac{(t - t_0) / t_1}{\beta_H + (t - t_0) / t_1} \right]^{(0.27)}$	$\left[ \frac{(t - t_0) / t_1}{\beta_H + (t - t_0) / t_1} \right]^{0.35}$

The following variables, which are defined below, were used in the equations in the Table 5-3:

$f_{cm}$  = mean compressive strength of concrete at 28 days (MPa)

$f_{cmo}$  = 10 MPa

$t_0$  = age of concrete at time of loading (days)

$t_1$  = 1 day

$t$  = age of concrete at the moment considered (days)

$$\beta_H = 150 \left\{ 1 + \left( 1.2 \frac{RH}{RH_0} \right)^{18} \right\} \frac{h}{h_0} + 250 \leq 1500$$

In addition to these parameters, the maturity function used in the CEB 90 method to account for curing conditions was changed. The following equation shows the original formulation:

$$t_T = \sum_{i=1}^n \Delta t_i \exp \left[ 13.65 - \frac{4000}{273 + \{T(\Delta t_i) / T_0\}} \right]$$

During the calibration process, the previous equation was updated with an activation energy of 45,000 J/mol, which provided the following equation for both the non-accelerated- and accelerated-cured specimens:

$$t_T = \sum_{i=1}^n \Delta t_i \exp \left[ 18.47 - \frac{5410}{273 + \{T(\Delta t_i)/T_0\}} \right]$$

where,

$t_T$  = temperature adjusted concrete age which replaces  $t$  in the corresponding equations (days)

$\Delta t_i$  = increment of days where  $T$  prevails

$T(\Delta t_i)$  = the temperature (°C) during the time period  $\Delta t_i$

$T_0$  = 1 °C

With the parameter modifications list above, predictions using the calibrated CEB 90 method, which is referred to as the Modified CEB 90 method, were completed in the manner described in Section 2.4.3.

Tables 5-4 and 5-5 show the results from the comparison statistics calculations that were performed to evaluate the Modified CEB 90 method. Also shown are the statistical values for the CEB 90 method. The statistics used in these tables are detailed in Section 5.2.1.

**Table 5-4 :** Error calculations for the non-accelerated-cured specimens

Non-Accelerated-Cured Samples					
	Mixtures				
	CTRL	MS-FA	MS-SL	HS-FA	HS-SL
<b>1. Percent Error (%)</b>					
<b>CEB 90</b>					
Positive Range	20	55	80	70	121
Negative Range	-35	-39	-66	-30	-32
<b>Modified CEB 90</b>					
Positive Range	40	98	129	117	153
Negative Range	-34	-29	-56	-19	-21
<b>2. Absolute Average Error (<math>\mu\epsilon</math>)</b>					
CEB 90	80	97	84	59	120
Modified CEB 90	73	83	90	60	134
<b>Best Method</b>	<b>Mod. CEB 90</b>	<b>Mod. CEB 90</b>	<b>CEB 90</b>	<b>CEB 90</b>	<b>CEB 90</b>
<b>3. Absolute Average Percent Error</b>					
CEB 90	15	16	27	13	38
Modified CEB 90	14	13	31	15	46
<b>Best Method</b>	<b>Mod. CEB 90</b>	<b>Mod. CEB 90</b>	<b>CEB 90</b>	<b>CEB 90</b>	<b>CEB 90</b>

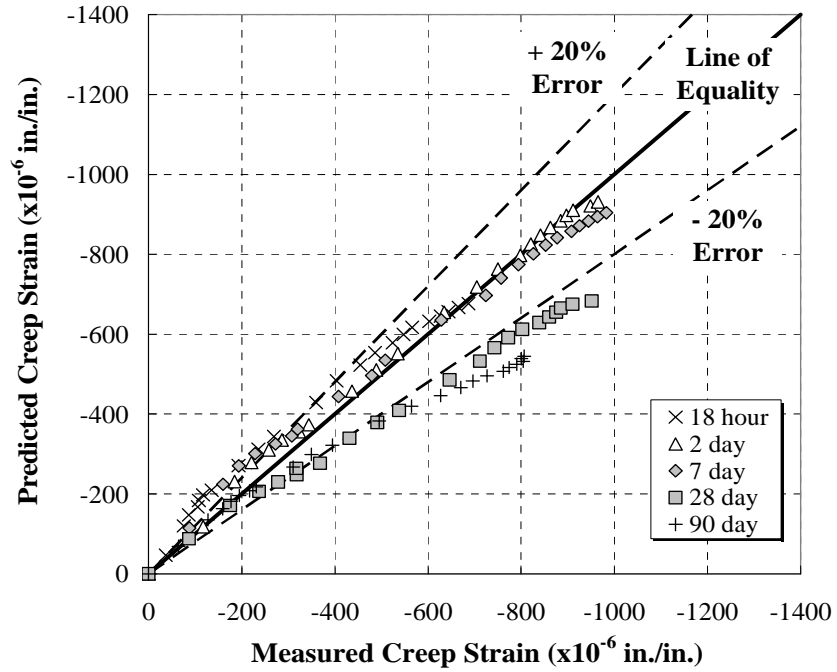
**Table 5-5:** Error calculations of the accelerated-cured specimens

Accelerated-Cured Samples					
	Mixtures				
	CTRL	MS-FA	MS-SL	HS-FA	HS-SL
<b>1. Percent Error (%)</b>					
<b>CEB 90</b>					
Positive Range	179	122	126	123	110
Negative Range	----	----	----	----	----
<b>Modified CEB 90</b>					
Positive Range	70	35	33	31	31
Negative Range	-1	-17	-38	-17	-4
<b>2. Absolute Average Error (<math>\mu\epsilon</math>)</b>					
CEB 90	203	91	106	156	239
Modified CEB 90	50	36	18	25	83
<b>Best Method</b>	<b>Mod. CEB 90</b>	<b>Mod. CEB 90</b>	<b>Mod. CEB 90</b>	<b>Mod. CEB 90</b>	<b>Mod. CEB 90</b>
<b>3. Absolute Average Percent Error</b>					
CEB 90	86	36	36	47	77
Modified CEB 90	27	11	10	7	23
<b>Best Method</b>	<b>Mod. CEB 90</b>	<b>Mod. CEB 90</b>	<b>Mod. CEB 90</b>	<b>Mod. CEB 90</b>	<b>Mod. CEB 90</b>

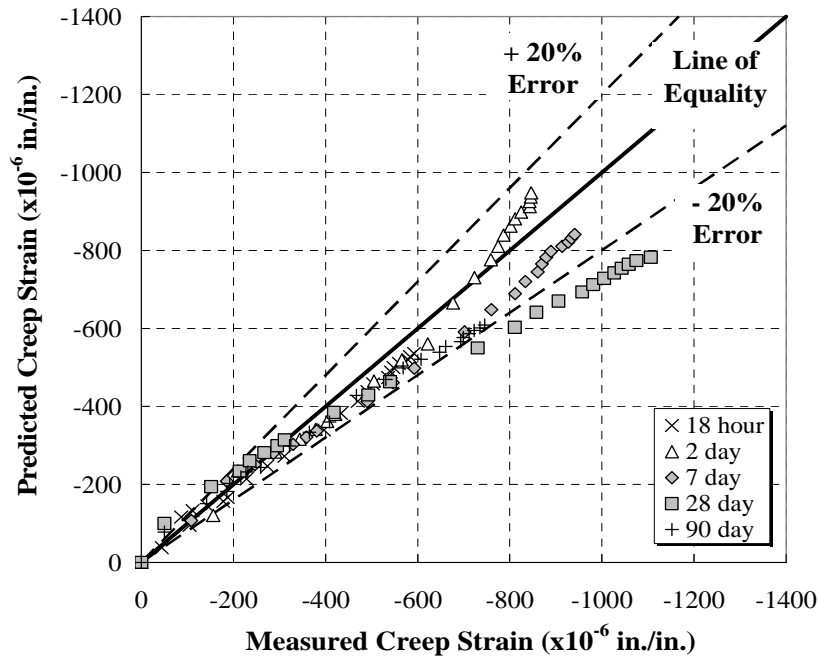
Figures 5-26 through 5-27 depict the estimated  $\epsilon_{CR}$  values calculated using the Modified CEB 90 method versus the measured creep values. From Figure 5-26 it can be seen that the Modified CEB 90 method provides accurate estimations of the  $\epsilon_{CR}$  for all loading ages of the conventional-slump mixture. In fact the only  $\epsilon_{CR}$  values that are outside of the  $\pm 20\%$  error range are the later ages of the 28- and 90-day specimens. Even these are within close proximity of the preferred tolerance. Furthermore, in Tables 5-4 and 5-5, the accuracy of this modified method is further reinforced. The  $AA\%E$  values displayed in both of these tables illustrate that this method is an improvement from the CEB 90 method, especially with regards to the accelerated-cured specimens.

Figure 5-27 shows the estimated versus measured  $\epsilon_{CR}$  values for the MS-FA mixture. From this figure it can be seen that the modified method provides accurate estimations of the  $\epsilon_{CR}$ . Here again the only  $\epsilon_{CR}$  values that are outside the  $\pm 20\%$  range are the later-age values 28-day specimens. The accuracy of this method is further revealed in Tables 5-4 and 5-5, which show an improvement in the  $AA\%E$  statistical values when comparing the CEB 90 method and the Modified CEB 90 method.

Figure 5-28 shows trends similar to Figures 5-26 and 5-27 in that the estimated values remain predominately within the  $\pm 20\%$  tolerance range. In contrast, Figures 5-29 and 5-30 show a decrease in the accuracy of this method as the strength level raises. In fact, the only improvement in accuracy from the CEB 90 method is associated with the accelerated-cured specimens. In Table 5-5 this can be seen in the form of the  $AA\%E$  values, where the Modified CEB 90 method has only a 23% error while the CEB 90 method has a 77% error.



**Figure 5-26:** Measured versus estimated creep strain for the conventional-s slump mixture using the Modified CEB 90 method



**Figure 5-27:** Measured versus estimated creep strain for the MS-FA mixture using the Modified CEB 90 method

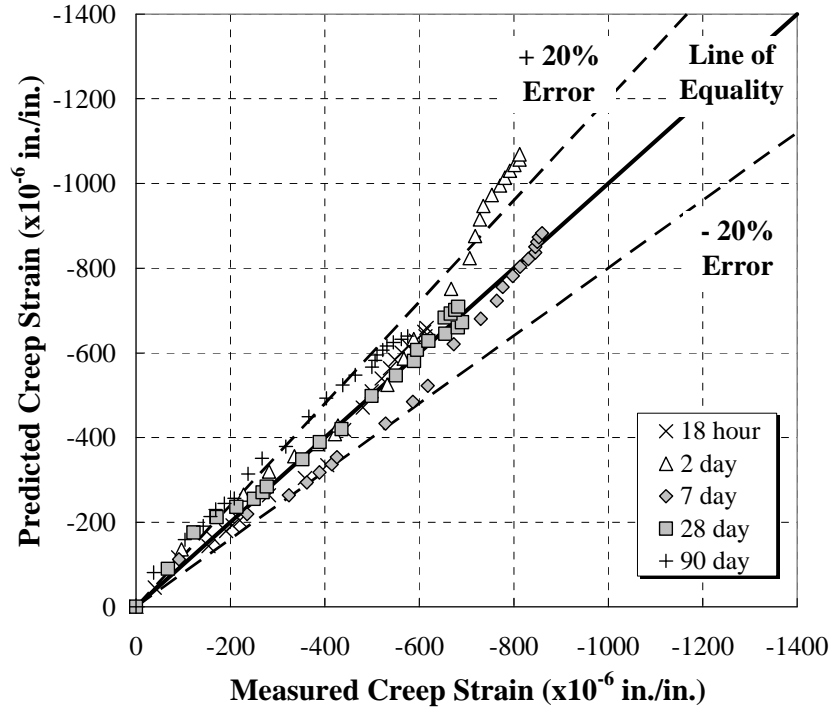


**Figure 5-28:** Measured versus estimated creep strain for the HS-FA mixture using the Modified CEB 90 method

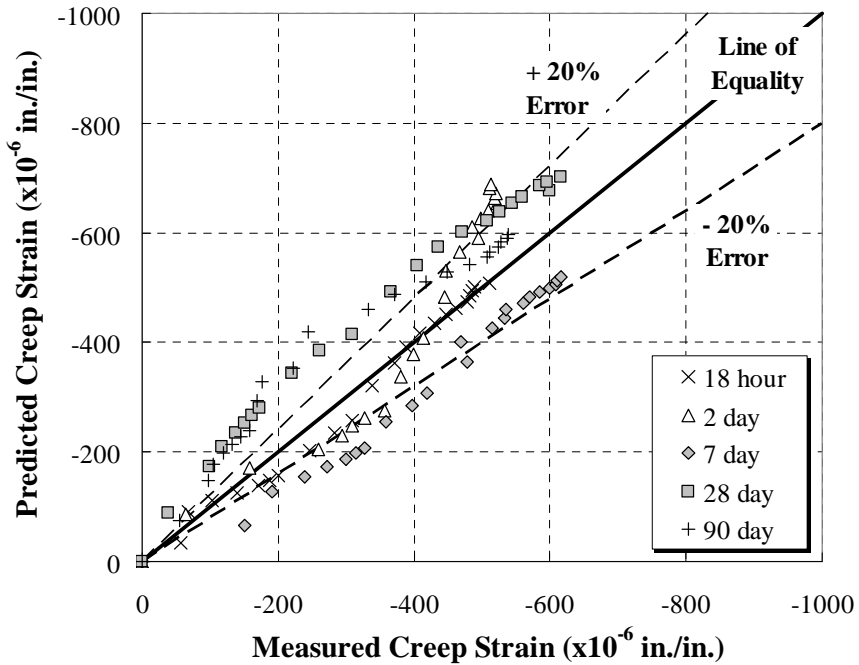


**Figure 5-29:** Measured versus estimated creep strain for the MS-SL mixture using the Modified CEB 90 method

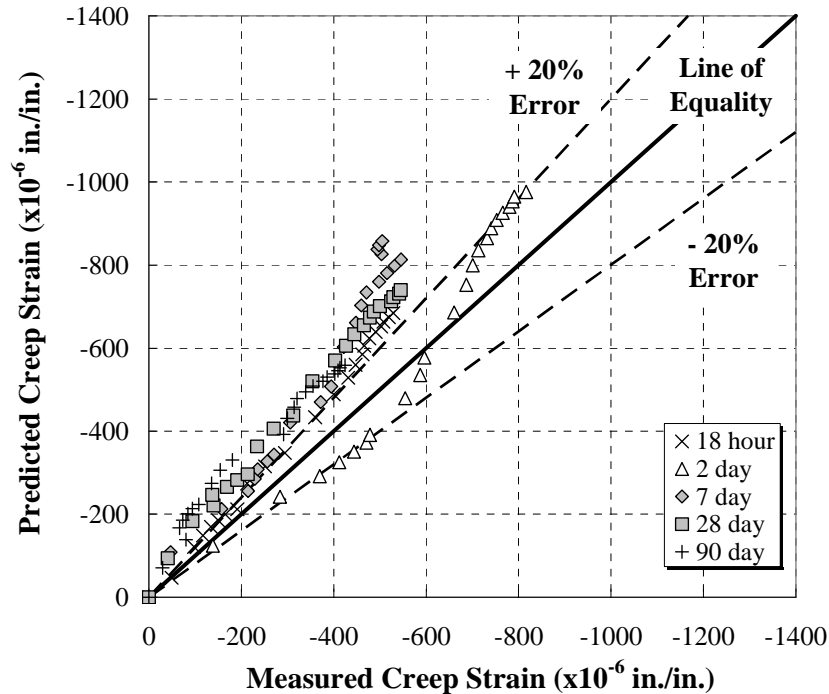


**Figure 5-30:** Measured versus estimated creep strain for the HS-SL mixture using the Modified CEB 90 method

## 5.9 SUMMARY OF CONCLUSIONS

From the results obtained through the analysis that is discussed in the previous sections of this chapter, the following conclusions can be drawn about all of the creep prediction methods:

- When curing was accelerated, ACI 209 provided the most accurate estimated creep strain values for the conventional-slump mixture.
- The ACI 209 creep prediction method was unable to accurately predict the creep strain in the high-strength concrete mixtures used in this study.
- In general, ACI 209 was one of the most accurate creep prediction methods of the five that were investigated in this study.

- In general, the AASHTO 2007 creep prediction method overestimates the creep strain of accelerated-cured concrete.
- In general, AASHTO 2007 underestimates the creep strain of early-age concrete and overestimates the creep strain of later-age concrete.
- In general, the AASHTO 2007 creep prediction method was among the most accurate of the five creep prediction methods investigated in this research.
- The CEB 90 method is the most accurate method for estimating creep strain for both conventional-slump concrete and SCC.
- In general, the GL 2000 creep prediction method overestimated the creep strain of both the conventional-slump and SCC mixtures.
- The GL 2000 model significantly overestimated the creep strain of the high-strength SCC mixtures used in this study.
- The GL 2000 method was unable to take accelerated curing into account; therefore, it significantly overestimated the creep strain of all accelerated-cured specimens.
- In general, the GL 2000 method was one of the least accurate creep prediction models investigated in this study.
- In general, the B3 creep prediction method overestimated the creep strain of all concrete mixtures used in this study.
- The B3 creep prediction method was unable to take accelerated curing into account; therefore, it significantly overestimated the creep strain of all accelerated-cured specimens.



- The B3 model significantly overestimated the creep strain of the high-strength SCC mixtures used in this study.
- In general, the B3 creep prediction method was one of the least accurate creep prediction methods investigated in this study
- The Modified CEB 90 method provides improved accuracy with regards to estimating the creep strain of all the moderate-strength mixtures in this study when compared to the CEB 90 method, except for the MS-SL mixture.
- The Modified CEB 90 method provides improved accuracy with regards to estimating the creep strain of all the accelerated-cured specimens in this study when compared to the CEB 90 method.

## **CHAPTER 6**

### **CONCLUSIONS AND RECOMMENDATIONS**

#### **6.1 SUMMARY OF LABORATORY WORK**

For this study, four SCC mixtures and one conventional-slump mixture were mixed and tested to determine the creep behavior of each. The SCC mixtures were comprised of varying types and quantities of constituent materials. This included Type III portland cement and two types of supplementary cementing materials (Class C fly ash and GGBF slag), for which the replacement percentages were varied. Two different water-to-cementitious materials ratios were also used for the various SCC mixtures. Compressive strength, creep, and drying shrinkage data were gathered for all mixtures. In addition, eight 6 in. x 12 in. cylinders were accelerated-cured at elevated temperatures similar to those used by the prestressing industry in the Southeastern United States.

For each SCC mixture, the slump flow, VSI, T-50, and total air content values were determined. The compressive strength testing was conducted on 6 in. x 12 in. cylinders in accordance with AASHTO T 22 (2003). Creep and drying shrinkage specimens were made from 6 in. x 12 in. cylinders and were tested according ASTM C 512 (2006). Specimens of each mixture were loaded at five loading ages to determine the creep response of each mixture. All specimens were loaded to 40 percent of their compressive strength at the time of insertion into the creep frames.

## **6.2 CONCLUSIONS**

### **6.2.1 FRESH PROPERTIES**

From this research, the following conclusion can be drawn about the fresh properties of SCC:

1. For a given SCM, as the  $w/cm$  decreases, the T-50 time increases, which indicates that the viscosity increases with a decrease in  $w/cm$ .
2. GGBF slag mixtures exhibited larger T-50 times than fly ash mixtures proportioned to provide similar 18-hour strength.

### **6.2.2 HARDENED PROPERTIES**

From this research, the following conclusions can be drawn about the hardened properties of SCC:

1. Mixtures containing GGBF slag gained compressive strength at a slower rate than those containing a cement replacement of Class C fly ash.
2. When curing is accelerated and the load is applied at 18 hours, the creep of all the SCC mixtures is less than the creep of the conventional-slump mixture.
3. Since the accelerated curing condition simulates plant conditions, excessive creep is not expected for full-scale members constructed with these SCC mixtures.

4. All SCC mixtures cured under elevated or standard laboratory temperature exhibited creep values similar to or less than the conventional-slump concrete mixture.
5. When curing is *not* accelerated, the creep behavior of the moderate-strength fly ash SCC and conventional-slump mixture is similar.
6. The high-strength mixtures had the highest paste content, but exhibited less creep than any of the moderate-strength mixtures. This is attributed to the increased strength and decreased permeability of the hydrated cement paste of these low- $w/cm$  mixtures.
7. At a fixed  $w/cm$ , SCC mixtures made with GGBF slag creep less than those made with fly ash, regardless of the age at loading.
8. All SCC mixtures exhibited lower drying shrinkage as the  $w/cm$  decreased.
9. All SCC mixtures exhibited drying shrinkage strains that were similar in magnitude to the conventional-slump mixture. For this reason, full-scale members constructed with SCC are not expected to experience excessive drying shrinkage.

### **6.2.3 CREEP PREDICTION METHODS**

Based on the results obtained through this research, the following conclusions can be drawn:

1. When curing was accelerated, ACI 209 provided the most accurate estimated creep strain values for the conventional-slump mixture.

2. The ACI 209 creep prediction method was unable to accurately predict the creep strain in the high-strength concrete mixtures used in this study.
3. In general, ACI 209 was one of the most accurate creep prediction methods of the five that were investigated in this study.
4. In general, the AASHTO 2007 creep prediction method overestimates the creep strain of accelerated-cured concrete.
5. In general, AASHTO 2007 underestimates the creep strain of early-age concrete and overestimates the creep strain of later-age concrete.
6. In general, the AASHTO 2007 creep prediction method was among the most accurate of the five creep prediction methods investigated in this research.
7. The CEB 90 method is the most accurate method for estimating creep strain for both conventional-slump concrete and SCC.
8. In general, the GL 2000 creep prediction method overestimated the creep strain of both the conventional-slump and SCC mixtures.
9. The GL 2000 model significantly overestimated the creep strain of the high-strength SCC mixtures used in this study.
10. The GL 2000 method was unable to take accelerated curing into account; therefore, it significantly overestimated the creep strain of all accelerated-cured specimens.
11. In general, the GL 2000 method was one of the least accurate creep prediction models investigated in this study.

12. In general, the B3 creep prediction method overestimated the creep strain of all concrete mixtures used in this study.
13. The B3 creep prediction method was unable to take accelerated curing into account; therefore, it significantly overestimated the creep strain of all accelerated-cured specimens.
14. The B3 model significantly overestimated the creep strain of the high-strength SCC mixtures used in this study.
15. In general, the B3 creep prediction method was one of the least accurate creep prediction methods investigated in this study.
16. The Modified CEB 90 method provides improved accuracy with regards to estimating the creep strain of all the moderate-strength mixtures in this study when compared to the CEB 90 method, except for the MS-SL mixture.
17. The Modified CEB 90 method provides improved accuracy with regards to estimating the creep strain of all the accelerated-cured specimens in this study when compared to the CEB 90 method.

### **6.3 RECOMMENDATIONS FOR FUTURE RESEARCH**

Before implementing SCC into prestressed construction, future research needs to be conducted. The following recommendations can be made based on the research detailed in this report:

- Further research is required to determine the long-term creep behavior of these SCC mixtures past one year.
- Creep and shrinkage testing should be performed on full-scale prestressed elements to determine the behavior of these SCC mixtures in real-world applications.

## REFERENCES

- AASHTO. 2007. *AASHTO LRFD Bridge Design Specifications: Customary U.S. Units*. 3<sup>rd</sup> ed. Washington D.C.: American Association of State Highway and Transportation Officials (AASHTO).
- AASHTO M 43. 2003. "Sizes of Aggregate for Road and Bridge Construction". In *Standard Specifications for Transportation Materials and Methods of Sampling and Testing*. Washington, DC: American Association of State Highway and Transportation Officials.
- AASHTO M 6. 2003. "Fine Aggregate for Portland Cement Concrete". In *Standard Specifications for Transportation Materials and Methods of Sampling and Testing*. Washington, DC: American Association of State Highway and Transportation Officials.
- AASHTO M 6. 2003. "Fine Aggregate for Portland Cement Concrete". In *Standard Specifications for Transportation Materials and Methods of Sampling and Testing*. Washington, DC: American Association of State Highway and Transportation Officials.
- AASHTO M 6. 2003. "Fine Aggregate for Portland Cement Concrete". In *Standard Specifications for Transportation Materials and Methods of Sampling and Testing*. Washington, DC: American Association of State Highway and Transportation Officials.



- AASHTO T 22. 2003. “Compressive Strength of Cylindrical Concrete Specimens”. In *Standard Specifications for Transportation Materials and Methods of Sampling and Testing*. Washington, DC: American Association of State Highway and Transportation Officials.
- AASHTO T 121. 2003. “Mass per Cubic Meter (Cubic Foot), Yield, and Air Content (Gravimetric) of Concrete”. In *Standard Specifications for Transportation Materials and Methods of Sampling and Testing*. Washington, DC: American Association of State Highway and Transportation Officials.
- AASHTO T 126. 2003. “Making and Curing Concrete Test Specimens in the Laboratory”. In *Standard Specifications for Transportation Materials and Methods of Sampling and Testing*. Washington, DC: American Association of State Highway and Transportation Officials.
- AASHTO T 231. 2003. “Capping Cylindrical Concrete Specimens”. In *Standard Specifications for Transportation Materials and Methods of Sampling and Testing*. Washington, DC: American Association of State Highway and Transportation Officials.
- AASHTO T 309. 2003. “Temperature of Freshly Mixed Portland Cement Concrete”. In *Standard Specifications for Transportation Materials and Methods of Sampling and Testing*. Washington, DC: American Association of State Highway and Transportation Officials.
- ACI 116. 2000. “Cement and Concrete Technology (ACI 116R)”. In *ACI Manual of Concrete Practice 2001: Part 1*. Farmington Hills, Michigan: American Concrete Institute, 116R-1-116R-73.

- ACI 209. 1997. "Prediction of Creep, Shrinkage, and Temperature Effects in concrete Structures (ACI 209R)". In *ACI Manual of Concrete Practice 2001: Part 1*. Farmington Hills, Michigan: American Concrete Institute, 209R-1-209R-47.
- ACI 233. 2000. "Ground Granulated Blast-Furnace Slag as a Cementitious Constituent in Concrete (ACI 233R)". In *ACI Manual of Concrete Practice 2001: Part 1*. Farmington Hills, Michigan: American Concrete Institute, 233R-1-233R-18.
- Al-Manaseer, A., Lam, J. P. 2005. Statistical Evaluation of Shrinkage and Creep Models. *ACI Materials Journal* 102, no.3: 170-176
- Assaad, J., Khayat, K. H. and Daczko, J. 2004. Evaluation of Static Stability of Self-Consolidating Concrete. *ACI Materials Journal* 101, no. 3: 207-215.
- ASTM C 150. 2006. "Specification for Portland Cement". *ASTM International*. West Conshohocken, Pennsylvania.
- ASTM C 512. 2006. "Standard Test for Creep in Concrete". *ASTM International*. West Conshohocken, Pennsylvania.
- ASTM C 1611. 2006. "Standard Test Method for Slump Flow of Self-Consolidating Concrete". *ASTM International*. West Conshohocken, Pennsylvania.
- Bazant, Z. P. 2001. Prediction of Concrete Creep and Shrinkage: Past, Present and Future. *Nuclear Engineering and Design* 203, no. 1: 27-38.
- Bazant, Z. P. and Baweja, S. 2000. "Description of Model B3 and Prediction Procedure". In *The Adam Neville Symposium: Creep and Shrinkage – Structural Design Effects*, ed. A. Al-Manaseer. Farmington Hills, Michigan: American Concrete Institute, 3-34.
- Carino, N.J., and Tank, R.C. 1992. Maturity Functions for Concrete Made with Various Cements and Admixtures. *ACI Materials Journal* 89, no. 2: 188-196

- CEB. 1990. "Creep and Shrinkage". In *CEB-FIP Model Code 1990*. Lausanne, Switzerland: Comite Euro-International du Beton (CEB), 53-65.
- Chopin, D., Francy, O., Lebourgeois, S. and Rougeau, P. 2003. "Creep and Shrinkage of Accelerated-cured Self-Compacting Concrete". In *Self-Compacting Concrete: Proceedings of the 3<sup>rd</sup> International RILEM Symposium*, ed. O. Wallevik and I. Nielsson. Bagnaux, France: RILEM Publications, 672-683.
- Colleparidi, M., Borsoi, A., Colleparidi, S., and Troli, R. 2005. "Strength, Shrinkage and Creep of SCC and Flowing Concrete". In *Second North American Conference on the Design and Use of Self-Consolidating Concrete and the Fourth International RILEM Symposium on Self-Compacting Concrete*, 911-920. Addison, Illinois: Hanley-Wood.
- D'Ambrosia, M. D., Lange, D. A., and Brinks, A. J., 2005. "Restrained Shrinkage and Creep of SCC and Flowing Concrete". In *Second North American Conference on the Design and Use of Self-Consolidating Concrete and the Fourth International RILEM Symposium on Self-Compacting Concrete*, 921-928. Addison, Illinois: Hanley-Wood.
- Domone, P. 2000. "Mix Design". In *State-of-the-Art Report (23) of RILEM Technical Committee 174-SCC*, ed. A. Skarendahl and O. Petersson. Cachan Cedex, France: RILEM Publications, 49-56.
- Gardner, N. J. and Lockman, M. J. 2001. Design Provisions for Drying Shrinkage and Creep of Normal-Strength Concrete. *ACI Materials Journal* 98, no. 2: 159-167
- Khayat, K. H. 1999. Workability, Testing, and Performance of Self-Consolidating Concrete. *ACI Materials Journal* 96, no. 3: 346-353.

- Khayat, K and Daczko, J. 2003. "The Holistic Approach to Self-Consolidating Concrete".  
In *First North American Conference on the Design and Use of Self-Consolidating Concrete 12-13 November 2002*, ed. S. Shah, J. Daczko, and J. Lingscheid. Addison, Illinois: Hanley-Wood, 9-14.
- Khayat, K., Hu, C. and Monty, H. 1999. "Stability of Self-Consolidating Concrete, Advantages and Potential Applications". In *Self-Compacting Concrete: Proceedings of the First International RILEM Symposium*, ed. A. Skarendahl and O. Petersson. Cachan Cedex, France: RILEM Publications, 143-152.
- Lee, Y., Yi, S. T., Kim, M. S. and Kim, J. K. 2006. Evaluation of a Basic Creep Model with Respect to Autogeneous Shrinkage. *Cement and Concrete Research* 36, no. 7: 1268-1278.
- Mindess, S., Young, J. F. and Darwin, D. 2003. *Concrete*, 2<sup>nd</sup> edition. Upper Saddle River, New Jersey: Prentice Hall.
- Muller, H. S. and Hillsdorf, H. K. 1990. "Evaluation of the Time-Dependent Behavior of Concrete, Summary Report on the Work of General Task Group 9". *CEB Bulletin d'Information*, no. 199: 290
- National Cooperative Highway Research Program (NCHRP). 2003. Report 496: Prestressed Losses in Pretension High-Strength Concrete Bridge Girders.
- Neville, A. M. 1996. *Properties of Concrete*, 4<sup>th</sup>. New York, New York: John Wiley & Sons, Inc.

- Okamura, H. and Ouchi, M. 1999. "Self-Compacting Concrete. Development, Present Use and Future". In *Self-Compacting Concrete: Proceedings of the First International RILEM Symposium*, ed. A. Skarendal and O. Petersson. Cachan Cedex, France: RILEM Publications, 3-14
- Pierard, J., Dieryck, V., and Desmyter, J. 2005. "Autogeneous Shrinkage of Self-Compacting Concrete". In *Second North American Conference on the Design and Use of Self-Consolidating Concrete and the Fourth International RILEM Symposium on Self-Compacting Concrete*, 1013-1022. Addison, Illinois: Hanley-Wood.
- Precast/Prestressed Concrete Institute (PCI). 2004. *Interim Guidelines for the Use of Self-Consolidating Concrete in Precast/Prestressed Concrete Institute Member Plants*, 1<sup>st</sup> edition. Chicago, Illinois: Precast/Prestressed Concrete Institute.
- Raghavan, K.P., Sarma, B.S., Chattopadhyay, D. 2003. "Creep, Shrinkage and Chloride Permeability Properties of Self-Consolidating Concrete". In *First North American Conference on the Design and Use of Self-Consolidating Concrete 12-13 November 2002*, ed. S. Shah, J. Daczko, and J. Lingsheit, 307-317. Addison, Illinois: Hanley-Wood.
- Roberts, J. 2005. Evaluation of Self-Consolidating Concrete for Use in Prestressed Girder Applications. M.S. Thesis, Auburn University.
- Schindler A.K., Barnes, R.W., Roberts, J.B., Rodriguez, S. 2006. Properties of Self-Consolidating Concrete for Prestressed Members. *ACI Materials Journal* 104, no.1: 53-61.

- Seng, V. and Shima, H. 2005. "Creep and Shrinkage of Self-Compacting Concrete with Different Limestone Powder Contents". In *Second North American Conference on the Design and Use of Self-Consolidating Concrete and the Fourth International RILEM Symposium on Self-Compacting Concrete*, 981-987. Addison, Illinois: Hanley-Wood.
- Tangtermsirikul, S. and Khayat, K. 2000. "Fresh Concrete Properties". In *State-of-the-Art-Report (23) of RILEM Technical Committee 174-SCC*, ed. A. Skarendahl and O. Petersson. Cachan Cedex, France: RILEM Publications, 17-22.

## **APPENDICES**

**APPENDIX A**  
**RAW TEST DATA**

**A.1 COLLECTED TEST DATA**

Tables A-1 through A-25 contain all creep test data collected during this study. Each table contains the total strain, drying shrinkage strain, creep strain, and applied load level for the individual loading age that is identified on the top line. Also provided are the compressive strength of the loading age and the target applied load level. Furthermore, the quality control compressive strength of the loading age is given. This test was done to ensure all batches of a mixture were similar in strength.



**Table A-6-1:** Raw collected data for the 18-hour loading age of the control mixture

<b>Mixture ID</b>		CTRL-18			
<b>Compressive Strength (psi)</b>		5,430			
<b>Target Applied Load (kips)</b>		62.6			
<b>Quality Control Compressive Strength (psi)</b>		8,400			
<b>Reading Interval</b>	<b>Shrinkage Strain (<math>\mu\epsilon</math>)</b>	<b>Total Strain (<math>\mu\epsilon</math>)</b>	<b>Creep Strain (<math>\mu\epsilon</math>)</b>	<b>Total Force (kips)</b>	
<b>Day One</b>	Pre-Load	----	----	----	----
	Post-Load	1	-541	-541	62.6
	2 to 6 hr	-11	-589	-578	62.5
<b>Week One</b>	1	-32	-649	-617	62.1
	2	-46	-674	-628	62.0
	3	-47	-694	-647	61.2
	4	-53	-702	-649	62.6
	5	-58	-716	-658	62.4
	6	-64	-740	-677	62.6
<b>Month One</b>	2	-93	-828	-735	61.2
	3	-112	-889	-777	61.1
	4	-132	-943	-811	61.3
<b>Months of Year One</b>	2	-188	-1089	-901	62.7
	3	-221	-1167	-945	62.4
	4	-248	-1244	-996	62.1
	5	-270	-1297	-1028	61.8
	6	-283	-1348	-1065	62.1
	7	-286	-1375	-1089	61.7
	8	-299	-1406	-1107	61.7
	9	-280	-1423	-1144	61.2
	10	-271	-1439	-1168	61.2
	11	-277	-1463	-1185	60.8
	12	-273	-1480	-1207	62.0
	13	-276	-1505	-1228	61.9

**Table A-6-2:** Raw collected data for the 2-day loading age of the control mixture

<b>Mixture ID</b>		<b>CTRL-2</b>			
<b>Compressive Strength (psi)</b>		5,850			
<b>Target Applied Load (kips)</b>		65.9			
<b>Quality Control Compressive Strength (psi)</b>		8,400			
<b>Reading Interval</b>	<b>Shrinkage Strain (<math>\mu\epsilon</math>)</b>	<b>Total Strain (<math>\mu\epsilon</math>)</b>	<b>Creep Strain (<math>\mu\epsilon</math>)</b>	<b>Total Force (kips)</b>	
<b>Day One</b>	Pre-Load	----	----	----	----
	Post-Load	0	-510	-510	65.9
	2 to 6 hr	-3	-631	-627	67.0
<b>Week One</b>	1	-20	-715	-695	67.5
	2	-22	-753	-731	67.5
	3	-26	-794	-768	67.4
	4	-29	-826	-796	67.0
	5	-39	-872	-833	67.2
	6	-47	-902	-855	67.3
<b>Month One</b>	2	-98	-1045	-947	66.9
	3	-130	-1130	-999	67.1
	4	-156	-1202	-1045	66.6
<b>Months of Year One</b>	2	-222	-1367	-1145	67.5
	3	-254	-1469	-1215	67.5
	4	-282	-1543	-1261	67.5
	5	-300	-1608	-1309	67.3
	6	-318	-1649	-1331	66.9
	7	-324	-1675	-1352	66.9
	8	-333	-1706	-1373	67.3
	9	-340	-1735	-1395	66.9
	10	-338	-1745	-1407	66.6
	11	-340	-1762	-1422	66.2
	12	-313	-1772	-1459	67.1
	13	-317	-1792	-1475	66.9

**Table A-6-3:** Raw collected data for the 7-day loading age of the control mixture

<b>Mixture ID</b>		<b>CTRL-7</b>			
<b>Compressive Strength (psi)</b>		7,660			
<b>Target Applied Load (kips)</b>		87.3			
<b>Quality Control Compressive Strength (psi)</b>		9,090			
<b>Reading Interval</b>	<b>Shrinkage Strain (<math>\mu\epsilon</math>)</b>	<b>Total Strain (<math>\mu\epsilon</math>)</b>	<b>Creep Strain (<math>\mu\epsilon</math>)</b>	<b>Total Force (kips)</b>	
<b>Day One</b>	Pre-Load	----	----	----	----
	Post-Load	-3	-628	-625	87.3
	2 to 6 hr	-3	-716	-713	86.9
<b>Week One</b>	1	-29	-814	-785	86.8
	2	-34	-853	-819	86.4
	3	-39	-893	-854	86.2
	4	-35	-934	-898	86.4
	5	-44	-977	-933	86.2
	6	-66	-1011	-946	85.4
<b>Month One</b>	2	-82	-1115	-1033	85.1
	3	-123	-1228	-1105	88.2
	4	-163	-1297	-1134	88.1
<b>Months of Year One</b>	2	-197	-1451	-1254	87.8
	3	-219	-1569	-1350	87.1
	4	-255	-1638	-1382	86.5
	5	-286	-1706	-1420	85.3
	6	-301	-1753	-1451	85.1
	7	-302	-1780	-1478	85.1
	8	-313	-1816	-1503	85.2
	9	-320	-1853	-1533	86.3
	10	-327	-1877	-1551	86.9
	11	-327	-1897	-1570	87.3
	12	-333	-1923	-1589	87.1
	13	-335	-1943	-1608	86.9

**Table A-6-4:** Raw collected data for the 28-day loading age of the control mixture

<b>Mixture ID</b>		<b>CTRL-28</b>			
<b>Compressive Strength (psi)</b>		9,090			
<b>Target Applied Load (kips)</b>		102.9			
<b>Quality Control Compressive Strength (psi)</b>		----			
	<b>Reading Interval</b>	<b>Shrinkage Strain (<math>\mu\epsilon</math>)</b>	<b>Total Strain (<math>\mu\epsilon</math>)</b>	<b>Creep Strain (<math>\mu\epsilon</math>)</b>	<b>Total Force (kips)</b>
<b>Day One</b>	Pre-Load	----	----	----	----
	Post-Load	-5	-626	-621	103.7
	2 to 6 hr	-7	-714	-708	104.0
<b>Week One</b>	1	-32	-828	-796	----
	2	-20	-878	-858	104.1
	3	-26	-925	-899	103.5
	4	-28	-967	-939	102.9
	5	-35	-974	-938	----
	6	-39	-1027	-988	103.2
<b>Month One</b>	2	-36	-1088	-1052	102.3
	3	-39	-1150	-1111	104.5
	4	-45	-1203	-1158	102.0
<b>Months of Year One</b>	2	-90	-1358	-1267	101.0
	3	-134	-1467	-1332	101.4
	4	-148	-1512	-1363	102.1
	5	-167	-1560	-1393	103.0
	6	-185	-1608	-1423	101.8
	7	-199	-1658	-1459	101.1
	8	-200	-1681	-1481	101.6
	9	-205	-1701	-1496	101.8
	10	-196	-1793	-1597	103.9
	11	-196	-1727	-1531	102.0
	12	-200	-1772	-1572	101.8
	13				

**Table A-6-5:** Raw collected data for the 90-day loading age of the control mixture

<b>Mixture ID</b>		<b>CTRL-90</b>			
<b>Compressive Strength (psi)</b>		8,330			
<b>Target Applied Load (kips)</b>		94.3			
<b>Quality Control Compressive Strength (psi)</b>		8,400			
<b>Reading Interval</b>	<b>Shrinkage Strain (<math>\mu\epsilon</math>)</b>	<b>Total Strain (<math>\mu\epsilon</math>)</b>	<b>Creep Strain (<math>\mu\epsilon</math>)</b>	<b>Total Force (kips)</b>	
<b>Day One</b>	Pre-Load	----	----	----	----
	Post-Load	0	-612	-612	95.4
	2 to 6 hr	-3	-679	-676	95.1
<b>Week One</b>	1	7	-733	-740	94.2
	2	-2	-773	-771	93.4
	3	-7	-796	-789	93.3
	4	-14	-821	-807	93.4
	5	-10	-839	-829	93.3
	6	-13	-857	-843	93.2
<b>Month One</b>	2	-23	-945	-922	96.1
	3	-29	-991	-962	95.5
	4	-28	-1035	-1006	93.7
<b>Months of Year One</b>	2	-46	-1153	-1107	93.3
	3	-62	-1239	-1176	93.2
	4	-74	-1313	-1239	92.6
	5	-65	-1347	-1282	92.9
	6	-68	-1376	-1308	92.4
	7	-67	-1406	-1339	92.4
	8	-59	-1432	-1374	92.5
	9	-69	-1455	-1386	92.7
	10	-74	-1477	-1402	92.6
	11	-78	-1495	-1416	93.9
	12	-83	-1495	-1412	93.6
	13	-83	-1521	-1438	93.3

**Table A-6-6:** Raw collected data for the 18-hour loading age of the MS-FA mixture

<b>Mixture ID</b>		<b>SCC-MS-FA-18</b>			
<b>Compressive Strength (psi)</b>		5,800			
<b>Target Applied Load (kips)</b>		66.9			
<b>Quality Control Compressive Strength (psi)</b>		10,020			
<b>Reading Interval</b>	<b>Shrinkage Strain (<math>\mu\epsilon</math>)</b>	<b>Total Strain (<math>\mu\epsilon</math>)</b>	<b>Creep Strain (<math>\mu\epsilon</math>)</b>	<b>Total Force (kips)</b>	
<b>Day One</b>	Pre-Load	----	----	----	----
	Post-Load	-3	-461	-459	66.9
	2 to 6 hr	-2	-505	-503	66.8
<b>Week One</b>	1	3	-560	-563	66.3
	2	-31	-576	-545	65.7
	3	-37	-607	-570	65.2
	4	-41	-643	-602	65.1
	5	-46	-683	-637	66.9
	6	-57	-703	-646	66.7
<b>Month One</b>	2	-100	-788	-687	65.4
	3	-143	-875	-732	64.5
	4	-170	-939	-769	65.0
<b>Months of Year One</b>	2	-227	-1082	-855	65.0
	3	-268	-1160	-892	65.3
	4	-245	-1180	-935	66.8
	5	-270	-1218	-949	65.6
	6	-275	-1236	-961	64.6
	7	-274	-1268	-994	64.5
	8	-292	-1293	-1000	64.5
	9	-310	-1315	-1006	65.2
	10	-299	-1317	-1018	65.7
	11	-293	-1331	-1038	65.6
	12	-299	-1341	-1042	65.7
	13	-301	-1352	-1051	67.0

**Table A-6-7:** Raw collected data for the 2-day loading age of the MS-FA mixture

<b>Mixture ID</b>		<b>SCC-MS-FA-2</b>			
<b>Compressive Strength (psi)</b>		5,700			
<b>Target Applied Load (kips)</b>		65.0			
<b>Quality Control Compressive Strength (psi)</b>		9,570			
<b>Reading Interval</b>	<b>Shrinkage Strain (<math>\mu\epsilon</math>)</b>	<b>Total Strain (<math>\mu\epsilon</math>)</b>	<b>Creep Strain (<math>\mu\epsilon</math>)</b>	<b>Total Force (kips)</b>	
<b>Day One</b>	Pre-Load	----	----	----	----
	Post-Load	-4	-558	-554	65.0
	2 to 6 hr	-3	-712	-710	64.9
<b>Week One</b>	1	-25	-789	-764	64.3
	2	-25	-869	-845	64.0
	3	-39	-936	-897	65.6
	4	-54	-986	-932	65.3
	5	-70	-1027	-957	65.4
	6	-82	-1056	-974	65.5
<b>Month One</b>	2	-130	-1188	-1059	65.3
	3	-159	-1279	-1119	65.3
	4	-187	-1362	-1176	65.5
<b>Months of Year One</b>	2	-238	-1469	-1231	64.7
	3	-258	-1535	-1277	63.3
	4	-294	-1606	-1313	63.3
	5	-306	-1634	-1328	64.2
	6	-318	-1658	-1340	64.2
	7	-328	-1684	-1356	64.4
	8	-327	-1692	-1365	63.7
	9	-323	-1701	-1378	63.6
	10	-311	-1708	-1397	65.2
	11	-325	-1722	-1397	64.4
	12	-323	-1723	-1400	64.5
	13	-329	-1729	-1400	64.7

**Table A-6-8:** Raw collected data for the 7-day loading age of the MS-FA mixture

<b>Mixture ID</b>		<b>SCC-MS-FA-7</b>			
<b>Compressive Strength (psi)</b>		7,570			
<b>Target Applied Load (kips)</b>		85.6			
<b>Quality Control Compressive Strength (psi)</b>		9,570			
<b>Reading Interval</b>	<b>Shrinkage Strain (<math>\mu\epsilon</math>)</b>	<b>Total Strain (<math>\mu\epsilon</math>)</b>	<b>Creep Strain (<math>\mu\epsilon</math>)</b>	<b>Total Force (kips)</b>	
<b>Day One</b>	Pre-Load	----	----	----	----
	Post-Load	-1	-622	-621	85.7
	2 to 6 hr	-4	-733	-729	86.8
<b>Week One</b>	1	-5	-811	-806	86.5
	2	-5	-873	-867	86.3
	3	-21	-928	-907	85.8
	4	-25	-975	-950	85.9
	5	-29	-1008	-979	87.3
	6	-36	-1037	-1001	87.3
<b>Month One</b>	2	-106	-1216	-1111	86.0
	3	-126	-1293	-1166	86.0
	4	-151	-1364	-1213	86.3
<b>Months of Year One</b>	2	-201	-1523	-1322	87.0
	3	-237	-1617	-1380	86.0
	4	-239	-1671	-1432	86.7
	5	-250	-1704	-1454	86.6
	6	-258	-1739	-1481	86.0
	7	-272	-1763	-1491	85.5
	8	-269	-1769	-1500	85.5
	9	-262	-1772	-1510	85.3
	10	-270	-1804	-1534	85.7
	11	-272	-1819	-1547	87.0
	12	-278	-1832	-1555	87.2
	13	-287	-1848	-1561	86.6



**Table A-6-9:** Raw collected data for the 28-day loading age of the MS-FA mixture

<b>Mixture ID</b>		<b>SCC-MS-FA-28</b>			
<b>Compressive Strength (psi)</b>		9,570			
<b>Target Applied Load (kips)</b>		108.2			
<b>Quality Control Compressive Strength (psi)</b>		----			
<b>Reading Interval</b>	<b>Shrinkage Strain (<math>\mu\epsilon</math>)</b>	<b>Total Strain (<math>\mu\epsilon</math>)</b>	<b>Creep Strain (<math>\mu\epsilon</math>)</b>	<b>Total Force (kips)</b>	
<b>Day One</b>	Pre-Load	----	----	----	----
	Post-Load	0	-750	-750	109.4
	2 to 6 hr	-3	-804	-800	107.6
<b>Week One</b>	1	-3	-905	-902	108.4
	2	-3	-967	-964	107.9
	3	-16	-1002	-986	108.9
	4	-17	-1035	-1017	108.4
	5	-15	-1060	-1045	107.9
	6	-24	-1085	-1061	108.0
<b>Month One</b>	2	-43	-1212	-1168	108.1
	3	-49	-1293	-1243	108.0
	4	-59	-1349	-1290	108.8
<b>Months of Year One</b>	2	-98	-1579	-1481	107.4
	3	-137	-1698	-1561	106.2
	4	-145	-1753	-1608	106.1
	5	-152	-1808	-1656	106.2
	6	-140	-1854	-1714	106.3
	7	-150	-1882	-1731	106.1
	8	-154	-1909	-1755	108.1
	9	-158	-1935	-1777	108.6
	10	-169	-1962	-1793	108.0
	11	-176	-1985	-1809	107.1
	12	-180	-2005	-1825	106.4
	13	-174	-2031	-1857	106.2

**Table A-6-10:** Raw collected data for the 90-day loading age of the MS-FA mixture

<b>Mixture ID</b>		<b>SCC-MS-FA-90</b>			
<b>Compressive Strength (psi)</b>		9,830			
<b>Target Applied Load (kips)</b>		112.8			
<b>Quality Control Compressive Strength (psi)</b>		9,570			
<b>Reading Interval</b>	<b>Shrinkage Strain (µε)</b>	<b>Total Strain (µε)</b>	<b>Creep Strain (µε)</b>	<b>Total Force (kips)</b>	
<b>Day One</b>	Pre-Load	----	----	----	----
	Post-Load	-1	-730	-730	112.8
	2 to 6 hr	-3	-782	-780	112.4
<b>Week One</b>	1	1	-871	-871	113.0
	2	-6	-921	-915	111.5
	3	1	-920	-922	113.3
	4	7	-939	-946	113.2
	5	8	-953	-961	113.1
	6	-13	-1001	-988	112.8
<b>Month One</b>	2	5	-1046	-1051	113.1
	3	4	-1090	-1094	113.3
	4	-18	-1156	-1138	113.3
<b>Months of Year One</b>	2	-25	-1222	-1196	112.5
	3	-45	-1306	-1261	113.0
	4	-45	-1344	-1298	113.3
	5	-38	-1375	-1337	113.1
	6	-30	-1407	-1377	112.4
	7	-38	-1428	-1390	113.2
	8	-39	-1462	-1423	113.4
	9	-59	-1487	-1428	113.3
	10	-69	-1510	-1441	111.9
	11	-78	-1530	-1452	110.8
	12	-81	-1545	-1465	110.0
	13	-87	-1562	-1475	110.1

**Table A-6-11:** Raw collected data for the 18-hour loading age of the HS-FA mixture

<b>Mixture ID</b>		<b>SCC-HS-FA-18</b>			
<b>Compressive Strength (psi)</b>		9,190			
<b>Target Applied Load (kips)</b>		102.5			
<b>Quality Control Compressive Strength (psi)</b>		12,790			
<b>Reading Interval</b>	<b>Shrinkage Strain (<math>\mu\epsilon</math>)</b>	<b>Total Strain (<math>\mu\epsilon</math>)</b>	<b>Creep Strain (<math>\mu\epsilon</math>)</b>	<b>Total Force (kips)</b>	
<b>Day One</b>	Pre-Load	----	----	----	----
	Post-Load	0	-653	-653	102.5
	2 to 6 hr	-3	-696	-693	101.9
<b>Week One</b>	1	-40	-782	-742	102.0
	2	-34	-841	-807	102.3
	3	-43	-859	-816	102.6
	4	-41	-885	-844	102.4
	5	-49	-907	-857	102.5
	6	-58	-931	-873	102.8
<b>Month One</b>	2	-104	-1039	-935	102.4
	3	-140	-1152	-1011	102.5
	4	-165	-1223	-1058	102.3
<b>Months of Year One</b>	2	-192	-1286	-1094	102.7
	3	-205	-1339	-1134	102.3
	4	-213	-1365	-1152	102.6
	5	-215	-1388	-1174	101.9
	6	-222	-1413	-1191	103.3
	7	-233	-1435	-1202	104.1
	8	-246	-1462	-1216	103.6
	9	-256	-1487	-1231	102.8
	10	-264	-1510	-1246	103.1
	11	-259	-1525	-1266	102.7
	12	-265	-1529	-1264	102.6
	13	-267	-1535	-1269	103.3

**Table A-6-12:** Raw collected data for the 2-day loading age of the HS-FA mixture

<b>Mixture ID</b>		<b>SCC-HS-FA-2</b>			
<b>Compressive Strength (psi)</b>		9,100			
<b>Target Applied Load (kips)</b>		101.3			
<b>Quality Control Compressive Strength (psi)</b>		12,970			
<b>Reading Interval</b>	<b>Shrinkage Strain (<math>\mu\epsilon</math>)</b>	<b>Total Strain (<math>\mu\epsilon</math>)</b>	<b>Creep Strain (<math>\mu\epsilon</math>)</b>	<b>Total Force (kips)</b>	
<b>Day One</b>	Pre-Load	----	----	----	----
	Post-Load	-1	-724	-723	101.3
	2 to 6 hr	-1	-821	-819	104.8
<b>Week One</b>	1	-17	-968	-951	105.0
	2	-39	-1044	-1004	105.0
	3	-61	-1119	-1058	105.0
	4	-57	-1164	-1107	104.9
	5	-57	-1201	-1144	105.0
	6	-66	-1216	-1150	104.8
<b>Month One</b>	2	-93	-1348	-1255	105.0
	3	-128	-1418	-1290	104.9
	4	-157	-1468	-1311	104.7
<b>Months of Year One</b>	2	-181	-1571	-1390	101.7
	3	-198	-1628	-1430	103.5
	4	-209	-1650	-1441	102.2
	5	-207	-1657	-1451	103.7
	6	-220	-1678	-1458	103.1
	7	-216	-1692	-1476	103.6
	8	-209	-1703	-1494	103.7
	9	-215	-1719	-1504	103.5
	10	-217	-1732	-1515	103.9
	11	-229	-1753	-1524	105.0
	12	-196	-1731	-1535	104.7
	13	-212	-1747	-1535	104.0

**Table A-6-13:** Raw collected data for the 7-day loading age of the HS-FA mixture

<b>Mixture ID</b>		<b>SCC-HS-FA-7</b>			
<b>Compressive Strength (psi)</b>		11,110			
<b>Target Applied Load (kips)</b>		128.2			
<b>Quality Control Compressive Strength (psi)</b>		12,800			
<b>Reading Interval</b>	<b>Shrinkage Strain (<math>\mu\epsilon</math>)</b>	<b>Total Strain (<math>\mu\epsilon</math>)</b>	<b>Creep Strain (<math>\mu\epsilon</math>)</b>	<b>Total Force (kips)</b>	
<b>Day One</b>	Pre-Load	----	----	----	----
	Post-Load	-2	-756	-754	128.2
	2 to 6 hr	-1	-846	-845	125.8
<b>Week One</b>	1	-9	-998	-989	124.1
	2	-12	-1089	-1077	125.4
	3	-19	-1135	-1115	125.4
	4	-32	-1174	-1142	126.2
	5	-41	-1210	-1168	126.6
	6	-49	-1228	-1179	124.3
<b>Month One</b>	2	-80	-1362	-1282	123.8
	3	-102	-1442	-1340	123.6
	4	-109	-1481	-1372	123.4
<b>Months of Year One</b>	2	-139	-1566	-1426	123.3
	3	-163	-1646	-1484	123.8
	4	-179	-1697	-1517	123.7
	5	-185	-1715	-1530	123.3
	6	-191	-1742	-1552	123.2
	7	-190	-1757	-1567	125.1
	8	-186	-1771	-1585	124.7
	9	-181	-1780	-1599	123.5
	10	-191	-1790	-1599	123.4
	11	-198	-1801	-1603	123.3
	12	-213	-1820	-1607	123.3
	13	-213	-1827	-1613	123.9

**Table A-6-14:** Raw collected data for the 28-day loading age of the HS-FA mixture

<b>Mixture ID</b>		<b>SCC-HS-FA-28</b>			
<b>Compressive Strength (psi)</b>		12,800			
<b>Target Applied Load (kips)</b>		145.1			
<b>Quality Control Compressive Strength (psi)</b>		----			
<b>Reading Interval</b>	<b>Shrinkage Strain (<math>\mu\epsilon</math>)</b>	<b>Total Strain (<math>\mu\epsilon</math>)</b>	<b>Creep Strain (<math>\mu\epsilon</math>)</b>	<b>Total Force (kips)</b>	
<b>Day One</b>	Pre-Load	----	----	----	----
	Post-Load	-1	-788	-786	145.1
	2 to 6 hr	-3	-857	-854	145.7
<b>Week One</b>	1	-1	-910	-908	145.2
	2	-3	-960	-957	145.0
	3	-6	-1005	-999	144.8
	4	-9	-1045	-1036	144.8
	5	-7	-1061	-1055	147.3
	6	-11	-1074	-1063	144.7
<b>Month One</b>	2	-27	-1166	-1139	144.6
	3	-27	-1202	-1176	144.6
	4	-36	-1258	-1222	142.6
<b>Months of Year One</b>	2	-56	-1342	-1285	142.4
	3	-67	-1404	-1337	142.7
	4	-60	-1435	-1375	143.6
	5	-84	-1466	-1382	143.0
	6	-86	-1492	-1406	142.7
	7	-68	-1509	-1441	143.0
	8	-74	-1542	-1468	144.4
	9	-89	-1566	-1477	144.3
	10	-109	-1549	-1440	143.7
	11	-114	-1567	-1453	142.7
	12	-119	-1581	-1462	142.7
	13	-125	-1593	-1469	142.6

**Table A-6-15:** Raw collected data for the 90-day loading age of the HS-FA mixture

<b>Mixture ID</b>		<b>SCC-HS-FA-90</b>			
<b>Compressive Strength (psi)</b>		13,630			
<b>Target Applied Load (kips)</b>		151.5			
<b>Quality Control Compressive Strength (psi)</b>		12,800			
<b>Reading Interval</b>	<b>Shrinkage Strain (<math>\mu\epsilon</math>)</b>	<b>Total Strain (<math>\mu\epsilon</math>)</b>	<b>Creep Strain (<math>\mu\epsilon</math>)</b>	<b>Total Force (kips)</b>	
<b>Day One</b>	Pre-Load	----	----	----	----
	Post-Load	-4	-891	-887	151.6
	2 to 6 hr	-6	-930	-924	151.2
<b>Week One</b>	1	-6	-996	-990	153.3
	2	-3	-1032	-1029	152.8
	3	-7	-1051	-1044	152.4
	4	-11	-1067	-1055	151.9
	5	-9	-1083	-1074	151.6
	6	-6	-1101	-1095	151.5
<b>Month One</b>	2	-11	-1135	-1124	151.2
	3	-15	-1168	-1154	151.2
	4	-11	-1214	-1204	150.6
<b>Months of Year One</b>	2	-2	-1255	-1253	149.5
	3	-37	-1327	-1290	149.3
	4	-32	-1356	-1324	149.2
	5	-33	-1384	-1351	148.7
	6	-21	-1407	-1386	147.2
	7	-35	-1428	-1393	146.6
	8	-49	-1447	-1397	146.1
	9	-57	-1466	-1409	145.6
	10	-58	-1476	-1418	144.9
	11	-63	-1495	-1432	145.1
	12	-67	-1515	-1449	147.3
	13	-71	-1533	-1462	147.0

**Table A-6-16:** Raw collected data for the 18-hour loading age of the MS-SL mixture

<b>Mixture ID</b>		<b>SCC-MS-SL-18</b>			
<b>Compressive Strength (psi)</b>		6,250			
<b>Target Applied Load (kips)</b>		71.1			
<b>Quality Control Compressive Strength (psi)</b>		9,100			
<b>Reading Interval</b>	<b>Shrinkage Strain (<math>\mu\epsilon</math>)</b>	<b>Total Strain (<math>\mu\epsilon</math>)</b>	<b>Creep Strain (<math>\mu\epsilon</math>)</b>	<b>Total Force (kips)</b>	
<b>Day One</b>	Pre-Load	----	----	----	----
	Post-Load	-2	-461	-459	71.1
	2 to 6 hr	-3	-518	-516	70.5
<b>Week One</b>	1	-63	-589	-526	70.5
	2	-80	-641	-561	70.2
	3	-90	-688	-598	70.2
	4	-96	-726	-630	70.6
	5	-93	-740	-647	70.6
	6	-110	-769	-659	70.2
<b>Month One</b>	2	-154	-859	-705	70.5
	3	-167	-910	-742	71.6
	4	-188	-955	-767	70.5
<b>Months of Year One</b>	2	-227	-1025	-798	69.9
	3	-257	-1087	-829	69.4
	4	-260	-1106	-846	69.4
	5	-257	-1124	-866	69.4
	6	-265	-1154	-889	69.4
	7	-268	-1173	-905	71.1
	8	-270	-1190	-920	70.6
	9	-265	-1202	-937	69.7
	10	-275	-1214	-940	69.8
	11	-286	-1230	-944	69.5
	12	-303	-1250	-947	69.4
	13	-293	-1264	-971	69.6



**Table A-6-17: Raw collected data for the 2-day loading age of the MS-SL mixture**

<b>Mixture ID</b>		<b>SCC-MS-SL-2</b>			
<b>Compressive Strength (psi)</b>		4,620			
<b>Target Applied Load (kips)</b>		53.0			
<b>Quality Control Compressive Strength (psi)</b>		8,890			
	<b>Reading Interval</b>	<b>Shrinkage Strain (<math>\mu\epsilon</math>)</b>	<b>Total Strain (<math>\mu\epsilon</math>)</b>	<b>Creep Strain (<math>\mu\epsilon</math>)</b>	<b>Total Force (kips)</b>
<b>Day One</b>	Pre-Load	----	----	----	----
	Post-Load	-1	-425	-424	53.0
	2 to 6 hr	-3	-492	-488	52.8
<b>Week One</b>	1	-19	-602	-582	51.8
	2	-33	-716	-683	52.0
	3	-54	-772	-718	51.9
	4	-70	-803	-733	52.3
	5	-78	-829	-751	52.5
	6	-64	-844	-780	52.1
<b>Month One</b>	2	-104	-908	-805	52.3
	3	-122	-946	-823	53.1
	4	-129	-967	-838	53.0
<b>Months of Year One</b>	2	-163	-1031	-868	51.9
	3	-188	-1059	-871	51.6
	4	-192	-1082	-890	51.3
	5	-189	-1107	-919	52.0
	6	-222	-1132	-910	51.4
	7	-222	-1145	-923	52.6
	8	-223	-1157	-934	52.7
	9	-217	-1164	-947	52.7
	10	-229	-1171	-942	52.9
	11	-231	-1176	-945	52.5
	12	-265	-1200	-935	52.1
	13	-273	-1211	-937	51.8

**Table A-6-18:** Raw collected data for the 7-day loading age of the MS-SL mixture

<b>Mixture ID</b>		<b>SCC-MS-SL-7</b>			
<b>Compressive Strength (psi)</b>		6,840			
<b>Target Applied Load (kips)</b>		78.3			
<b>Quality Control Compressive Strength (psi)</b>		8,890			
<b>Reading Interval</b>	<b>Shrinkage Strain (<math>\mu\epsilon</math>)</b>	<b>Total Strain (<math>\mu\epsilon</math>)</b>	<b>Creep Strain (<math>\mu\epsilon</math>)</b>	<b>Total Force (kips)</b>	
<b>Day One</b>	Pre-Load	----	----	----	----
	Post-Load	-2	-405	-403	78.3
	2 to 6 hr	0	-554	-554	77.3
<b>Week One</b>	1	-71	-666	-595	76.5
	2	-76	-718	-642	77.4
	3	-90	-764	-675	77.1
	4	-96	-800	-704	76.4
	5	-111	-829	-718	77.4
	6	-130	-861	-730	76.5
<b>Month One</b>	2	-173	-934	-762	76.4
	3	-181	-982	-800	76.5
	4	-194	-1016	-822	76.4
<b>Months of Year One</b>	2	-227	-1109	-882	77.0
	3	-274	-1146	-873	78.8
	4	-260	-1178	-918	77.4
	5	-265	-1202	-937	77.2
	6	-286	-1224	-938	77.0
	7	-274	-1237	-964	78.7
	8	-283	-1256	-973	78.8
	9	-277	-1265	-988	77.2
	10	-274	-1277	-1003	76.2
	11	-279	-1291	-1012	75.9
	12	-283	-1296	-1013	77.6
	13	-301	-1321	-1019	78.7

**Table A-6-19:** Raw collected data for the 28-day loading age of the MS-SL mixture

<b>Mixture ID</b>		<b>SCC-MS-SL-28</b>			
<b>Compressive Strength (psi)</b>		10,610			
<b>Target Applied Load (kips)</b>		120.8			
<b>Quality Control Compressive Strength (psi)</b>		----			
<b>Reading Interval</b>	<b>Shrinkage Strain (<math>\mu\epsilon</math>)</b>	<b>Total Strain (<math>\mu\epsilon</math>)</b>	<b>Creep Strain (<math>\mu\epsilon</math>)</b>	<b>Total Force (kips)</b>	
<b>Day One</b>	Pre-Load	----	----	----	----
	Post-Load	-1	-710	-708	120.7
	2 to 6 hr	-3	-750	-747	120.5
<b>Week One</b>	1	11	-797	-808	119.9
	2	-12	-838	-826	118.3
	3	-7	-852	-845	118.3
	4	-5	-865	-859	118.1
	5	-5	-875	-870	118.1
	6	-4	-885	-881	118.1
<b>Month One</b>	2	-13	-941	-928	120.5
	3	-9	-979	-970	119.3
	4	-27	-1045	-1017	119.0
<b>Months of Year One</b>	2	-40	-1115	-1075	118.6
	3	-43	-1156	-1113	118.5
	4	-56	-1199	-1144	119.1
	5	-59	-1239	-1180	119.8
	6	-60	-1277	-1216	119.3
	7	-72	-1306	-1235	119.3
	8	-80	-1332	-1252	118.9
	9	-89	-1356	-1267	119.3
	10	-91	-1399	-1307	119.6
	11	-97	-1389	-1292	119.3
	12	-106	-1410	-1304	119.6
	13	-113	-1437	-1324	119.6

**Table A-6-20:** Raw collected data for the 90-day loading age of the MS-SL mixture

<b>Mixture ID</b>		<b>SCC-MS-SL-90</b>			
<b>Compressive Strength (psi)</b>		11,580			
<b>Target Applied Load (kips)</b>		128.5			
<b>Quality Control Compressive Strength (psi)</b>		8,890			
<b>Reading Interval</b>	<b>Shrinkage Strain (<math>\mu\epsilon</math>)</b>	<b>Total Strain (<math>\mu\epsilon</math>)</b>	<b>Creep Strain (<math>\mu\epsilon</math>)</b>	<b>Total Force (kips)</b>	
<b>Day One</b>	Pre-Load	----	----	----	----
	Post-Load	-1	-754	-753	128.5
	2 to 6 hr	-3	-811	-808	128.8
<b>Week One</b>	1	6	-844	-850	128.5
	2	-9	-867	-858	129.0
	3	-7	-879	-872	128.9
	4	-5	-890	-885	128.6
	5	-2	-899	-897	128.5
	6	-9	-920	-912	128.4
<b>Month One</b>	2	-14	-936	-922	128.5
	3	-21	-952	-930	128.4
	4	-22	-997	-975	129.1
<b>Months of Year One</b>	2	-22	-1020	-998	128.6
	3	-25	-1111	-1085	128.8
	4	-31	-1156	-1125	128.6
	5	-29	-1199	-1170	129.7
	6	-26	-1228	-1202	128.9
	7	-24	-1259	-1235	128.8
	8	-31	-1292	-1261	128.5
	9	-36	-1301	-1265	129.2
	10	-58	-1334	-1276	129.1
	11	-67	-1349	-1281	128.5
	12	-81	-1370	-1289	128.8
	13	-101	-1393	-1292	129.4

**Table A-6-21:** Raw collected data for the 18-hour loading age of the HS-SL mixture

<b>Mixture ID</b>		<b>SCC-HS-SL-18</b>			
<b>Compressive Strength (psi)</b>		9,600			
<b>Target Applied Load (kips)</b>		106.9			
<b>Quality Control Compressive Strength (psi)</b>		12,880			
<b>Reading Interval</b>	<b>Shrinkage Strain (<math>\mu\epsilon</math>)</b>	<b>Total Strain (<math>\mu\epsilon</math>)</b>	<b>Creep Strain (<math>\mu\epsilon</math>)</b>	<b>Total Force (kips)</b>	
<b>Day One</b>	Pre-Load	----	----	----	----
	Post-Load	-1	-681	-680	106.9
	2 to 6 hr	-5	-734	-729	106.8
<b>Week One</b>	1	-33	-811	-778	107.9
	2	-43	-840	-797	106.8
	3	-53	-867	-815	106.6
	4	-60	-890	-830	106.7
	5	-67	-912	-845	107.0
	6	-58	-929	-871	106.5
<b>Month One</b>	2	-96	-988	-893	106.7
	3	-130	-1062	-932	107.1
	4	-137	-1111	-974	107.2
<b>Months of Year One</b>	2	-142	-1182	-1040	106.5
	3	-163	-1243	-1080	106.9
	4	-158	-1270	-1111	106.5
	5	-166	-1293	-1128	106.5
	6	-172	-1314	-1142	107.8
	7	-188	-1334	-1146	107.1
	8	-200	-1357	-1157	107.1
	9	-211	-1382	-1171	107.0
	10	-215	-1398	-1183	106.9
	11	-213	-1401	-1188	107.0
	12	-219	-1419	-1199	107.2
	13	-223	-1432	-1209	107.4

**Table A-6-22:** Raw collected data for the 2-day loading age of the HS-SL mixture

<b>Mixture ID</b>		<b>SCC-HS-SL-2</b>			
<b>Compressive Strength (psi)</b>		8,830			
<b>Target Applied Load (kips)</b>		101.7			
<b>Quality Control Compressive Strength (psi)</b>		12,490			
<b>Reading Interval</b>	<b>Shrinkage Strain (<math>\mu\epsilon</math>)</b>	<b>Total Strain (<math>\mu\epsilon</math>)</b>	<b>Creep Strain (<math>\mu\epsilon</math>)</b>	<b>Total Force (kips)</b>	
<b>Day One</b>	Pre-Load	----	----	----	----
	Post-Load	0	-662	-662	101.7
	2 to 6 hr	0	-800	-800	100.6
<b>Week One</b>	1	-74	-1019	-946	99.6
	2	-78	-1110	-1032	101.6
	3	-97	-1171	-1074	101.4
	4	-111	-1217	-1106	101.7
	5	-122	-1255	-1133	101.8
	6	-143	-1284	-1141	100.0
<b>Month One</b>	2	-159	-1376	-1216	98.9
	3	-166	-1415	-1249	98.9
	4	-190	-1449	-1259	98.6
<b>Months of Year One</b>	2	-213	-1535	-1323	98.8
	3	-230	-1579	-1349	99.7
	4	-237	-1600	-1363	100.7
	5	-252	-1627	-1375	100.6
	6	-263	-1658	-1394	100.2
	7	-264	-1667	-1403	100.6
	8	-268	-1683	-1414	101.7
	9	-260	-1688	-1428	100.6
	10	-257	-1699	-1442	99.7
	11	-262	-1711	-1449	98.9
	12	-263	-1715	-1453	99.2
	13	-260	-1739	-1479	101.6

**Table A-6-23:** Raw collected data for the 7-day loading age of the HS-SL mixture

<b>Mixture ID</b>		<b>SCC-HS-SL-7</b>			
<b>Compressive Strength (psi)</b>		10,580			
<b>Target Applied Load (kips)</b>		118.4			
<b>Quality Control Compressive Strength (psi)</b>		12,880			
<b>Reading Interval</b>	<b>Shrinkage Strain (<math>\mu\epsilon</math>)</b>	<b>Total Strain (<math>\mu\epsilon</math>)</b>	<b>Creep Strain (<math>\mu\epsilon</math>)</b>	<b>Total Force (kips)</b>	
<b>Day One</b>	Pre-Load	----	----	----	----
	Post-Load	-1	-736	-734	118.4
	2 to 6 hr	-3	-784	-781	117.4
<b>Week One</b>	1	-26	-918	-891	120.2
	2	-24	-973	-949	119.6
	3	-36	-999	-963	118.2
	4	-45	-1014	-970	120.4
	5	-52	-1043	-990	120.6
	6	-60	-1065	-1005	120.6
<b>Month One</b>	2	-77	-1117	-1040	120.4
	3	-91	-1197	-1106	120.3
	4	-115	-1244	-1129	119.7
<b>Months of Year One</b>	2	-134	-1290	-1156	119.4
	3	-148	-1331	-1182	119.6
	4	-150	-1344	-1194	121.1
	5	-147	-1352	-1205	121.0
	6	-132	-1365	-1233	120.8
	7	-143	-1393	-1250	117.8
	8	-143	-1409	-1266	120.0
	9	-142	-1422	-1280	120.1
	10	-175	-1413	-1238	122.0
	11	-203	-1433	-1229	120.7
	12	-213	-1445	-1232	121.7
	13	-225	-1464	-1239	121.6

**Table A-6-24:** Raw collected data for the 28-day loading age of the HS-SL mixture

<b>Mixture ID</b>		<b>SCC-HS-SL-28</b>			
<b>Compressive Strength (psi)</b>		12,880			
<b>Target Applied Load (kips)</b>		143.7			
<b>Quality Control Compressive Strength (psi)</b>		----			
<b>Reading Interval</b>	<b>Shrinkage Strain (<math>\mu\epsilon</math>)</b>	<b>Total Strain (<math>\mu\epsilon</math>)</b>	<b>Creep Strain (<math>\mu\epsilon</math>)</b>	<b>Total Force (kips)</b>	
<b>Day One</b>	Pre-Load	----	----	----	----
	Post-Load	-1	-824	-823	143.7
	2 to 6 hr	-3	-866	-863	143.2
<b>Week One</b>	1	4	-913	-917	143.1
	2	4	-958	-962	143.0
	3	5	-955	-960	145.7
	4	-7	-998	-992	145.4
	5	-11	-1025	-1014	145.1
	6	-15	-1051	-1037	145.1
<b>Month One</b>	2	-18	-1075	-1057	144.3
	3	-21	-1113	-1093	146.1
	4	-23	-1158	-1135	146.0
<b>Months of Year One</b>	2	-23	-1200	-1177	144.7
	3	-23	-1249	-1226	144.2
	4	-28	-1277	-1249	145.4
	5	-31	-1299	-1267	143.0
	6	-32	-1320	-1288	143.7
	7	-43	-1344	-1301	143.4
	8	-53	-1362	-1309	143.6
	9	-60	-1383	-1323	145.1
	10	-47	-1395	-1347	145.0
	11	-57	-1409	-1352	144.0
	12	-61	-1426	-1365	143.5
	13	-87	-1455	-1367	142.8



**Table A-6-25:** Raw collected data for the 90-day loading age of the HS-SL mixture

<b>Mixture ID</b>		<b>SCC-HS-SL-90</b>			
<b>Compressive Strength (psi)</b>		13,670			
<b>Target Applied Load (kips)</b>		153.5			
<b>Quality Control Compressive Strength (psi)</b>		12,880			
<b>Reading Interval</b>	<b>Shrinkage Strain (<math>\mu\epsilon</math>)</b>	<b>Total Strain (<math>\mu\epsilon</math>)</b>	<b>Creep Strain (<math>\mu\epsilon</math>)</b>	<b>Total Force (kips)</b>	
<b>Day One</b>	Pre-Load	----	----	----	----
	Post-Load	-1	-778	-777	153.5
	2 to 6 hr	-3	-809	-807	152.9
<b>Week One</b>	1	-2	-859	-857	152.1
	2	-5	-848	-843	151.6
	3	-16	-867	-851	151.6
	4	-26	-887	-861	151.6
	5	-24	-895	-871	151.6
	6	-13	-898	-885	151.7
<b>Month One</b>	2	-16	-929	-913	151.6
	3	-28	-960	-932	151.7
	4	-31	-989	-958	151.6
<b>Months of Year One</b>	2	-25	-1093	-1069	152.8
	3	-12	-1089	-1077	151.6
	4	-13	-1105	-1091	151.6
	5	-32	-1130	-1097	152.0
	6	-41	-1158	-1117	152.2
	7	-56	-1189	-1133	151.6
	8	-51	-1205	-1154	151.6
	9	-58	-1221	-1163	152.2
	10	-60	-1239	-1179	153.5
	11	-63	-1250	-1187	152.8
	12	-68	-1259	-1191	153.6
	13	-75	-1276	-1201	152.1